Development of an imaging model of a CNS infection with African trypanosomes

Hollie Burrell-Saward

Thesis submitted in accordance with the requirements for the degree of

Doctor of Philosophy

of the

University of London

January 2015

Department of Immunology and Infection

Faculty of Infectious Tropical Diseases

LONDON SCHOOL OF HYGIENE & TROPICAL MEDICINE

Funded by: Bill and Melinda Gates Foundation

Research group affiliation: Croft Group

Declaration

I, Hollie Burrell-Saward, confirm that the work presented in this thesis is my own. Where information has been derived from other sources, I confirm that this has been indicated in the thesis.

Signed:……

Contributors

The work carried out within this PhD was part of the Bill and Melinda Gates funded grant and involved a number of contributors.

1. The design of construct was carried out by Dr. Martin Taylor, with the transfections of the *T. b. brucei* strains were carried out by Alex McLatchie at the London School of Hygiene and Tropical Medicine (LSHTM). The *in vitro* assessments (bioluminescence and growth curves) were also carried out by Alex McLatchie.

2. All *in vivo* assessments of strains were carried out by author as well as the production of samples for pharmacokinetic studies. The drug and DNA extractions were also carried out by author.

3. The design and optimisation of primers for qPCR were carried out by Dr. Eleanor Barnwell (LSHTM), with all qPCR experiments and analysis carried out by author.

4. Analysis of samples from pharmacokinetic studies (produced by the author) was carried out by Dr. Hatem Sallam and Dr. Andy Harris at Pharmidex, UK. This involved the LC-MS/MS analysis of generated samples (see above) and dose ranging studies.

See individual chapters for breakdown of contributors.

Abstract

The study of late-stage human African trypanosomiasis (HAT) within mouse models is lengthy and complex, with the removal of brain tissue being required to monitor parasitic burden. This results in the inability to track real-time infections within the central nervous system (CNS).

With nearly 70 million people at risk of HAT infection in Africa every year, research into new drug therapies which are capable of crossing the blood brain barrier and efficacious towards the parasite are imperative. However, progress has been slow and difficult, partly due to the limitations with the current drug relapse mouse model for African trypanosomiasis (*T. b. brucei* GVR35), which requires a follow-up time of 180-days.

In this study, we report the generation of highly bioluminescent parasites and their use in an *in vivo* imaging model of late-stage African trypanosomiasis. Bloodstream forms of the chronic model strain GVR35 were transfected with a "red-shifted" luciferase, which produced detectable signal in CNS at 21-days p.i mimicking that of the wild type line. This model enabled the tracking of a single animal through the entire chronic infection, with the detection of parasites occurring earlier than blood film microscopy.

The model was further employed to assess the effects of known anti-trypanosomal drugs on bioluminescence, and to demonstrate how the reduction in bioluminescent signal combined with qPCR can determine a dose-dependent effect after treatment.

The non-invasive *in vivo* imaging model will reduce the time and numbers of mice required to assess preclinical efficacy of new anti-trypanosomal drugs.
This study shows the development and optimisation of a new, efficient method to evaluate novel anti-trypanosomal drugs *in vivo* with the added advantage of reducing the current drug relapse model from 180-days to 90-days.

Acknowledgements

I would like to begin by thanking my supervisor Professor Simon Croft for giving me his constant support and guidance throughout, especially during the writing of my thesis. Simon, your direction has been invaluable and I will be eternally grateful for it.

I am also thankful to all those involved in the Gates HAT project for their suggestions and feedback during this project. In particular I would like to thank Dr. Jean Rodgers, Dr. Martin Taylor, Dr. Theresa Ward and Professor John Kelly, for their help with animal models, PCR and imaging.

I am indebted to my esteemed colleagues at morning coffee: Dr. Sam Alsford, Dr. Matt Rogers, Dr. Vanessa Yardley and Lindsay Stewart, for their help and patience with my persistent questions and moaning.

A big thanks goes to my colleagues and friends in 480: to Ross Paveley for providing IT and statistics help and to Liz McCarthy and Rachel Gregory for providing support, encouragement and much needed biscuits. Extra special thanks go to Andrea and Tash, whose continual friendship has been unwavering in spite of my constant distractions.

It is also important that I thank my beloved London Rockin' Rollers who were always on hand to smash around the track when I needed to decompress.

Finally I would like to say a massive thank you to my family for their endless support and encouragement. I owe my biggest thanks to my husband Tim who was always there to calm me down when stressed, encourage me through the tough times and without whom I would never have started (l*et al*one finished) this PhD.

This thesis was powered by McVities Chocolate Penguins.

Index

TABLE OF CONTENTS

List of figures and tables

ADME	absorption, distribution, metabolism and excretion
AIDS	Acquired Immune Deficiency Syndrome
AUC	Area under the curve
BAL	dimercaptopropanol
BBB	blood brain barrier
BLAST	Basic Local Alignment Sequence Tool
BLI	bioluminescence live imaging
BSF	blood-stage form
CBR	click beetle luciferase
CCLR	cell culture lysis reagent
cDNA	complimentary DNA
CI	confidence interval
CM	cerebral malaria
CNS	central nervous system
CSF	cerebrospinal fluid
CVO	circumventricular organ
D1, D2, D3 etc	Day 1, Day 2, Day 3 etc
DA	diminazene aceturate
DEA	disease endemic areas
DFMO	α-difluoromethylornithine or eflornithine
DNA	deoxyribonucleic acid
DNDi	Drugs for neglected diseases initiate
DPBS	Dulbeccos phosphate buffered saline
ED50	effective dose to kill 50% parasite population
ED90	effective dose to kill 90% parasite population
F Luc	firefly luciferase
f.o.v	field of view
FMO	flavin-containing monooxygenase
GFP	green fluorescent protein
HAART	highly active anti-retroviral therapy
HAT	Human African trypanosomiasis
HCl	hydrochloride
hi-FCS	heat-inactivated foetal calf serum
i.p	intraperitoneal

i.v	intravenous
IC_{50}	Inhibitory concentration to kill 50% parasite population
IC_{90}	Inhibitory concentration to kill 90% parasite population
iCAM	intercellular adhesion molecule
IFN	interferon
iRBC	infected red blood cell
ISG	invariant surface glycoprotein
IVIS	*in vivo* imaging system
JAM	junctional adhesion molecules
LC-MS/MS	Liquid chromatography- tandem mass spectrometry
LSHTM	London School of Hygiene and Tropical Medicine
M1, M2, M3 etc	Mouse 1, Mouse 2, Mouse 3 etc
MelB	melarsoprol
MIC	minimum inhibitory concentration
MSF	Medécins Sans Frontières
NECT	nifurtimox and eflornithine combination therapy
NK	natural killer cells
ns	not significant
NTD	neglected tropical diseases
NTR	nitroreductase
ODC	ornithine decarboxylase
p-value	probability value
p.i	post-infection
p.o	per os (oral dose)
p/s	photons/second
PBS	phosphate buffered saline
PBS-G	phosphate buffered glucose saline
PCR	polymerase chain reaction
PD	pharmacodynamics
PfEMP	*Plasmodium falciparum* erythrocyte membrane protein
PK	pharmacokinetics
PPP	public- private partnership
PTRE	post-treatment reactive encephalopathy
qPCR	quantitative polymerase chain reaction

R Luc	renilla luciferase
R-value	correlation coefficient
RBC	red blood cell
RLU	relative luminescence units
RNA	ribonucleic acid
RNAi	RNA interference
ROI	region of interest
rpm	rotations per minute
RT	room temperature
SCID	severe combined immuno-deficient
SD	standard deviation
SEM	standard error of the mean
Swiss TPH	Swiss Tropical and Public Health institute
T. brucei	*Trypanosoma brucei*
TE	toxoplasmosis encephalitis
v/v	volume to volume
VSG	variant surface glycoprotein
VSL	variant surface lipoprotein
w/v	weight to volume
WBCs	white blood cells
WHO	world health organisation
WT	wild type

CHAPTER 1: Introduction

1.1 Challenges of central nervous infections

One of the hardest challenges facing drug development projects in neglected diseases, is the treatment of neurological parasitic infections. The complex balance of anti-parasitic activity and low toxicity is problematic. The therapeutic needs to be able to cross into the brain at concentrations that are effective to kill the pathogen for a sustained period of time to reduce complex treatment regimens (Nau *et al*., 2010).

New treatments are always a priority when dealing with disease and infections, but the ability to diagnose and understand the pathogen and its burden is essential in elimination and eradication programmes. Burden is an inherently difficult aspect to assess in neglected tropical diseases. The remote nature of most endemic areas and the limited access to medical facilities, prevents the recording of the disease and correct diagnosis (Jannin and Gabrielli, 2013). Neurological infections are often mis-diagnosed based on symptoms rather than the infective pathogen. This has resulted in epilepsy being a widely recorded condition in endemic areas as seizures are a common manifestation of most central nervous system (CNS) infections. The diagnosis of epilepsy has resulted in many diseases remaining untreated (Jannin and Gabrielli, 2013).

The pathogenic invasion of the CNS during an infection is often rare but can cause severe complications for the host if left untreated (Finsterer and Auer, 2013). For some pathogens, the CNS may not always be the intended destination, for others CNS invasion acts as an important survival step of host evasion (Masocha and Kristensson, 2012).

In order for a pathogen to successfully reach the CNS, they need to breach, cross or evade physical and immunological barriers. The two most well-known physical barriers within the CNS are the blood-cerebrospinal fluid (blood-CSF) barrier and the blood-brain barrier (BBB), both of which are responsible for keeping potentially harmful substances circulating in the blood, away from the brain and spinal cord.

1.1.1 Blood-cerebrospinal fluid (Blood-CSF) barrier and CSF-brain interface

The CSF is a clear liquid produced by the choroid plexus that is responsible for providing an optimum environment for neurological mechanisms (Finsterer and Auer, 2013). CSF circulates around the brain and spinal cord within the ventricular system, and can be used as a marker in determining brain dysfunction through the analysis of lumbar puncture samples. To ensure that the internal environment remains regulated and protected against unwanted molecules, a blood-CSF barrier exists within the choroid plexus (Fig 1.1).

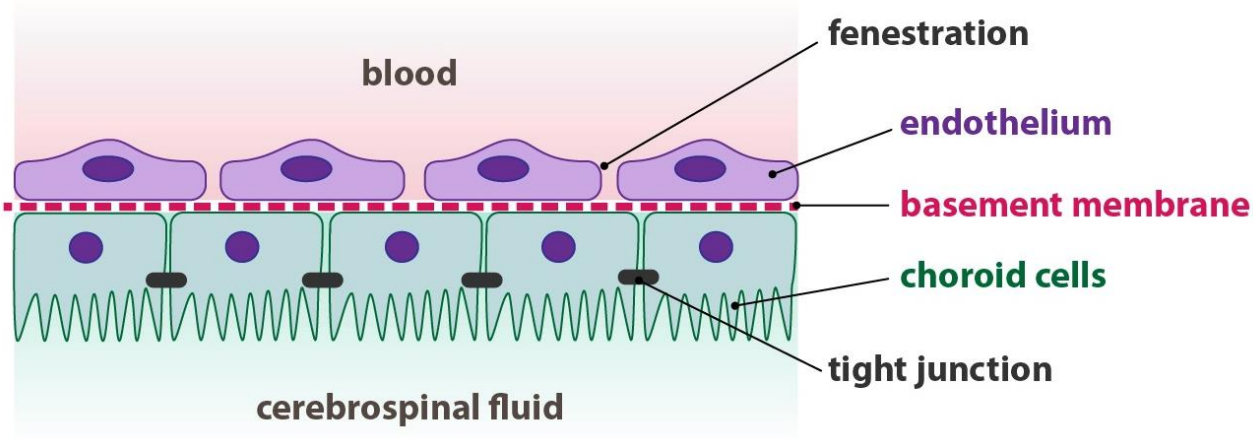

Figure 1.1. Blood-CSF barrier. The endothelial cells have large gaps between them allowing easy access to the basement membrane. Further entry into the CSF is halted by tight junctions being present between the choroid cells (Source: http://fblt.cz/en).

The barrier consists of three parts; choroidal epithelial cells, basement membrane and endothelium of the pia mater capillaries.

As a barrier it is relatively permeable, with the movement of plasma proteins being possible through active transport or pinocytosis. Permeability of the barrier is due to gaps (fenestrations) in the endothelium of pia mater capillaries. Plasma proteins and macromolecules are able to pass through the endothelium, but due to the choroid epithelial cells being connected by tight junctions they become trapped within the basement membrane. It is thought that the tight junctions provide the selectivity of the barrier, limiting the movement of molecules through and into the CSF as no fenestrations are present between the choroid cells (Kristensson *et al.*, 2013).

Structures are present that separate the CSF and the brain tissue, whilst these are not barriers they do consist of similar cells seen in both the blood brain barrier (BBB) and blood-CSF. The structures; pia-covered surface of spinal cord and brain, perivascular extensions of the subarachnoid space and the ependymal surface. The notable difference between these structures and the barriers, is the lack of tight junctions, which may explain why molecules are able to pass through from the CSF into the central nervous system with little resistance (Masocha and Kristensson, 2012).

1.12 Blood-brain barrier (BBB)

The blood-brain barrier (BBB) isolates and protects the CNS from the blood to provide a stable environment free from microbes and large or hydrophilic molecules. The structure of the barrier is a complex, highly specific, semi-permeable membrane that restricts the movement of molecules from blood vessels to the brain (Kristensson *et al*., 2013).

BBB occurs along the capillaries in the CNS and like the blood-CSF barrier, consists of three parts; a layer of endothelial cells, basement membrane and astrocytic feet (Fig. 1.2).

The first point of contact of the blood is a wall of tightly packed endothelial cells with no fenestrations (normally present in other endothelium, as in the blood-CSF). The endothelial cells are interconnected by tight junctions that cause the selectivity of the barrier and prevent the passage of molecules through. The tight junctions themselves are a collection of transmembrane proteins such as occludin, claudins and junctional adhesion molecules (JAM), which are fixed to the endothelial cells by protein complexes (Kristensson *et al*., 2013).

The basement membrane (also known as the basal membrane) is a matrix of basal lamina of astrocytes and basal lamina of endothelial cells. It separates the endothelial cells from the astrocytes and acts as an additional barrier in the protection of the CNS.

The astrocytes are glial cells found on the neural basement membrane, adhering to the outer surface of the capillary wall via astrocytic “feet” (Fig. 1.2).

The cells do not have a substantial role in the maintenance of the BBB, but are involved in the regulation of blood flow into the brain (Masocha and Kristensson, 2012).

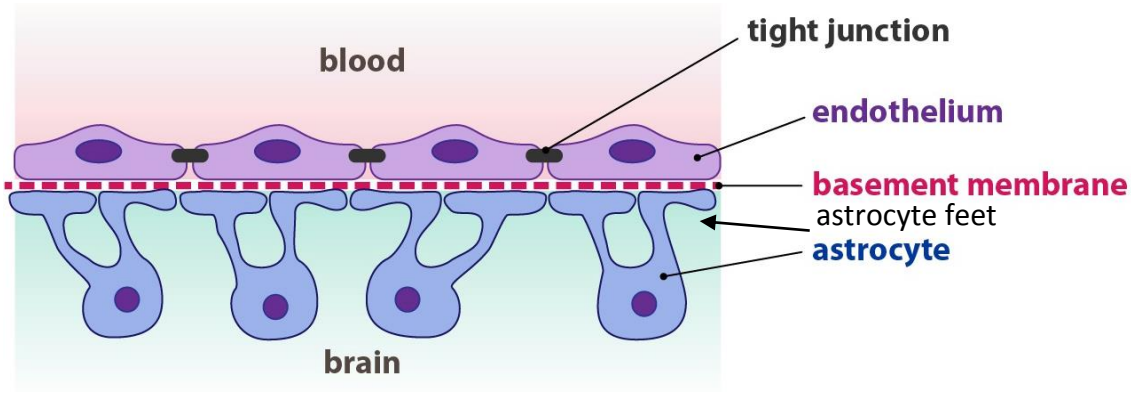

Figure 1.2. Structure of the blood-brain barrier BBB. Unlike the blood-CSF barrier, the tight junctions appear in between the endothelium with no fenestrations being present. The astrocytic feet anchor the astrocytes to the basement membrane (adapted from http://fblt.cz/en).

The permeability of the membrane is related to the size of the molecule. Larger molecules move slowly across the barrier (glucose etc.), whereas water and gas are able to pass through readily. Plasma proteins and compounds with large molecular weight (> 60, 000 kDa) are unable to cross (Masocha and Kristensson, 2012). The overall structure of the BBB results in a hydrophobic nature, allowing only lipophilic substances to penetrate unless appropriate transport channels are expressed by the endothelial and astrocytes (Fig. 1.3)

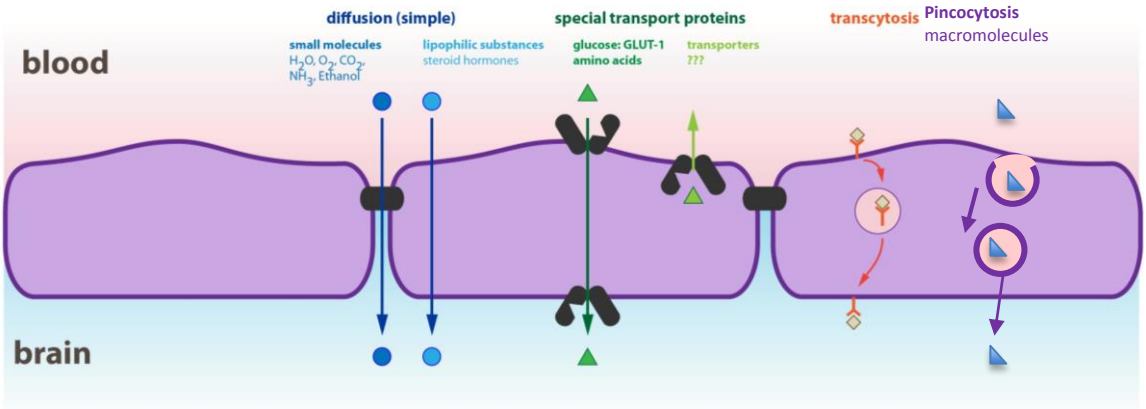

Figure. 1.3. Passage of molecules through the BBB. Small and lipophilic molecules are able to move through the BBB freely by passive diffusion. Facilitated diffusion and active transporters allow glucose, GLU-1 and amino acids passage into the brain. Specific larger and macromolecules can be transferred using transcytosis and pinocytosis. (Source: http://fblt.cz/en 2013).

As described above, the prominent role of the BBB is to maintain an internal environment within the brain, free from unwanted molecules and pathogens. But

in the event of a CNS infection, the BBB also acts as a protective layer against the entry of antibodies and drugs. The CNS was once thought as being an "immune-privileged" site, where the presence of immune cells were unable to enter resulting in a lack of inflammatory response. However, over the past twenty years this theory has been challenged as CNS macrophages (microglia) have been detected within the system, and there is evidence that an interaction of peripheral immune cells with the CNS endothelium occurs (Kristensson *et al*., 2013).

Not all areas of the brain have a BBB. The circumventricular organs (CVOs) have large vasculature providing an alternative route for hormones and other molecules to enter the CNS (Kristensson *et al*., 2013).

1.2 CNS parasitic infections

As mentioned earlier, not all pathogens have the CNS as their target for infection. Parasites that infect the CNS fall into two categories. (i) Single-celled protozoa such as, malaria, toxoplasmosis and Human African trypanosomiasis and (ii), multi-cellular metazoan such as, flatworms (including trematoda and crestoda) and roundworms (Pittella, 2013). The diagnosis of CNS infections is extremely difficult as most parasites either cause a self-limiting infection or are asymptomatic (Finsterer and Auer, 2013). Here, we provide a brief overview of single-celled protozoan infections, their interaction and in some cases invasion of the CNS.

1.2.1 Cerebral malaria

Cerebral malaria (CM) is the neurological complication of severe *Plasmodium falciparum* (*P. falciparum*) malaria infection (Pittella, 2013). *P. falciparum* is a intracellular apicomplexan parasite that is transmitted by the *Anopheleine* mosquito during a blood meal and causes one million deaths each year (Postels and Birbeck, 2013). The complication of severe malaria and consequently CM occurs in patients with little or no background immunity to the parasite, and causes nearly half of the total deaths from malaria each year (Newton *et al*., 2000).

P. falciparum undergoes a complex multi-staged life-cycle, that involves a vertebrate host (human) and an invertebrate host (mosquito), and it is the human host that we will focus on. There are three distinct phases within the human host. (1) The exo-erthrocytic schizogony occurs after the injection of plasmodial

sporozoites into the host by the mosquito. The sporozoites rapidly migrate to the liver and undergo asexual reproduction in infected hepatocytes to produce hepatic schizonts. (2) The erythrocytic schizogony stage occurs after the matured hepatic schizonts rupture, releasing merozoites into the bloodstream. At this stage the merozoites rapidly invade the red blood cells (RBCs) and undergoes maturation from young ring to schizont, containing 16-32 merozoites. Not all infected red blood cells (iRBCs) become schizonts, a proportion of rings commit to differentiate from the asexual to sexual (3) stage to become macro or microgametocytes which are taken up by mosquitos during a blood meal (Madigan, 2006).

Clinical presentation of CM include; the asexual forms of the *P. falciparum* being present in the peripheral blood films and patients being in a potentially reversible unarousable coma (with no other possible causes). The coma is either spontaneous or it can develop one hour after a seizure (Idro *et al*., 2010).

As with most CNS infections the exact cause of CM is largely unknown, but the invasion of *P. falciparum* parasite into the CNS is not responsible for the neurological effects (Medana and Turner, 2006). Post-mortem samples of CM patients and work carried out with the rodent model *P. berghei* ANKA, has found that the sequestration of iRBCs to the endothelium in the cerebral vessels is necessary for the development of CM, but the initiation and maintenance pf coma requires other factors (Adams *et al*., 2002). The adhesion of the iRBCs to the endothelium requires a number of endothelial receptors including; intercellular adhesion molecule (ICAM)-1 and the scavenger receptor CD36. The adherence is mediated by the parasite antigen PfEMP-1 (*Plasmodium falciparum* erythrocyte membrane protein-1) (Idro *et al*., 2010). The receptors responsible for the sequestration are also involved in recruiting leukocytes during an inflammatory response.

The cytoadherance of the iRBCs to the endothelial cells and the host immune response, causes a change in the BBB permeability which in turn leads to neural injury. The 'leaky' BBB is confirmed in patients with CM as an increase in albumin is found in the CSF, whereas normally the molecule is too large to pass through the barrier (Adams *et al*., 2002).

Upon treatment, CM coma can be reversed and many patients do not suffer any lasting neurological effects (Finsterer and Auer, 2013). But there have been cases where survivors have a sustained brain injury, manifesting as long-term neuro-cognitive impairments. Current treatment therapies involve the intramuscular or intravenous injection of artesunate followed by a complete course of artemisinin combinational therapy (ACT). In children that may have signs of neurological impairment, cognitive rehabilitation is recommended, such as; behavioural and speech therapy as well as hearing aids, but unfortunately strict guidelines on assessing impairment have not been established (Idro *et al*., 2010).

1.2.2 Toxoplasmosis

Toxoplasma gondii (*T. gondii*) is an apicomplexan obligate intracellular parasite, which has the ability to infect and replicate in any nucleated mammalian or avian cell (Kamerkar and Davis, 2012). Toxoplasmosis effects a third of the world population and is one of the most common human zoonotic infection, with many patients being asymptomatic (Saadatnia and Golkar, 2012). CNS complications arise in immunocompromised hosts, where a reactivation of the latent infection occurs and can lead to the patient developing serious symptomatic manifestations (Saadatnia and Golkar, 2012).

The zoonotic parasite exists as three forms; (1) the oocyst contains sporozoites and is produced during the sexual stage within the small intestine of felines. This is the infectious stage and can infect humans via cat excrement contaminated water, soil or vegetables. After ingestion, the oocysts rupture in the intestine and the sporozoites are able to infect the surrounding cells of the lumen. (2) the tissue cyst is the more common form ingested by humans and is normally present in undercooked meat, like the oocysts, the tissue cysts also rupture when in the intestine. The rupturing of the tissue cyst produces bradyzoites that then proceeds to infect surrounding cells. (3) the final form is the tachyzoite, which is rapidly-dividing with the ability to infect any nucleated cells. They are then able to disseminate to different tissues and produce a reactivation of a latent infection. The infection of sporozoites and bradyzoites into the intestinal cells, also results in differentiation to the proliferative tachyzoites which circulate in the blood and lymphatic system (Saadatnia and Golkar, 2012).

In addition to oral transmission, *T. gondii* is able to cross the placenta and infect the foetus in pregnant women with latent infections. The manifestations of the foetal infections can be severe and devastating, with symptoms including hydrocephaly, mental retardation, seizures, inflammation of the eyes and miscarriage or still-birth. The severity of the infection is dependent upon the point at which the mother is infected. Prior to pregnancy the foetus is protected due to the mothers antibodies, but later in pregnancy the symptoms become more severe (Saadatnia and Golkar, 2012).

Toxoplasmosis in healthy individuals is usually controlled by the immune system. When the illness does manifest, it usually causes flu-like symptoms that may last for weeks or months before becoming dormant, it is then only reactivated during immunosuppression (Pittella, 2013). It is the major opportunistic infection in immunosuppressed patients (e.g. AIDS and organ transplant patients), with the reactivation of an infection giving rise to the symptoms of fever, confusion, headaches, seizures, nausea, poor coordination and the potentially fatal toxoplasmic encephalitis (TE) (Finsterer and Auer, 2013).

The exact movement of *T. gondii* into the CNS is poorly understood and the parasite is able to move both intra and extracellularly (though predominantly it remains as an intracellular parasite) (Masocha and Kristensson, 2012). Research carried out by Lachenmaier *et al* found evidence to support the 'Trojan horse' theory. The infection of nerve cells, astrocytes and microglia in combination with a T-cell-mediated response, allows the parasites to enter the brain via transendothelial migration of the BBB (Fig. 1.4) (Lachenmaier *et al*., 2011).
In immunosuppressed patients it has also been found that *T. gondii* can localise in the choroid plexus at the blood-CSF barrier which could be a potential point of entry into the CNS (Masocha and Kristensson, 2012).

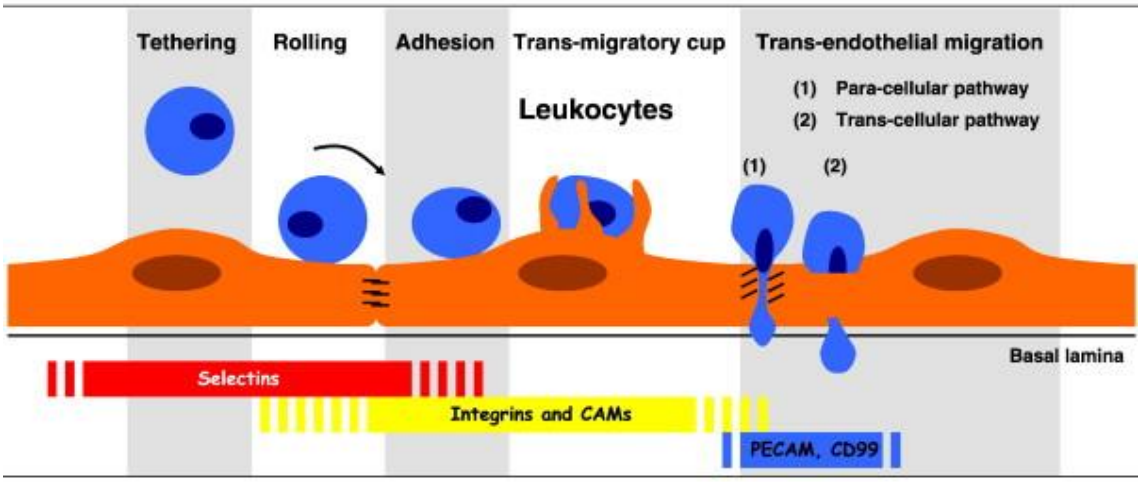

Figure 1.4. Endothelial transmigration. Various adhesion molecules and their receptors on the endothelial cells modulate the entry of the infected leukocytes through the BBB. The tachyzoites infected cells induce an upregulation of activated cellular adhesion molecules on the inflamed endothelial cells, resulting in a leaky BBB. (Weiss *et al*., 2009)

Educating individuals on how to avoid personal exposure to toxoplasmosis is currently the best method of prevention as no vaccine is currently available for humans, although not out of reach as life-long protection would occur (Saadatnia and Golkar, 2012). Early diagnosis in immunocompromised individuals can help in the treatment to prevent the onset of TE, and currently highly active anti-retroviral therapy (HAART) has effectively reduced the number of AIDS patients presenting with TE (Saadatnia and Golkar, 2012). Healthy symptomatic patients infected with toxoplasmosis can undergo an effective combination treatment regime of pyrimethamine, sulfadiazine and folinic acid, though the treatment is limiting for established TE infections (Finsterer and Auer, 2013).

1.3. Human African trypanosomiasis

Human African trypanosomiasis (HAT) is a multi-stage disease that manifests in two stages of an early and late stage, and it is the latter that involves the invasion of parasites into the CNS (Pentreath, 2004), and the focus of this study.

HAT causes fewer than 8000 cases (as reported in 2013) a year with almost 70 million people at risk within the African continent (WHO, 2013). Prevalence has greatly fluctuated over the last 100 years due to medical intervention and socio-economic unrest. Despite the high risk of infection, HAT is still classed as a

Neglected Tropical Disease (NTD) by the World Health Organisation (WHO) with very little advance in drug development over the past 50 years (Simarro, 2011).

African trypanosomiasis is caused by an extracellular, unicellular kinetoplastid protozoan parasite *Trypanosoma brucei* (*T. b*) and transmitted by an infected tsetse fly (*Glossina sp.*) during a blood meal (Stevens, 2004).
There are three subspecies of *Trypanosoma brucei*; *T. b. brucei*, *T. b. gambiense* and *T. b rhodesiense* (the latter two being responsible for the human infection) (Brun *et al*., 2010).

T. b. gambiense is responsible for approximately 95% of all reported cases of HAT every year within central and western Africa and produces a chronic infection that may take anything from three months to two years to manifest (Kaiser *et al*., 2011). *T. b. rhodesiense* is a zoonotic parasite, with the primary reservoir being within game and livestock in eastern and southern Africa and causes an acute infection, with symptomatic manifestations occurring in a matter of weeks (Steverding, 2008). The third subspecies; *T. b. brucei,* found in cattle, causes the disease known as *nagana* and is non-infectious to humans. However, it can be used as a surrogate parasite in the study of trypanosomiasis (Brun *et al*., 2010).

1.3.1 Parasite, lifecycle and pathogenesis

Despite the differences in host infectivity and infection pathogenesis, the parasite and lifecycle of the three subspecies are identical (Fig 1.5).

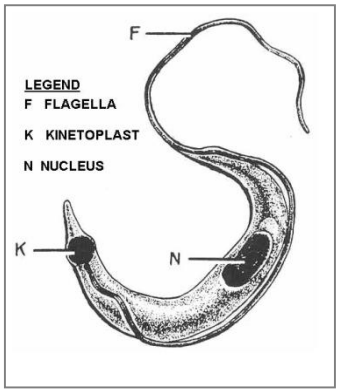

Figure 1.5 The trypanosome (Source: http://armymedical.tpub.com). (F) Flagellum is attached via the parabasal body at the posterior end of the trypanosome near the kinetoplast (K), and runs the entire length of the parasite. (K) contains mitochondrial DNA and is essential in reproduction and metabolism. (N) Nucleus contains DNA arranged in the form of genes and chromosomes. Its

position varies depending on which form the trypanosome is in. (S) Surface coat is a dense structure that encases the entire cell body and flagellum (Nolan, 2004).

Trypanosomes are pleiomorphic and exhibit three different morphological forms within the mammalian host, consisting of slender, intermediate and stumpy forms (Fig.1.6 and Table 1).

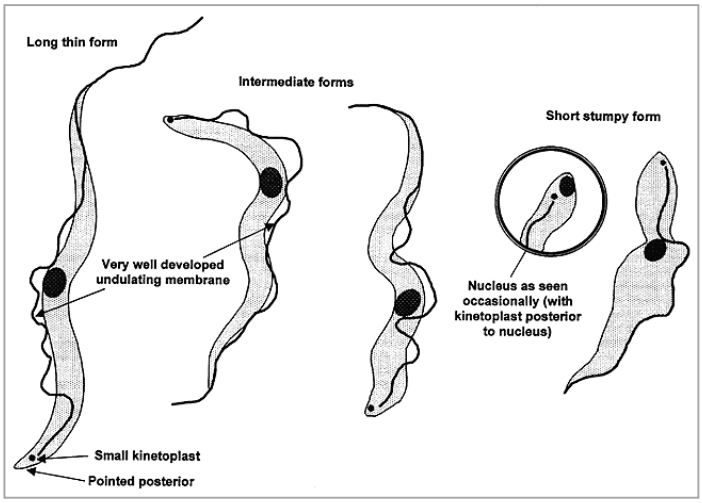

Figure 1.6 Pleiomorphic stages of *T. brucei* (Source: http://www.fao.org)

During the early stages of trypanosomiasis, the slender forms are rapidly dividing and cause the haemolymphatic parasitaemia to increase logarithmically. Once cell-density reaches a threshold, activation of density-sensing factors occurs and results in halting parasite division. At this point the slender forms morphologically differentiate into the non-replicating stumpy form (Nolan, 2004). The intermediate stage is often seen in *in vivo* models and appears neither slender nor stumpy.

Recent studies have shown that trypanosomes isolated from the brains of mice infected with *T. b. brucei* AnTaT 1.1, have a very long slender morphology (extensively thinner and longer than in Fig. 1.6) and are highly motile moving in straight lines at high speed, therefore distinctly different from the blood slender forms (Mogk *et al*., 2014).

Stage	Length	Position of Nucleus	Flagellum
Slender	23-30μm	Central	Free, spirals around parasite body
Intermediate	23-25μm	Off-centre, nearer posterior end	Free, but slightly shorter than in the slender form
Stumpy	17-22μm	Nearer kinetoplast	No

Table 1 Morphological differences between different life-cycle stage of trypanosomes.

The extracellular slender forms found in the blood, are under constant challenge by the host immune system. The trypanosomes are able to evade the host immune attack by expressing approximately 1 x 10^7 variant surface glycoprotein (VSG) on their surface coat, which protects the parasite against lymphocytes and complement. The trypanosome contains several hundred VSG genes but only one VSG protein is expressed on the surface at a time in a process known as antigenic variation. (Barry, 2001). The process of antigenic variation is clonal and rapid, with each individual trypanosome undergoing spontaneous antigenic switching. This allows the parasite to evade the host immune response, as the formation of VSG-specific antibodies will only clear part of the clonal population in the blood, as parasites that have already switched VSG are protected and will proliferate. (Barry, 2004). Once the slender forms have differentiated into stumpy parasites they are no longer able to undergo antigenic variation and are therefore susceptible to immune response (Mogk *et al*., 2014).
Understanding how antigenic variation occurs and a way to disrupt it can provide a potential drug target, as trypanosomes would then become vulnerable to an attack by the host immune system.

T. brucei undergoes a complex multi-stage life-cycle involving a mammalian host and an invertebrate host (the tsetse fly) (Fig. 1.7). Within the human host the infection has three distinct phases; chancre formation, early (first) stage and late (second) stage HAT.

The trypanosomal chancre is a localised inflammatory response to the tsetse fly bite and initial injection of parasites. It typically appears approximately 48 hours after the fly has taken a blood meal and is the first sign of an infection. Patient reaction to the chancre typically differs; some find it disappears within a couple of days, whereas others find it very painful, persisting for up to three weeks (Sternberg and Maclean, 2010). The early stage of infection occurs some weeks later as the parasite invades the haemolymphatic system (Pentreath, 2004). It is at this point that the differences between *T. b. gambiense* and *T. b. rhodesiense* infections are evident. In the acute infection of *T. b. rhodesiense*, symptoms can occur immediately, as the infection progresses at a much faster rate. With a *T. b. gambiense* infection a patient may not see symptoms for several years.

The common symptoms present during the early stages (haemolymphatic stage) of HAT include an irregular fever pattern, joint pain, itching, enlargement of the spleen and in gambiense infections, a characteristic enlargement of the lymph nodes known as Winterbottom's sign (enlargement of the posterior cervical group of lymph nodes) (Bʊscher, 2004).

The late stage, also known as the meningoencephalitis stage is characterised by the parasites invading the central nervous system (CNS) through the blood-brain barrier (BBB). How the parasites pass through the BBB remains under investigation and there are many theories regarding the mechanism of action. These theories include the involvement of immune cells and the use of intracellular junctions (Brun *et al*., 2010). The symptoms for the late stage are neurological and include confusion, personality changes, tremors and psychiatric symptoms. The primary symptom of the late stage is the disruption in sleep patterns, which is due to the infection causing a deregulation in the circadian rhythm. The differences between the late stages of the chronic (*gambiense*) and acute (*rhodesiense*) infection are more obvious, but in both cases, if left untreated the second stage will progress to coma leading to eventual death (Pentreath, 2004, Brun *et al*., 2010).

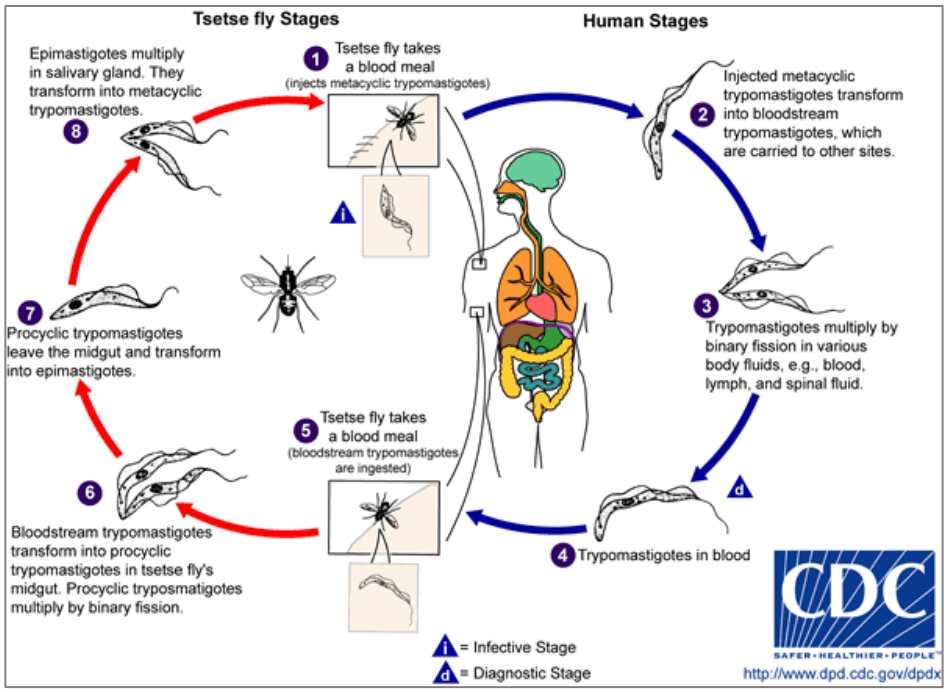

Figure 1.7. The life-cycle of Human African trypanosomiasis (CDC, 2009)

1.3.2 CNS invasion by trypanosomes

The penetration of trypanosomes into the CNS is still under investigation but they do exhibit some similarities with that of toxoplasmosis in its CNS penetration. Unlike *P. falciparum, Trypanosoma* and *Toxoplasma* do not actively damage the BBB to invade the CNS, and it is theorised that both use the presence of leukocytes and an immune response to gain entry (Finsterer and Auer, 2013).

During early stages of infection, trypanosomes have been found to concentrate around the circumventricular organs and choroid plexus and are believed to cross into the choroid plexus and CVOs due to the lack of BBB. But despite being at the CSF-Brain interface, the trypanosomes do not cross the ependymal cell layer to the brain parenchyma (Kristensson *et al.*, 2013).

The introduction of trypanosomes within the choroid plexus and CVOs causes inflammatory changes in the brain parenchyma as well as an upregulation of adhesions molecules, and other immune cells (e.g., chemokine, cytokines etc.). This is evident by the increased number of white blood cells (WBCs) that are found in the CSF, which is used as a diagnostic tool. This influx of leukocytes is believed to be the 'blanket of cover' the trypanosomes require in order to access the brain, as it is theorised that the parasite enters the brain through important and short-lived

openings in the BBB caused by the entrance of T-cells (Masocha and Kristensson, 2012).

Masocha *et al* established that the migration of trypanosomes into the brain requires lymphocytes to be present, by using a rodent model of African trypanosomiasis which lacked B and T cells (RAG-1 mice). The model failed to establish a CNS infection, suggesting that trypanosomes penetrate the BBB using mechanisms similar to leukocytes or, that leukocytes alter the integrity of the basement membranes (Masocha *et al*., 2004). The study also confirmed that pro-inflammatory cytokines played an important role in the parasite invasion as IFN-γ secreted by T and natural killer cells (NK) is predominantly responsible for the induction of macrophage trypanotoxic activities (Burgos *et al*., 2003). However, in IFN-γ or IL-12 (major inducer of IFN-γ) deficient mice, a reduction in trypanosome infiltration into the brain parenchyma is seen, although an increase in systemic parasitaemia occured (Masocha *et al*., 2004).

The detection of trypanosomes in the brain is inherently difficult and time-consuming due to low parasitaemia. Neuropathological changes associated with African trypanosomiasis have been studied from histopathology samples obtained from animal models (due to a lack of post-mortem reports from human patients) and indicate that neuropathogenesis is predominantly due to an inflammatory response presenting as meningitis, encephalitis and perivascular cuffing (Bʊscher, 2004). The occurrence of perivascular cuffing (accumulation of lymphocytes) in areas of vascularisation such as the thalamus, hypothalamus and choroid plexus, is common and indicative of CNS involvement in HAT but have not been proven to be responsible in the clinical features of late stage HAT (Burri, 2004).

1.3.3 HAT Drugs

When a patient presents with HAT it is preferable to know the strain and stage (early or late) of the infection (though this is not always performed) before treatment is administered. This is due to the four registered anti-trypanosomal drugs being both strain and stage specific.

	Early stage	Late stage
T. b. gambiense	pentamidine	• melarsoprol • eflornithine (DFMO) • DFMO & nifurtimox combination therapy (NECT)
T. b. rhodesiense	suramin	• melarsoprol

Table 1.2. Current therapies in the treatment of gambiense and rhodesiense HAT (WHO, 2009)

As the main focus of this study is on late stage HAT, the treatments for the early stages of gambiense and rhodesiense trypanosomiasis of pentamidine and suramin will be covered briefly.

Suramin was developed in Germany and first used in the treatment of sleeping sickness in 1922. It is now produced by Bayer under the name Germanin® (Burri, 2004). It was initially used for first stage treatment in both *T. b. rhodesiense* and *T. b. gambiense* and also in the clearance of *Onchocerca spp.* infections (Brun *et al*., 2010). However, due to some patients developing a severe allergic reaction to the clearance of *Onchocerca* infections in *T. b. gambiense* endemic areas, suramin treatment is now only carried out in *T. b. rhodesiense* cases (Burri, 2004).
After suramin treatment for gambiense ceased, pentamidine was introduced in 1941 under the commercial name of Pentacarinat (Dorlo and Kager, 2008).
Despite having a high cure rate of 98% in gambiense infected patients, failures are extensive in rhodesiense sleeping sickness which may be due to poor uptake by the rhodesiense parasite (Burri, 2004).

As the infection moves into the later stage of the disease and invades the CNS, different drugs are required that are able to cross the blood brain barrier. Table 1.3 indicates the current therapies for late stage disease are; melarsoprol, eflornithine (as a 2nd line treatment to melarsoprol failures) and the combinational therapy NECT (nifurtimox and eflornithine).

Melarsoprol (Arsobal®) was the most widely used drug in the treatment of late stage HAT in both *gambiense* and *rhodesiense* infections and has been used for HAT

since 1949. The wide use of the drug is in part due to its affordability and currently it is the only treatment available for *rhodesiense* infection (Barrett *et al*., 2007). Melarsoprol can produce a severe toxic side effect known as post-treatment reactive encephalopathic (PTRE) syndrome (table 1.3)(Stein *et al*., 2014). Chapter 4 provides further details on melarsoprol.

Eflornithine (DL-α-difluromethylornithine, DFMO) is one of the newer drugs to be introduced for the treatment of late-stage HAT. Originally designed for use in tumour chemotherapy, it was first trialed as an alternative to melarsoprol in 1981 by Van Nieuwenhove *et al*, after Bacchi *et al* confirmed its anti-trypanosomal efficacy *in vivo* (Bacchi, 1980, Van Nieuwenhove, 1981b). It is currently produced by Sanofi under the brand name of Ornidyl®. As mentioned earlier, DFMO can be used as a 2nd line treatment in melarsoprol failures, and is known as the "resurrection drug" as comatosed patients recover shortly after administration. The use of DFMO in the treatment of *rhodesiense* infections is strongly discouraged due to the drugs poor efficacy to the parasite (Burri, 2004). The very short half-life (3 hours) of DFMO means that the treatment administration requires intravenous infusion of large doses (Stein *et al*., 2014). In the early use of DFMO, it was given as an oral treatment as a way to reduce the need of hospitalisation for patients in rural areas. However, pharmacokinetic studies found absorption and effectiveness were seriously hindered with this method of administration (Na-Bangchang, 2004). Chapter 5 provides more information on DFMO and its mechanism of action.

Nifurtimox was introduced in the 1960s for the treatment of American trypanosomiasis (Chagas disease). In the 1980s, it was found to be poorly effective in studies with African trypanosomiasis, but there was still interest in using nifurtimox in combination with DFMO to treat late stage infection (Priotto, 2006). NECT (nifurtimox and eflornithine combinational therapy) was placed on the WHO Essential Medicines List in 2009 as an approved alternative treatment to melarsoprol and is currently the first-line treatment for late-stage HAT due to its less painful application than the individual monotherapies (Stein *et al*., 2014, Simarro, 2011). Chapter 5 provides further details on nifurtimox.

Currently there are two drugs in clinical trials for the treatment of HAT; fexinidazole and SCYX-7158 (DNDi, 2014).

Fexinidazole is an oral nitroimidazole drug re-purposed by the Drugs for Neglected Diseases initiative (DNDi) and is currently in Phase-2 and 3 clinical trials, with the plan of drug registration by the end of 2016 (DNDi, 2014). Preliminary studies have shown that it is orally effective in curing both chronic and acute stages of the disease in mice (Kaiser *et al*., 2011) (further details on the drug can be found in chapter 6).

SCYX-7158 is an orally-active benzoxaborole that has been shown to be effective in the cure of both early and late stage HAT in murine models at low doses (25mg/kg). The mechanism of action is understood to be the inhibition of serine proteases, which is common with boron-containing compounds. SCYX-7158 is currently in Phase-1 clinical trials and is one of the first candidate to enter clinical trials from the DNDi Lead Optimization Consortium, with drug registration planned for the end of 2018 (Nare *et al*., 2010, Wring *et al*., 2014).

Drug	Class of compound	Pharmacokinetics						Treatment Regime	Side effects
		Oral absorption	Distribution	Metabolism	Excretion	Plasma Protein Binding	Plasma half-life		
pentamidine	diamidine	Negligible	Large distribution throughout body and retained by tissue.	Liver	Renal	70%	6.5 hours	4mg/kg/day i.m x 7-days	Well tolerated, complications reversible with cessation of treatment. Local irritation, vomiting. Severe: - hypotension, hyperglycaemia, hypoglycaemia
suramin	naphthalene	Poor	High tissue distribution.	Not known	80% by renal clearance	99.7%	Approx. 44 days	1g i.v on days 1, 3, 5, 14 and 21. A test dose of 100mg carried out prior to treatment to test blood pressure stability.	Slow intravenous infusion reduce febrile reactions (nausea, vomiting). Severe: - renal damage, jaundice and leucopoenia.
melarsoprol	organometal	Not known	1-2% max plasma levels of melarsen oxide accumulates across the BBB	Microsomal enzymes; to melarsen oxide. Further metabolised into non-toxic compounds.	In the urine and faeces	80%	35 hours	2.2mg/kg/day i.v x 10 days	Severe: - post-treatment encephalopathic (PTRE) syndrome. Convulsions, fever, headaches, progressive coma and eventually death.
eflornithine (DFMO)	polyamine	55%	Poor distribution	Not metabolised	Renal,80% unchanged in urine	Very low	3 hours	100mg/kg daily i.v infusions for 14 days	Diarrhoea, reversible anaemia Severe: - Convulsions and seizures
nifurtimox	nitrofuran	Not known	Poor.	Rapid and extensive	Renal, only 1% unchanged	~ 39%	3 hours	Not used as a monotherapy, see text for NECT combination-therapy	Vomiting, insomnia, headache and disorientation. Cease upon the end of treatment

Table 1.3. Comparison of current drug therapies used in the treatment of HAT

1.3.4 Rodent Models of HAT

The use of animal models in the study of any infectious disease, can not only provide useful information about the interactions of the pathogen with the host immune system. It can also be a helpful tool in drug discovery programmes to determine targets and are necessary for efficacy testing of the drug in an infected host.

T. b. brucei, the parasite responsible for some forms of trypanosomiasis in cattle, is the most commonly used parasite line in both the laboratory and animal unit for the study of African trypanosomiasis. The strain *T. b. brucei* Lister 427 is a well-defined monomorphic line, remaining solely as the blood-stream form (BSF) of the parasite.

Lister 427 is often used in efficacy trials of drugs aimed at the blood-stage of the disease, as it can easily infect outbred mice and, due to its virulence, kills mice within 7-10 days making it a very quick high-throughput drug experiment.

T. b. brucei GVR35 is a pleiomorphic strain that is commonly used to study CNS infection, as trypanosomes are able to cross the blood brain barrier, with a survival rate of approximately 40 days in mice. This model allows drug relapse to be detected in either the CNS or peripheral parasitaemia. Currently the GVR35 model requires 180-days of follow up to allow parasites to move into the periphery from the CNS, and therefore detectable via blood films (Jennings *et al*., 2002).

GVR35 can also be easily cultured *in vitro,* but at a slower rate than Lister 427 and requires different culturing techniques due to the parasite having the ability to differentiate to the stumpy form.

Models of *T. b. rhodesiense* are often used to assess drug efficacy against the early-stage of the disease due to the acute nature of infection, and normally used as a secondary screen after successful data obtained from Lister 427. STIB 900, derived from STIB704 is a commonly used strain both *in vitro* and *in vivo* as it is drug sensitive and can be easily cultured. STIB900 can successfully infect inbred strains of mice, without the requirement of immunosuppression and mice are normally overwhelmed by parasitaemia and die at approximately day 6 post-infection (Kaiser *et al*., 2011).

Though a chronic infection model of *T. b. gambiense* in albino rodents (rats and mice) was first obtained in 1981 by Beckers *et al* (Beckers, 1981), use and reproduction of the model has been limited in recent years. The key problem with rodent models of *T. b. gambiense* is the low virulence in immunocompetent mice, with very low parasitaemia that can take many months to appear. The low parasitaemia can be problematic when studying drug efficacy, as numbers are too low to determine if an effective dose has been reached. Using immunosuppressed or severe combined immune-deficient (SCID) mice can help to obtain initial infections and to boost parasitaemias. The use of cyclophosphamide and irradiation to immunosuppress mice prior to infection helps to increase parasitaemia to $>10^6$/ml, enabling the harvest of parasites much easier. However, immunosuppression does not always produce uniform infections and low CNS infections (confirmed primarily by the presence of immune cells within the brain) usually occurs. There is also some discrepancy on how often mice should be treated with the immunosuppressant, not to mention the added problem of drug-treating mice prior to a drug study, as drug to drug interaction may be an issue (Brun, 1999). Due to GVR35 being able to replicate a CNS infection within mice, it is commonly used as a surrogate in the drug evaluation and study of CNS infection in HAT.

When carrying out studies in rodents it is important to understand the limitations of the models and be aware of the physical differences between rodents and humans. In CNS infection studies this is especially important as there is limited access to infected human brain tissue for comparison. Although the brain organisation of humans and mice are similar, anatomical and cellular differences are more apparent (Simeonova and Huillard, 2014). Anatomically the most striking difference between the human and mouse brain is the structure of the neocortex. Within the mouse brain, the neocortex is smooth and only covers the top of the brain, whereas the human neocortical surface covers the entire brain and has many folds (or sulci). Within the folds there are several subclasses of astrocytes, whose function is currently unknown (Simeonova and Huillard, 2014). On a cellular level, the astrocytes present in the human brain are larger, more complex and signal considerably faster than that of the mouse. This explains how humans

are able to process complex information faster than rodents (Oberheim *et al*., 2009).

These differences may result in alterations in CNS invasion and persistence within the rodent model compared to human infections but it is difficult to predict to what extent. Regardless of these issues, the use of predictive mouse models have provided information about the relationship between CNS and parasites that would of otherwise remained a mystery.

1.4 Drug discovery and development

Inefficiency and resistance of drugs are not the only factors preventing control and elimination of HAT. One of the major problems with the drugs currently used in HAT treatments are their availability and costs to the poorer rural towns in Africa. The complex and prolonged treatment regimens for the drugs, force the overall cost of treatment to levels that could never be afforded in the disease endemic areas (DEAs). A campaign led by the WHO is currently in place to ensure that much-needed drugs are available and supplied to the DEA. This has been achieved by the public-private partnership (PPP) of Bayer and Sanofi with the WHO to donate and distribute the anti-trypanosomal drugs. The campaign was first set up in 2001, initially for 5 years and was continually renewed based upon evidence that the number of patient cases have continued to decline since its inception (Simarro, 2011).

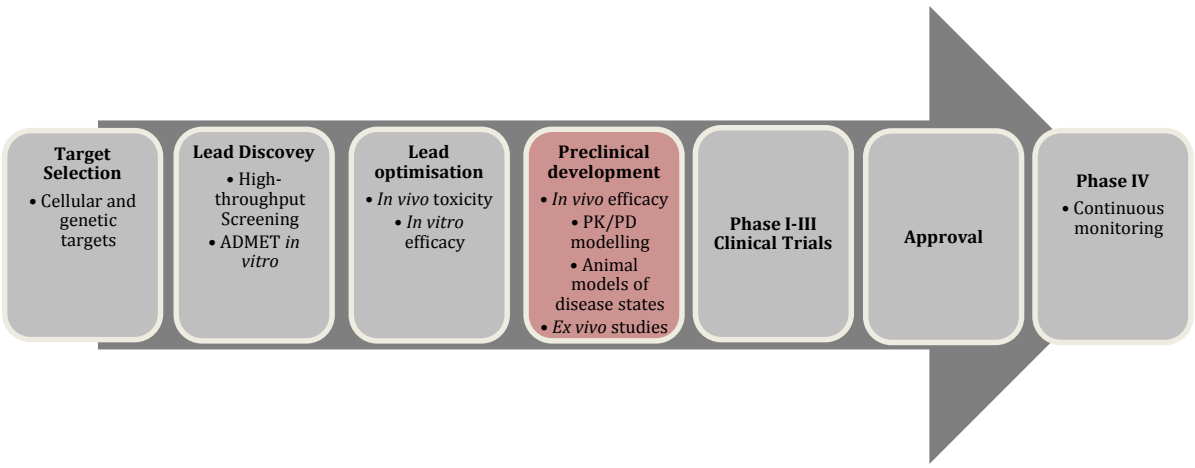

Figure 1.8 Process involved in drug discovery. It can take an average of 12 years for a new drug to enter the pharmacy. Preclinical development (highlighted in red) is the area where discoveries made in this project will be most beneficial.

Whilst the access to free treatment has markedly improved the availability of drugs, the number of cases being reported, by no way detracts from the need to develop new chemotherapies, as resistance is slowly emerging in the small number of drugs available. But without the full understanding of the parasite and pathology of the disease, new drugs are difficult to discover and therefore a switch in research to understand both parasite and pathology becomes paramount in drug discovery, which can be achieved by using animal models to reproduce infections.

1.4.1 Importance of pharmacokinetics and pharmacodynamics

Within drug development, efficacy of a new compound to the pathogen is only part of the challenge. By understanding the pharmacology of a compound at early stages of development, a more effective approach to drug research and development can be achieved.

Pharmacological studies look at two important factors; (i) the effect the host has on the drug (pharmacokinetics, PK) in terms of its absorption, distribution, metabolism and excretion (ADME), and (ii) the effect the drug has on the host/pathogen in terms of its drug action (pharmacodynamics, PD) (Drusano, 2004).

Establishing the PK-PD relationship of a new drug determines the interactions between the drug's potency, its exposure in target tissue (in the case of late stage HAT, the brain) and also the length of time the tissue is exposed to the drug to ensure cure (Wring *et al*., 2014).

Whereas previously the study of PK-PD usually occurred towards the end of pre-clinical trials when potency of a drug is established, by using PK-PD predictive models at early stages of drug development we can determine if the plasma (central compartment) and target tissue (peripheral compartment) concentrations of the drug are at a relevant therapeutic level to render cure (Wring *et al*., 2014).

PK-PD predictive models determine optimised dosing regimens that enable the minimum inhibitory concentration (MIC) of the drugs to be maintained in tissue. This is carried out by assessing the total drug exposure over time (calculated by the area under the curve, AUC) and ensuring that levels are above the MIC (Fig. 1.9).

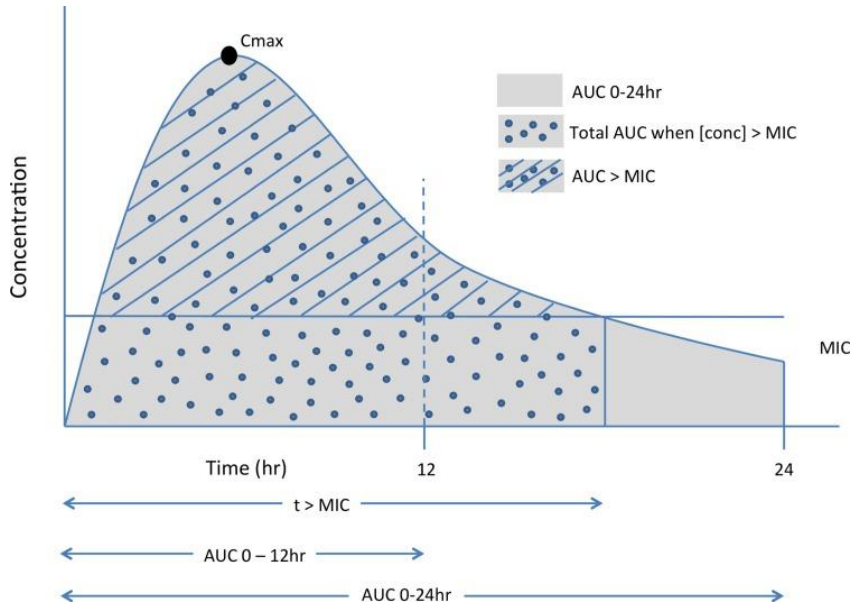

Figure 1.9. PK-PD relationship of drug concentrations against time. For a drug to kill a pathogen it needs to remain above the MIC in the target tissue for an extended period of time. The C_{max} is the maximum concentration of drug after a single dose Source (Wring *et al*., 2014).

The determination of the MIC is normally obtained from a static inhibition assay after a set period of time (frequently used trypanosome assays is 72 hours). The methodology to determine the AUC/MIC relationship has been the most commonly used and well established, but it fails to take into consideration protein binding, tissue distribution and kill-rate of the drug. By also assessing the C_{max}/MIC it is possible to look at how the maximum concentrations obtained after a single dose can alter the efficiency and rate of pathogen death.

Using a dynamic predictive model in combination with the AUC/MIC and/or C_{max}/MIC models we can gain a greater understanding of the relationship between time and concentration of drug. This can also be achieved with *in vitro* time-kill assays where the rate of kill of a drug can be assessed to be either concentration or time dependent (Mueller *et al*., 2004).

The penetration of drugs entering the CNS is restricted due to the highly specific BBB, with many drugs being denied access or encountering a slow diffusion (water soluble drugs) through the tightly linked endothelium, whereas lipid soluble drugs are able to move rapidly into the brain through passive diffusion and would therefore provide rapid concentrations after dose (Wring *et al*., 2014). Assessing the plasma and brain concentrations of drugs in infected and uninfected mice can establish the proportion of dose that is able to pass through the BBB, and whether that differs in an infected host. As detailed earlier, some CNS infections can cause an increase in permeability in BBB, which will allow a larger proportion of drug to enter which is important to establish for dose ranging purposes.

By confirming tissue distribution, dose-ranging properties through AUC/MIC, protein binding and time-kill in early stages of drug development, long lengthy *in vivo* efficacy studies can be avoided in potential failure compounds. Most PK-PD studies can be carried out *in vitro* or in uninfected mice, making them easily achievable in most laboratories.

1.5 Bioluminescence Imaging

The method of bioluminescence imaging (BLI) has become a powerful tool in monitoring real-time infections in a single animal.

BLI is based on the emission of light in the visible-spectrum (Fig. 1.10) produced by a luciferase-catalysed reaction. The emitted photons are then detected by a charge coupled device (CCD) camera, which is able to convert the light photons to electrons (Sadikot and Blackwell, 2005).

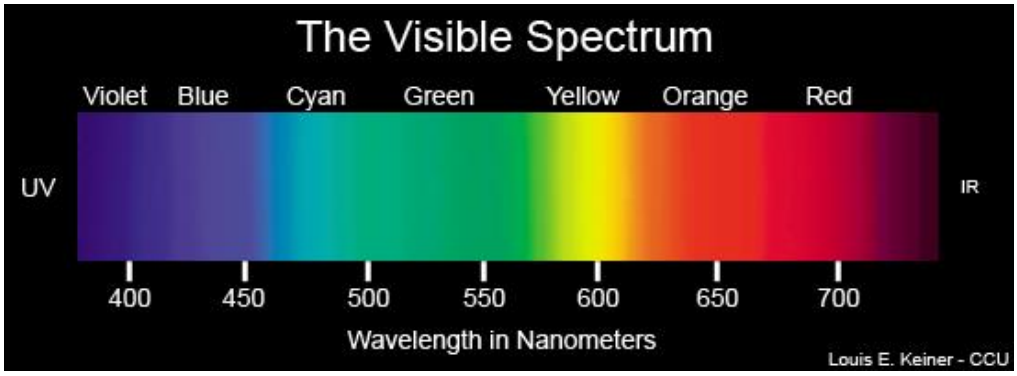

Figure 1.10 The visible spectrum. The human eye is able to see electromagnetic radiation (light) from wavelengths 390-700 nm. (http://myweb.rollins.edu/jsiry/Biophysical.html)

The naturally-occurring luciferase enzymes involved in the genetic manipulation of pathogens or (for some studies) mice, can be obtained from a number of different sources including; (1) bacteria *Vibrio fischeri* and *Vibrio harveyi* (bioluminescent marine bacteria). (2) the jellyfish *Aequorea.* (3) insects such as the North American firefly (*Photinus pyralis*) that produces the firefly luciferase FLuc and the click beetle (*Pyrophorus plagiophthalamus*) producing click beetle luciferase, CBR. (4) the sea pansy (*Renilla reniformis*) which produces the *Renilla* luciferase, RLuc (Sadikot and Blackwell, 2005). The most widely used reporters are RLuc and FLuc.

The benefit of using bioluminescent rather than fluorescent reporters, is that bioluminescence has a very high signal-to-noise ratio which allows the system to be very sensitive due to the lack of intrinsic bioluminescence. Unlike fluorescence, bioluminescence does not require excitation, which results in negligible background signal (Keyaerts *et al*., 2012). For the luciferase reporters to emit light, a luciferase-catalysed reaction is required, but the substrate needed depends on the reporter. RLuc requires the presence of the substrate coelentrazine and oxygen to produce light in the blue region of the spectrum at 480nm. For FLuc, the substrate D-luciferin in addition to oxygen and ATP is needed to produce light in the green area of spectrum at 562 nm (Taylor and Kelly, 2014). Both substrates are not produced by mammalian cells and therefore require them to be added (or injected) prior to imaging (Hutchens and Luker, 2007).

Bioluminescent transfected lines can be used *in vitro* and *in vivo*, providing a range of research opportunities. By using opaque tissue culture plates, spectrophotometers with the ability to detect bioluminescence can be used for fast, highly sensitive assays. However, with the advancements in technology over the last decade whole animal bioluminescence *in vivo* imaging has become affordable and groundbreaking for many inaccessible, difficult areas of research (Fig 1.11) (Sadikot and Blackwell, 2005).

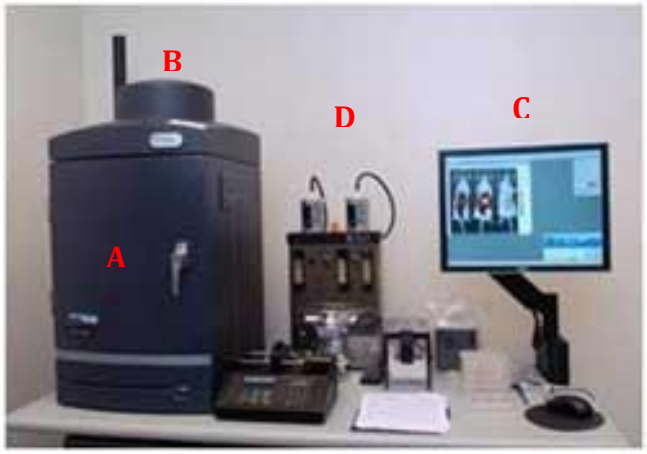

Figure 1.11 *In vivo* imaging system. The IVIS Lumina is a light-tight box (A) with a super-cooled CCD camera mounted above (B). The super-cooling and light-tight box reduces the background noise to negligible quantities allowing highly sensitive imaging to take place. The camera is controlled by a computer that carries out image acquisition and analysis (C). An inhalation anaesthesia unit (D) provide a slow pump of iso-flourane into the chamber allowing the animals to be safely imaged with minimal stress and fast recovery.

Photographs of the animals are first taken and a bioluminescent image overlaid. The bioluminescent image is a heat-map scale, with areas of high bioluminescence signal (high photonic output) represented in the red area of the scale (Fig. 1.12). Without specialised software the images are purely qualitative, indicating areas of high luminescence emitting cells. The software is able to quantify the signal as the number of photons per second of exposure in a region of interest (ROI).

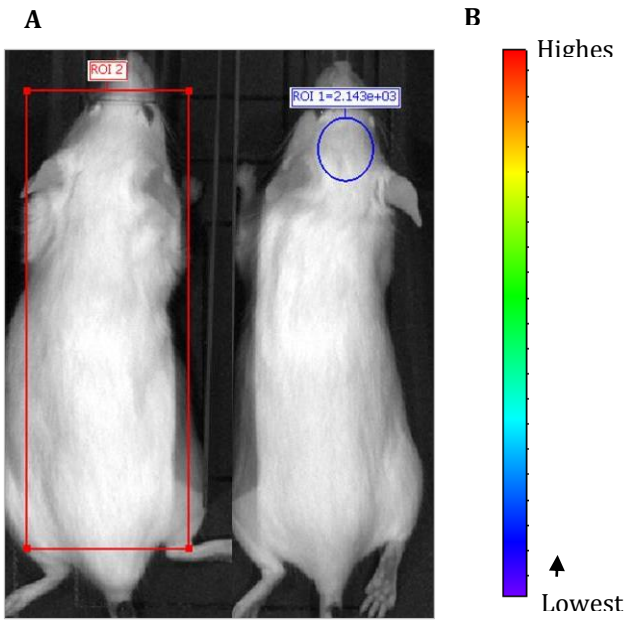

Figure 1.12 BLI analysis and heat map scale (A) the bioluminescence can be quantitated and therefore compared by analysing the same size of area animal on each acquired image. (B) The heat map scale indicating high photonic signal in red and low signal in blue. The scale ranges can be altered at analysis stage using imaging software. Depending on the ranges and strength of bioluminescent strains, two scales maybe needed during the course of an infection (showing low infection and high infection) or a logarithmic scale can be used.

1.5.1 Limitations

As with all technologies there are limitations to BLI but advances have been made to try and overcome some of the restrictions.

The catalytic reaction requires all factors to be present, oxygen, substrate and (in the case of FLuc) ATP. If any of these are not present in large quantities or if the substrate is not uniformly distributed throughout the animal after administration, light emission may not be a true representation of bioluminescence activity (Badr and Tannous, 2011). For example, coelentrazine has shown poor distribution and difficulty in crossing cellular membranes which would provide a false representation of bioluminescent cells (Hutchens and Luker, 2007). D-luciferin however, has been shown to distribute throughout the mouse and is able to penetrate blood-tissue barriers. It can also be administered via a number of dosing route, but intraperitoneally (i.p.) is often chosen for ease of use, but does not affect the level of signal produced, reaching a plateau at 10 minutes post administration (Keyaerts *et al*., 2012).

The transmission of light through tissue is wavelength dependent and is one of the biggest problems with BLI. Tissue absorption is at its highest when bioluminescence at the lower end of the spectrum is used. This is due to an increase in light scatter at the shorter wavelengths. In addition to this haemoglobin is a chromaphore that absorbs light in the 420 - 550nm part of the spectrum (blue-green), resulting in poor signal intensity (Fig 1.13.)

To avoid high levels of tissue absorption, reporters that emit light above 600nm are best to use. By genetically manipulating the reporters, a "red-shifted" FLuc has been produced known as PpyRE9, which emits light at a maximum of 617nm (Branchini *et al*., 2010).

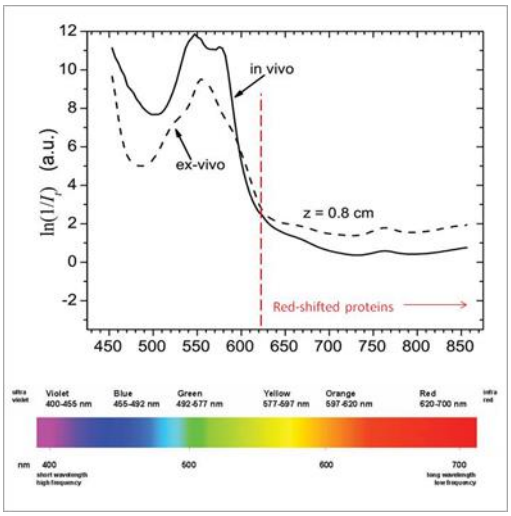

Figure 1.13. Tissue absorption in *in vivo* imaging. A reduction in tissue absorption is seen with bioluminescent reporters producing light above 600nm (Source: Adapted from (Deliolanis, 2008).

1.5.2 Bioluminescence models of infectious disease

Prior to the development of new technologies, the study of host-pathogen interactions and the progress of infections involved the euthanasia of vast numbers of experimental animals at multiple time points to determine pathogen burden. The conventional method provided many limitations, the spread of pathogens to tissues and organs could not be effectively monitored without invasive measures, the course of infection could not be traced within an individual animal for an entire experiment and the setting of multiple time points may miss certain infection events.

The development of BLI addressed these limitations and enabled researchers to gain a more rounded understanding of infection processes in different pathogens. The engineering of bioluminescent strains has been carried out in viruses, bacteria, yeast, and protozoa. Here, we briefly detail the advancements in bioluminescence protozoa models over the last decade.

Bioluminescence models have been developed for *Toxoplasma gondii* to study virulence between strains, infection susceptibility after immune manipulations (various toll-like receptor knock-out mice), as well as reactivation of parasites during a chronic infection (Hitziger *et al*., 2005, Saeij *et al*., 2005). The models all express FLuc, emitting light in the green part of the spectrum, which affect the depth of tissue imaging possible, nevertheless the models have shown that the manipulation of *T. gondii* is possible and that BLI can be used to further investigate the pathology (Hutchens and Luker, 2007).

The parasite responsible for cutaneous Leishmaniasis, *L. amazonensis,* has been successfully manipulated to produce a firefly bioluminescent model of infection. The model has been predominantly used in cell culture for drug therapy evaluation, but it has also provided information on parasite burden in excised organs from mice (Lang *et al*., 2005).

To gauge a better understanding of malaria, the rodent malaria strain *Plasmodium berghei* was engineered to express the firefly luciferase by Franke-Fayard *et al*. The strain was able to provide bioluminescence in all parasite life stages, they were able to locate iRBCs (infected with schizonts) sequestered in the microvasculature of the lung and also adipose tissues (Franke-Fayard *et al*., 2005). Due to the complete lifecycle being able to express the bioluminescence, closer investigations can be carried out to understand the parasites interactions at each stage and monitor pathogenesis in the host.

Chagas disease (*Trypanosoma cruzi*) has been difficult to study in animal models due to the lengthy experimental times (often up to six months), the lack of circulating extracellular trypamastigotes and the sub patent parasitaemia means that parasite burden is difficult to determine. Hyland *et al* developed a transfected

strain of *T. cruzi* that utilised the FLuc reporter expressing light in the blue-green spectrum. Whilst this model was able to demonstrate the dissemination of the *T. cruzi* infection throughout the mouse model, the level of bioluminescence was very low, which would cause potential issues when dealing with drug therapy analysis and imaging parasites deep within tissues (Hyland *et al*., 2008).

To overcome the restrictions with this model, Lewis *et al* developed a new bioluminescent strain of *T. cruzi* using a red-shifted FLuc. This model provided a greater sensitivity and tissue penetration due to the longer wavelength of 617nm (Lewis *et al*., 2014a). The greater sensitivity has also enabled the model to be used as a drug evaluation model for the chronic infection as relapse can be detected (Lewis *et al*., 2014b).

Other *Trypanosoma sp.* that has benefited from the development of BLI are those responsible for African trypanosomiasis. Claes *et al* were the first to develop a *T. b. brucei* bioluminescence imaging model expressing *Renilla* luciferase (emits light at 490nm, purple-blue), in both a monomorphic and pleiomorphic strain (Claes *et al*., 2009). Limitations with the model included the use of coelentrazine (as mentioned earlier) having a poor distribution around the body and is chemiluminescent resulting in high background bioluminescence. The *Renilla* produces light within the blue part of the spectrum which is largely absorbed by the tissues within the mice, making deep tissue imaging difficult (Taylor and Kelly, 2014).

An advancement on the model was made by the University of Glasgow with a FLuc transfected line *T. b. brucei* GVR35 LUC2 emitting light in the green spectrum at approximately 500nm. By using the D-luciferin substrate a uniform distribution occurred, reducing the problems with luciferase-substrate reaction. In addition to the substrate issues, the sensitivity was increased as a longer wavelength than the *Renilla* was emitted and the model was successful in determining drug relapse (Myburgh *et al*., 2013). However, based on figure 1.12 the level of tissue absorption is still an issue at these wavelengths, resulting in the possibility of residual parasite being present but not detectable using the current BLI model.

The development of an African trypanosomiasis bioluminescence imaging model utilising red-shifted proteins would enable a model to be produced that could detect drug relapse earlier. This would result in the length of experiment being

reduced, as the signal would be detected before peripheral parasitaemia is measurable. Ultimately this would enable a more efficient method of analysing drug efficacy.

CHAPTER 2: Materials and methods

2.1 Parasite culture

T. b. brucei Lister 427, isolated from cattle in Tanganyika (now Tanzania) in 1956 was transferred to the Lister institute in London where it underwent serial syringe passage, was provided by Dr. Martin Taylor, LSHTM. *T. b. brucei* GVR35 WT/Cl.1, isolated in 1966 from a wildebeest in the Serengeti (Tanzania), was provided by Dr. Jean Rodgers, University of Glasgow.

Frozen monomorphic strains (WT and transfected 427 lines) were fast thawed to room temperature (RT) and added to 9ml of modified HMI-9 media in a filter-top culture flask. Modified HMI-9 media (Hirumi and Hirumi, 1994) in powdered form (Invitrogen, UK) was re-suspended in dH_2O supplemented with 10% v/v heat-inactivated foetal calf serum, hi-FCS (Gibco, Life Technologies, UK) and 0.3% w/v sodium bicarbonate (Sigma Aldrich, UK). Parasites were monitored via haemocytometer counts 24 hours later and the HMI-9 media changed. Parasites were counted and passaged every 2-3 days.

The pleiomorphic strains (WT and GVR35 transfected lines) were thawed as above and cultured in modified HMI-9 with the addition of sterile 0.01% w/v methyl cellulose (Sigma, UK). Due to the pleomorphic nature and slower growth of GVR35 a lower parasitaemia needed to be maintained, passaging every 2-3 days at approx. 2×10^4 trypanosomes/ml, to ensure the culture did not differentiate into the stumpy (non-replicating) form.

2.2 Cryopreservation of trypanosomes

Parasite morphology (in the replicating stage, slender) was examined by microscopy and parasitaemia was determined. The cells were mixed with a freezing buffer to protect the parasites. The total stabilate produced contained 8% glycerol (Sigma, UK), 20% hi-FCS and 72% of media (or blood) containing parasites. Parasites were aliquoted and slowly frozen at -80°C using a Mr. Frosty™ Freezing container (Nalgene, UK), before being transferred to liquid N_2.

2.3 Construct development and transfection

The pTb-AMLuc construct (McLatchie *et al*., 2013) containing the red-shifted firefly luciferase gene PpyRE9H (Branchini *et al*., 2010) was designed to integrate into the ribosomal RNA locus to provide strong RNA polymerase 1 – mediated transcription, resulting in high levels of expression (for further details see McLatchie *et al*., 2013). The construct was transfected into *T. b. brucei* 427 and GVR35 strains using the protocol described by Burkard *et al* 2007(Burkard et al., 2007) by A. McLatchie. Parasites were selected with puromycin (1 µg/ml). The transfections produced the following strains.

***T. b. brucei* strain**	**Transfected line**
427	VSG - 4, 5, 10, 17 and 20
GVR35	VSL – 1, 2, 4, 8, 21, 22, 29, 40, 42, and 51

Table 2.1 *T. b. brucei* strains produced from transfection with pTb-AMLuc construct

2.4 Bioluminescence assessment *in vitro* of transfected strains

Parasites were pelleted at 1000*g* for 10 minutes, washed once in Phosphate buffered saline (PBS) and then lysed in CCLR (cell culture lysis reagent) buffer (Promega, UK). The luciferase activity was assessed using the Promega Luciferase assay kit (Promega, UK) and the bioluminescence read on the Spectramax plate reader (Molecular Devices) at 610 -620nm.

The transfected lines that produced high bioluminescence and performed well *in vitro* were selected for further investigation *in vivo.*

2.5 *In vivo* validation

2.5.1 Mice

Female CD1 mice in weight range of 20-25g (Charles River, UK) were housed in groups no larger than five in specific pathogen-free individually vented cages, and were fed *ad libitum*. All work was carried out under the approval of the UK Home Office Animals (Scientific Procedures) Act 1986, Project Licence PPL 70/6997, and the London School of Hygiene & Tropical Medicine AWERB (Animal Welfare and Ethics Review Body). ARRIVE guidelines are followed in this report (Kilkenny *et al*., 2010).

2.5.2 Infection of passage and experimental mice

A frozen stabilate was thawed and trypanosomes diluted to $2x10^4$ in phosphate buffered glucose saline (PBS-G) pH 8.0 as described (Jennings *et al*., 2002). The diluted trypanosomes were injected into donor mice by the intraperitoneal route (i.p.).
Peripheral parasitaemia was monitored via blood films and after approximately 5-7 days post-infection (p.i), mice were culled via cardiac puncture and blood collected.

Experimental mice were infected as per Kennedy *et al* with minor modifications (Kennedy et al., 1997). From a donor mouse (detailed above), 2 x 10^4 trypanosomes/mL were diluted in PBS-G as described (Jennings *et al*., 2002) and injected by the intravenous (i.v) route. Mice were then randomised into groups of 6 (2 cages of 3 mice).

2.5.3 *In vivo* bioluminescence imaging

Infected mice (detailed in 2.4.2) were monitored every 7 days via blood microscopy and by whole animal imaging (all VSL-2 mice and a control group of WT mice). Luciferase substrate D-luciferin was administered i.p at 150 mg/kg (Perkin Elmer, UK diluted in Dulbecco's Phosphate Buffered Saline) and after 10 minutes (see appendix 1 for luciferin kinetics), imaged using a standard set of exposure times in an IVIS® Lumina II (Perkin Elmer, UK) under anaesthesia (2% isofluorane/O_2 mix at 2.5 L/min). All images were acquired using the following exposure times; 1, 3, 10, 30, 60 and 180 seconds, with medium binning, 1 f/stop and an open filter, and field of view E (12.5 x 12.5 cm).
To confirm CNS infection, *ex vivo* imaging of perfused brains was performed. After whole animal imaging, mice were culled via cardiac puncture under terminal anaesthesia, and the blood was mixed with a chaotropic salt (6M guanidine HCl-2M EDTA) in a 50/50 solution and stored at 4°C for DNA extraction and qPCR (see 2.6). Mice were then perfused with 20 mL of 1% D-Luciferin in PBS via the heart. The brain was then excised and transferred to a Petri dish. Prior to imaging, 50 µL of 15 mg/mL luciferin was pipetted onto the brain and imaged using the settings as above. All images were analysed using Living Image® software as detailed in 2.5.4.

After imaging the brains were snap frozen on dry ice and stored at -80°C for DNA extraction and qPCR.

2.5.4 Quantification of bioluminescence

Bioluminescence was quantified using the region of interest (ROI) with Living Image® v.4.2 software (Perkin Elmer) and corrected for background bioluminescence.

The ROI was determined by removing the signal from the image and a rectangular ROI (for whole animal quantitation) was positioned on the image to cover (as close to, due to varying size) tip of the nose to base of the tail of the mouse. The same size box was used for every animal and every time point. When looking at the ROI for the brain a circular ROI was used in the same way, positioning it where the brain would be (see figure 2.1).

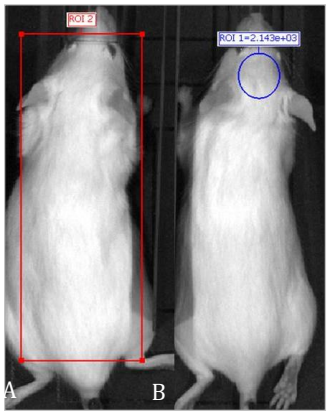

Figure 2.1. ROI calculation for both whole animal (A) and brain (B)

2.6 Real-time quantitative PCR to determine parasite load.

Real-time quantitative PCR was used to determine parasite load of *T. b. brucei* GVR35 (WT and transfected lines) in cardiac blood and perfused brain material, using a primer sequence to target the invariant surface glycoprotein (ISG-75). Primer sequence was designed by Dr. Eleanor Barnwell by determining a gene present in trypanosomes and not mice (using GeneDB and checking in BLAST, Basic Local Alignment Search Tool), and supplied by Sigma Aldrich, UK.

DNA was extracted from whole brain homogenate and cardiac blood using Roche High Pure PCR template kit according to manufacturer's instruction (Roche UK) and quantified by spectrophotometry on a Nanodrop ND1000 instrument (Thermo Scientific, UK).

Standards for the gene ISG-75 were generated by conventional PCR from *T. b. brucei* GVR35-derived cDNA, followed by purification using the QIAquick PCR purification kit (Qiagen, UK,). Copy numbers were calculated based on the fragment length, and standards were used in subsequent assays to generate standard curves ranging from 10^8 copies to 10 copies/reaction. The levels of ISG-75 in the indicated samples were measured by real-time quantitative PCR using SYBR® Green (Applied Biosystems) incorporation in an ABI Prism 7000 sequence detection system (Applied Biosystems) relative to the standard curve. Each reaction was performed in duplicate with 4 µL DNA, 10 µL SYBR® Green master mix, 0.2 µL each primer (final concentration 200 nM), and 5.6 µL water, to produce a reaction volume of 20 µL. PCR conditions were 10 min 95°C denaturation step, followed by 40 cycles of 95°C: 15 s/60°C: 1 min/72°C: 1 s.
Primer sequences were: ISG FW: 5'-TTGCTGATAAAGTTGCAGAGGA .3', and

ISG RW: 5' – CAACTCGAACTCTATATAACCAGCA-3'

2.7 *In vivo* drug efficacy and relapse evaluation

Mice (as detailed in 2.5.1) were infected with *T. b brucei* GVR35 WT and VSL-2 as described in 2.5.2. A CNS control group treated with analytical grade diminazene aceturate, DA (Sigma-Aldrich, UK) at 40 mg/kg intraperitoneally (i.p), which clears peripheral parasitaemia, a drug-treated positive control group of melarsoprol treated mice with 15 mg/kg i.p for 3 days and a negative control group of untreated infected mice, was included for both strains. Mice were randomised into groups of six with a single group per drug/dose.
Details of drugs and administration is detailed in table 2.2 and drug structures can be found in Figure 2.2

Drug	Source	Dose (mg/kg)	Carrier	Route	Duration (days)
Melarsoprol	Sanofi, FR	10, 6, 3, 1	IV formulation consisting of 10% v/v 1, 3-Dimethyl-2-imidazolidinone (Sigma Aldrich, UK), 10% v/v 1-Methyl-2-pyrrolidinone (Sigma Aldrich, UK), 35% v/v propylene glycol (Sigma Aldrich, UK) and 45% v/v 50 mM glycine/HCl (Sigma Aldrich, UK), which was then diluted to 10% v/v in 5% dextrose solution	i.v	4
Fexinidazole	Sanofi, FR	200, 66.7, 22.2, 7.41	Oral formulation 0.5% w/v Methylcellulose (Sigma, UK) and 5% v/v Tween 80 (Sigma, UK) dissolved in sterile H_2O.	p.o (oral)	5
DFMO	Sanofi, FR	1000, 800, 400, 200	Dissolved in sterile physiological saline (0.9% w/v sodium chloride; Sigma, UK)	i.v	4
Nifurtimox	Bayer Schering, DE	200	Oral formulation 0.5% w/v Methylcellulose (Sigma, UK) and 5% v/v Tween 80 (Sigma, UK) dissolved in sterile H_2O.	p.o	4
Diminazene aceturate	Sigma Aldrich	40	Dissolved in sterile dH2O	i.p	1

Table 2.2 Drug doses and formulations

Mice were monitored via imaging and blood films (from the tail vein) every 4-5 days until D35. At D35 mice were culled and qPCR analysis carried out on blood and brain samples to determine parasite burden as detailed in 2.6.

To assess relapse, two doses (10 mg/kg and 6 mg/kg) of melarsoprol were used and, following the same protocol described above, mice were infected and dosed. Mice were imaged and blood filmed (from the tail vein) every 7 days from D35 to D180. Mice were culled when humane endpoints (weight loss >20% total body weight, reluctance to move or feed for > 4-6 hrs and/or hind-leg paralysis) of the experiment were reached.

2.8 Pharmacokinetic studies

To assess the concentration of melarsoprol and the qualitative PK profile of fexinidazole present in the brain and plasma, pharmacokinetic studies and analysis were carried out in collaboration with Dr. Hatem Sallam and Dr. Andy Harris at Pharmidex, UK on samples prepared by the author using LC-MS/MS.

2.8.1 *In vivo*

Groups of 3 mice per time point were infected with VSL-2 as detailed in 2.5.2. An additional group of 3 mice per time point were used as uninfected controls. At D24 p.i, a single dose of melarsoprol or fexinidazole (10 mg/kg and 200 mg/kg respectively) was administered to both uninfected and infected mice (see table 2.2 for formulation). At certain time points (see figure 4.7, p 94 and figure 6.6, p 120) mice were culled via cardiac puncture (collecting a minimum of 500 µl of blood) under terminal anaesthesia, and plasma was collected by centrifugation of heparinized blood at 2000 *g* for 10 minutes. The plasma was then snap frozen on dry ice and stored at -80°C. Perfused brains (with PBS via the hepatic portal vein) were also collected (as detailed in 2.5.3), snap frozen on dry ice and stored at -80°C.

2.8.2 Drug extractions from brain tissue

Brains were weighed and 0.1% v/v formic acid was added at a weight : volume ratio of 1:1 into 1.5ml SuperLock Microcentrifuge tubes (StarLab, UK). Then 4-5 1.0 mm zirconium oxide beads (Next Advance, UK) were added and the tube was placed in a Bullet blender BBY5E (Next Advance, UK) for 5 minutes at speed 8.
In a clean microcentrifuge tube, 50 µl of homogenised brain was added to 150 µl of extraction buffer (containing internal standard tolbutamide) provided by Pharmidex. The tube was vortexed for 1 minute and further centrifuged at 3000 *g* at 4°C for 20 minutes. The supernatant was then collected and stored at -20°C for further analysis by LC-MS/MS at Pharmidex (see 2.8.4).

2.8.3 Drug extractions from plasma

For drug extraction 50 μl of plasma was added to 150 μl of extraction buffer in a clean microcentrifuge tube and vortexed for 1 minute. The tube was then centrifuged at 3000 *g* at 4°C for 20 minutes. The supernatant was then collected and stored at -20°C for further analysis by LC-MS/MS at Pharmidex, UK.

For melarsoprol, a standard curve was generated for both plasma and brain samples using a serial dilution of melarsoprol. The dilutions were added to homogenized brain or plasma of an untreated mouse and extracted as detailed above.

2.8.4 Pharmacokinetic analysis

The drug extractions were analysed using an Agilent 1200 HPLC and auto sampler combined with an Agilent 6410A triple quadrupole mass spectrometer (Agilent Technologies, UK). All work was carried out at Pharmidex, UK by Dr. Hatem Sallam and Dr. Andy Harris.

2.8.5 Melarsoprol binding assays

The free fraction of melarsoprol in plasma and brain tissue was determined by Rapid Equilibrium Dialysis. Using a dual compartment well separated by a dialysis membrane, melarsoprol-spiked plasma or brain homogenate was loaded into the first compartment (bound) with PBS placed in the other (free). The well was sealed and incubated at 37°C on an orbital shaker for 4 hours to achieve equilibrium between the two compartments. After incubation, the samples underwent extraction (as described in 2.8.3) and the concentration of melarsoprol was quantified using LC-MS/MS with the results expressed as either % bound or free.

2.9 Data analysis

All data was analysed using Microsoft© Excel and GraphPad Prism® v.6.02 for statistical analysis (see figures for tests used)

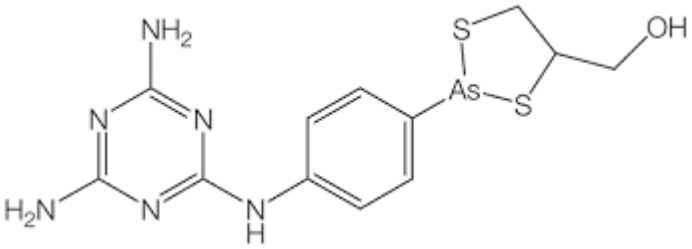

Melarsoprol

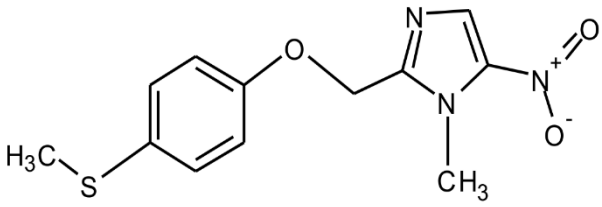

Fexinidazole

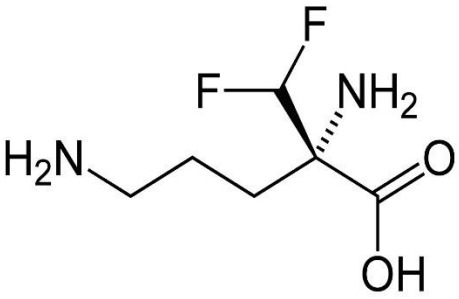

Eflornithine, DFMO

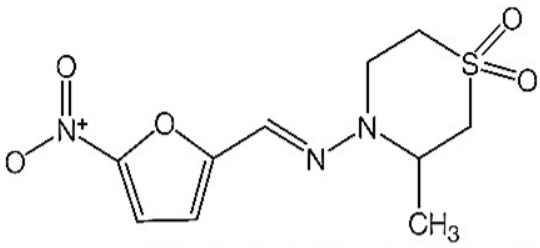

Nifurtimox

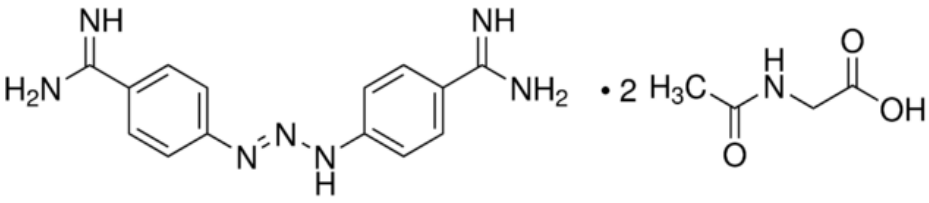

Diminazene aceturate

Figure 2.2 Drug structure of current anti-trypanosomals.

CHAPTER 3: Development of *T. brucei* bioluminescence imaging model

3.1 Introduction

Currently, mouse models involved in HAT drug development are used either for the early stage of the infection, using the monomorphic line *T. b. brucei* Lister 427 (or a derivative), or for the late stage, using the 'gold standard' pleiomorphic strain *T. b. brucei* GVR35 (Jennings, 1977).

One of the first *T. brucei* strains to be maintained within the axenic culture method developed by Hirumi was *T. b. brucei* 427 (Hirumi *et al*., 1977).
Lister 427 was first isolated from cattle in Tanganyika in 1956, and was transferred to the Lister Institute in London where it was serially passaged through mice for 15 passages before being frozen at -70°C (Claes *et al*., 2009).
The strain *T. b. brucei* 427 is a well-defined monomorphic line and remains solely as the bloodstream form (BSF) of the parasite (Cui *et al*., 2008). The parasites have the characteristic long and slender form, and produce high parasitaemia both *in vitro* and *in vivo.* 427 adaptation to *in vitro* culture has made it an invaluable tool in molecular biology (Claes *et al*., 2009).

The use of *T. b. brucei* 427 has not been limited to genetic studies; its rapid infection rates meant it was quickly adopted into drug discovery programmes.

The development of a colorimetric assay utilising the substrate resazurin, (or its commercial counterpart Alamar blue®), resulted in the strain being widely used in initial drug screens *in vitro* to determine drug efficacy against BSF (Raz *et al*., 1997). The *in vitro* assay could determine inhibitory concentrations (IC_{50} and IC_{90}) within three days, providing a huge breakthrough in the first stages of drug discovery programmes, by ascertaining whether the compound was active against the trypanosome. However, the substrate requires an incubation time of approximately six hours, which has limited the use of the assay for anything other than endpoint studies. Time-kill evaluation of drugs can only currently be carried out by manually counting parasites, especially if short time points are being determined (under six hours for example).

With access to an easily cultured BSF of *T. b. brucei*, other areas of the infection could be investigated further, such as the parasites ability to switch its variable surface glycoprotein (VSG) to evade host immune defenses (Claes *et al*., 2009). The strain is also easy to genetically manipulate by the insertion or deletion of certain genes. This methodology has been used in the study of RNA interference (RNAi), to discover new drug targets and resistance (Kristensson *et al*., 2013, Jayakumar *et al*., 2013).

As discussed in chapter one, 427 is also infectious to mammalian hosts (rodents) but remains within the first stage of the disease. This has made the strain ideal as a model for the study of the acute stage of infection and drug evaluation, especially as it is non-infective to humans therefore making it a safer alternative to *T. b. rhodesiense* (Finsterer and Auer, 2013). But *T. b. brucei* 427's monomorphic nature and inability to invade the CNS is the most limiting factor in terms of mimicking the infection of African trypanosomiasis.

The pleiomorphic strain *T. b. brucei* GVR35 was isolated from a wildebeest in 1966 in the Serengeti and further developed by Jennings *et al* in the 1970s to study drug therapies of late-stage infection (Jennings, 1977). The line can be easily cultured *in vitro* but grows at a slower rate than Lister 427 requiring a different culture technique, as the parasites require passaging more frequently to ensure the dividing population remains in culture (slender). Culturing at a lower density also prevents the trypanosomes from becoming stressed, therefore transforming to the stumpy form (Myburgh *et al*., 2013).

The development of the reproducible CNS model for trypanosomiasis using GVR35 in outbred immunocompetent mice, was to primarily produce a model for melarsoprol-related PTRE (post-treatment reactive encephalopathy) (Johanson *et al*., 2011). However, the model enhanced the understanding of the late stage, as a CNS infection established 21 days post infection (p.i). This development made it possible to carry out efficacy testing on late-stage drugs, by following a 180-day drug relapse method (Jennings *et al*., 2002).

The prolonged amount of time for follow-up was determined as it is known that trypanosomes can remain in the CNS for extended periods of time, and due to the parasites inaccessibility for quantification (unless the mouse is culled and brain

excised), 180-days allows the parasites to relapse in the blood stream if the drug is ineffective (Pittella, 2013).

The development of a new model that is able to determine infection without the need for parasites to be present in the periphery, or require the culling and qPCR analysis on the extracted brain tissue, could greatly reduce the time, cost and numbers of animals needed to study CNS infection in late-stage trypanosomiasis.

Bioluminescence imaging (BLI) can provide highly sensitive, non-invasive detection of parasite distribution in a mouse model that can be followed in a single animal for the entirety of the experiment. An initial bioluminescent model, GVR35-LUC2 used green light-emitting luciferase (wavelength 520nm) expressed in GVR35 was developed to study HAT in a mouse model (Myburgh *et al*., 2013). But with problems of tissue absorption (as detailed in chapter 1) that can occur in the green-shifted bioluminescence, it was decided that a red-shifted model will provide a more sensitive study tool in the study of trypanosomiasis infection.

An optimized pTb-AMluc-v construct integrated with a humanised red-shifted luciferase PpyRE9H that emits light at 617nm (Figure 3.1), was produced by A. McLatchie. The incorporation of the luciferase into the ribosomal RNA produced a high expression of luciferase. This is due to the ribosomal array within trypanosomes containing 10 copies and being well characterised (McLatchie *et al*., 2013). The luciferase was surrounded by sequences that modulated the expression within the trypanosome, as well as a puromycin selectable drug marker. After transfection a clonal population was selected for further analysis (McLatchie *et al*., 2013).

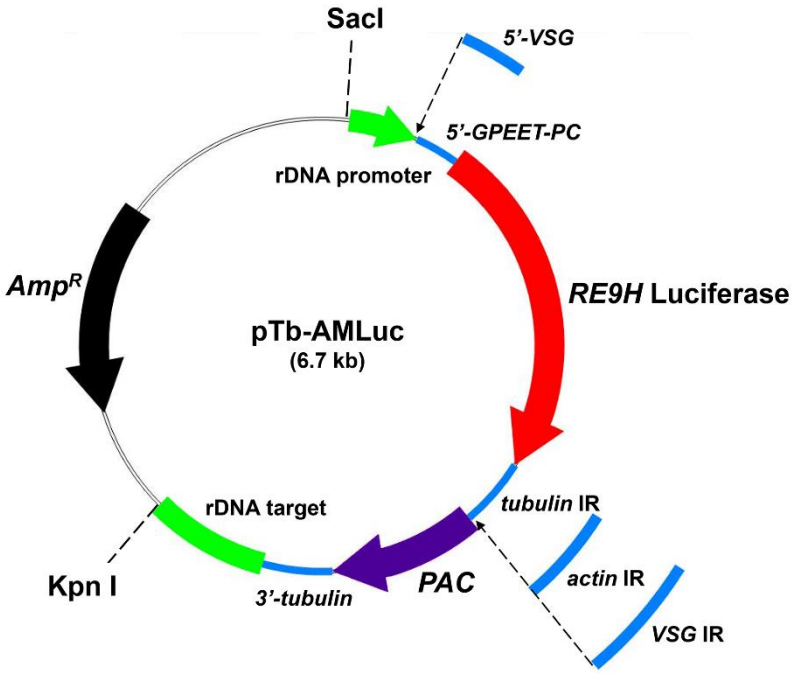

Figure 3.1 pTb-AMluc construct. (McLatchie *et al*., 2013)

As discussed in chapter one, one of the major issues with BLI is with the signal not being detectable in whole body imaging, as well as the instability of the construct within the transfected line.

The ultimate goal is to study bioluminescence during a CNS infection, it is essential that strains have a high intensity signal that can be detected through the skull.

Here, we describe the development of a red-shifted bioluminescence model of African trypanosomiasis integrated with the pTb-AMluc-v construct (McLatchie *et al*., 2013).

3.2 Aims and Objectives

The main aims of this chapter were to develop and validate a red-shifted bioluminescence strain of *T. b. brucei* that is able to produce a signal that can be detected *in vivo*. The two aims were investigated.

1. Using *T. b. brucei* 427 as a proof of principle to assess construct stability within the trypanosome the following objectives were investigated:

- Establish a bioluminescence strain that mimics the infection kinetics of a wild type strain both *in vitro* and *in vivo*.
- Produce a bioluminescence strain with high intensity signal that can be detected in whole animal imaging.

- Determine the correlation between traditional blood film parasitaemia and bioluminescence.

2. Validation of the pleiomorphic line GVR35 with the following objectives were investigated:

- Establish a bioluminescence strain that mimics the infection kinetics of a wild type strain *in vitro.*
- Produce a bioluminescence strain with high intensity signal that can be detected in whole animal imaging and through the skull of an infected mouse.
- The bioluminescence strain will also have the ability to produce a CNS infection that will be visible both in whole animal imaging and *ex vivo* imaging of brain.

3.3 Contributors

The pTb-AMluc-v construct was designed by Dr. Martin Taylor at the London School of Hygiene and Tropical Medicine (LSHTM). The transfections and *in vitro* assessment (growth curves and luciferase activity) were carried out by Alex McLatchie. All *in vivo* experiments were carried out by author including qPCR analysis.

3.4 Results

3.4.1 Growth and bioluminescence of transfected 427

Using the pTb-AMluc-v construct containing RE9H luciferase reporter genes, a number of transfected strains of 427 were produced, using the methodology described (McLatchie *et al*., 2013).

The bioluminescence of 1 x 10^6 trypanosomes/ml of each strain was assessed using the Promega Luciferase Kit and read on a Molecular Devices Spectramax M3 (Fig. 3.2)

Rather than carrying out an endpoint bioluminescence analysis at a single wavelength, the samples were analysed over a spectrum of wavelengths from 550 nm to 750 nm to ensure the transfected red-shifted luciferase was emitting light at the correct and optimal wavelength.

All of the transfected lines peaked at 610 nm. However, the magnitude of bioluminescence emitted differed between the lines.
VSG5 produced the maximum level of bioluminescence at 610 nm, peaking at 22 991 relative luminescence units (RLU), significantly (p-value = 0.046) higher than VSG17 (the next highest performing strain), which peaked at 10 978.9 RLU.

Based on the bioluminescence analysis the top four transfected lines (VSG4, VSG5, VSG10 and VSG17) were chosen, and to ensure the transfection process did not alter the infectivity, the growth rate was assessed against the WT (Fig. 3.3). The cumulative *in vitro* growth of VSG-lines were compared to that of the wild type daily for 10 days, with a starting parasitaemia of (and diluted down to) 1 x 10^5 trypanosomes/ml. Daily haemocytometer counts were recorded and the parasites were diluted back to the starting parasitaemia. Figure 3.3 shows that there is no significant difference in the growth of the transfected lines to that of the wild type, indicating that the infectivity of the strain was not compromised with the addition of the pTb-AMluc construct.
The spectral and growth analysis data provides sufficient evidence that VSG5 is the optimum transfected line to be further investigated *in vivo.*

3.4.2 Evaluation of bioluminescence *in vivo* using whole animal imaging.

To confirm that bioluminescence could be detected *in vivo* and that the strain exhibited the same infection kinetics within an animal host, a 4-day infection was performed (Fig. 3.4). The experiment was also able to determine whether the use of bioluminescence imaging (BLI) can detect trypanosomal infection earlier than the traditional blood film method.
At D1 post infection (p.i), bioluminescence can be seen at the infection site as parasites reside within the intraperitoneal cavity. For three days the bioluminescence remains focal as seen on D1 but steadily increasing in bioluminescence (represented by the yellow and red areas of the heat map scale), and disseminated around the infection site.
At D4 p.i a clear systemic infection can be seen as the signal disseminated throughout the mouse, with a peak area of bioluminescence remaining at the injection site.

The bioluminescence of the entire mouse was quantified using the region of interest (ROI) and compared to blood films detecting peripheral parasitaemia (Fig. 3.5). Despite signal being detected as early as D1 p.i at approximately 10^7 photons/seconds (100-fold higher than the background bioluminescence), no parasitaemia is observed within the blood films. At D2 parasitaemia is detectable, albeit very low, at an average of 10 trypanosomes/10 fields of view (f.o.v).
With an increase in peripheral parasitaemia, the bioluminescence also increased and by D4 p.i the bioluminescence had reached 10^{10} photons/second, and the parasitaemia peaked at approximately 100 trypanosomes/10 fields. At this point the mice were culled due to the monomorphic virulent nature of 427, visible in mice by weight loss and anaemia. The parasites continue to divide until the animal becomes overwhelmed and eventually dies.

The data also showed how bioluminescence has little variance between animals, which is indicated by the narrow error bars seen on the graph. Yet the detection of parasites in the blood had a larger margin of error, which may be due to the objectiveness of the person counting the slides.
A direct correlation analysis of bioluminescence vs. parasitaemia of VSG-5, ascertained that there was a significant positive correlation between the two measurements with an r-value 0.85 and a p-value of <0.0001 (Fig 3.6), indicating that for VSG-5 bioluminescence could be used as a quantitative method.

Based on the success of the integration of the construct into *T. b. brucei* 427 to produce a stable bioluminescence line, the construct was transfected into the pleiomorphic strain *T. b. brucei* GVR35.

3.4.3 GVR35 transfected strain validation

A number of transfected lines were produced and the bioluminescence assessed as detailed in 2.4. The *in vitro* test showed that all the top four transfected lines (Fig. 3.7) produced a bioluminescence signal that was at least 10-fold higher than the *T. b. brucei* 427-VSG5 strain. The top four producing lines (VSL-1, VSL-2, VSL-8 and VSL-21), all produced bioluminescence above 5×10^4 RLUs, with VSL-2 producing the maximum bioluminescence *in vitro* of 2×10^5 RLUs. It is important to note that the assessment of bioluminescence of the lines is by lysing the parasites first

before a catalyst is added to produce the signal. This results in a high bioluminescence signal that is not always indicative of what can be seen in the animal model. In order to determine if the bioluminescence could be detected through live-animal imaging and if the transfected strain was able to produce a CNS infection , the top four producing lines were infected into three CD1 mice via a donor as described in Chapter 2.5.2 as a preliminary observation at the performance of the strain *in vivo.*

VSL-8 and VSL-21

A presentation of animals infected with VSL-8 and VSL-21 over the 35 days experiment as detailed by Jennings, can be seen in figure 3.8 (Jennings, 1977). As early as D7 p.i, bioluminescence was detected in the lower back of both the VSL-8 and VSL-21 infected mice. In VSL-8 infected mouse signal was also visible in the snout, which may in part be due to the blood being closer to the surface of the skin. By D14 signal increased and was distributed throughout the entire body of VSL-21 infected mouse. The bioluminescence in the VSL-8 mouse appeared not to have increased, but became more focal with signal only present in the lower back of the mouse. Prior to treatment with diminazene aceturate (DA) the total bioluminescent signal (ROI) calculated for the VSL-8 infected mice decreased from 1.7×10^8 to 6×10^7 photons/second (p/s), due to a disseminated signal (Fig. 3.9). Prior to treatment at D21 bioluminescence in the VSL-8 mice had decreased, with very low signal around the ears and nose. High bioluminescence of 1.2×10^{10} p/s was dispersed through the entire VSL-2 infected mouse at D21 just before treatment with DA.

After DA treatment, bioluminescence dropped and became undetectable in both the VSL-8 and VSL-21 mice. At the end of the experiment at D35 the mice were imaged before being culled. At this point bioluminescence was still undetectable, with the head region also clear of bioluminescence. The brains of the perfused mice were imaged, and as with the whole animal imaging, no bioluminescence was detected in the excised brains for either of the transfected lines.

VSL-8 had a starting parasitaemia 10 times higher than VSL-21 of 40 trypanosomes /10 f.o.v. Over the 35-day experiment the peripheral parasitaemia decreased, and reduced to zero parasites after DA treatment for both VSL-8 and

VSL-21 (Fig 3.9). The bioluminescence for VSL-8 followed a similar pattern as the peripheral parasitaemia. Bioluminescence started at approximately 10^9 photons/second, but gradually decreased to $\sim 10^8$ at D21 before rapidly falling to below background bioluminescence at D35. Despite the low peripheral parasitaemia exhibited by VSL-21, there is a stark contrast in the bioluminescence produced. During the first 21 days p.i the bioluminescence remained high at approximately 10^{10} photons/second until DA treatment, cleared the signal to below background (Fig. 3.9).

Possible explanations for the lack of signal in the brain include: (i) parasites are present but the strain had lost the ability to produce bioluminescent signal, indicating that the transfected clone was unstable. (ii) the transfected lines had lost the capability to invade the CNS, which may be due to the length of time the wild-type was in culture prior to transfection, or (iii) that the BBB became damaged due to infection and host inflammatory response, resulting in the DA passing through and cleared the brain infection.

The quantitative PCR (qPCR) data (Fig. 3.9) and *ex vivo* imaging (Fig. 3.8) confirmed that there were no trypanosomes present in the brain homogenate, indicating that either there was an inability of the clones to enter the CNS, or that BBB damage occurred and therefore enabled clearance by DA.

Due to the lack of CNS infection produced from both VSL-8 and VSL-21, both lines were discontinued within this study, and further transfections were carried out.

VSL-1 and VSL-2

Due to the inability to produce a CNS infection in strains VSL-8 and VSL-21, it was decided that the length of time GVR35 remained in culture prior to and post transfection, should be kept to a minimum. The strains VSL-1 and VSL-2 produced exceptional bioluminescence when tested *in vitro* (Fig 3.7).

VSL-1 and VSL-2 were intravenously infected into 3 mice per strain and the infection was monitored through blood films and imaging every 7-days, with DA treatment carried out on D21 to clear peripheral parasitaemia. At D7 p.i both VSL-1 and VSL-2 mice had signal in the lower back and snout (Fig. 3.8), VSL-2 had additional signal present in axillary/brachial lymph node area. Seven days later signal for VSL-1 mice had become visually undetectable on this heat map scale,

whereas VSL-2 mice had strong bioluminescence dissipated throughout the entire animal, with intense signal (indicated in red of the scale) present in areas with high blood flow at the surface, such as the eyes, and ears of the mouse. After treatment with DA, bioluminescence in both strains decreased to background (~10^5 photons/second) with VSL-1 remaining clear of bioluminescence at D35. The *ex vivo* imaging further confirmed no late stage infection present.

VSL-2 infected mice had a re-emergence of bioluminescence focused in the head region of the mouse. The *ex vivo* imaging of the brain and qPCR confirmed that an infection was present and that VSL-2 had successfully infected the CNS.

The parasitaemia for VSL-1 and VSL-2 over the 35 day experiment followed the same pattern but the VSL-1 was approximately 50% lower than VSL-2 (Fig. 3.9). Both transfected lines peaked at D14 (VSL-1 40 trypanosomes /10 fields and VSL-2 85 trypanosomes/ 10 fields) and cleared after DA treatment at D21, and remained undetectable at D35 p.i.

The bioluminescence for VSL-1 was overall low compared to the other transfected lines, with a starting bioluminescence at D7 p.i of 1 x 10^7 photons/second, only 100-fold higher than the background bioluminescence of 2 x 10^5 photons/second (Fig. 3.10). There was a small amount of fluctuation (drop at D14 before it increased again at D21), before the administration of DA caused the bioluminescence to decrease to below background level by D35. In contrast, VSL-2 had a high starting bioluminescence of 1.3 x 10^8 photons/second (albeit lower than VSL-8 and VSL-21), which increased to 5.45 x 10^9 photons/second at D14 and remained high until treatment at D21. DA caused a rapid decrease in bioluminescence to 5 x 10^5 photons/second, just above background before a rise at D35 to 2.9 x 10^6 photons/second.

3.4.4 VSL-2 Validation

As the VSL-2 transfected line produced bioluminescence in both the early and late-stage of infection in the GVR35 model, further studies were needed to ensure that the model was both reproducible and consistent as a new model for human African trypanosomiasis. This involved assessment of VSL-2 growth *in vitro* compared to the wild type, repeating the course of infection experiment with a larger group of

animals (six), the correlation of bioluminescence and parasitaemia, and determining the detectable bioluminescent limit of the model.

In vitro growth rate

The cumulative *in vitro* growth of VSL-2 was compared to that of the wild type (Fig. 3.10). The parasite growth was monitored daily for 10 days, with a starting parasitaemia of (and diluted down to) 1 x 10^5 trypanosomes/ml. Daily haemocytometer counts were recorded and the parasites were diluted back to the starting parasitaemia and the cumulative growth calculated

The growth of VSL-2 was not affected after the transfection of the luciferase. This is evident by the growth curve for VSL-2 overlaying that of the wild type.

In vivo bioluminescence assessment

A repeat of the strain assessment was carried out for VSL-2 with a greater number of mice (six).

A patchy signal was evident throughout the mouse that resided predominantly in the lower back region and lymph nodes at D7 p.i (Fig 3.11). The trypanomastigotes continued to multiply and spread throughout the blood and lymphatic system, and on D14 signal was observed throughout the animal. By D21 a similar signal distribution was seen, although the bioluminescence was much higher, peaking at 1 x 10^8 photons/second. From the heat-map scale it can be seen that the liver/spleen area displays the highest bioluminescence, providing further evidence that the lymphatic system is heavily infected.

Following treatment with DA at D21, bioluminescence in infected animals at D28 was greatly reduced, with a focal signal found only in the head region, as the clearance of peripheral parasitaemia revealed possible CNS infection. By D35, the bioluminescence signal in the head region became more intense, as the cranial concentration of parasites appeared to increase, with a 10-fold increase in flux between D28 and D35.

Quantification of the images revealed that as the infection progressed, the bioluminescence increased from 10^8 to less than 10^{10} total flux until DA treatment was administered (Fig. 3.12). In comparison parasitaemia was not detectable via microscopy until D14 and then was undetectable following treatment with DA.

Peripheral parasitaemia remained undetectable until the end of the experiment at D35 despite bioluminescence signal clearly apparent in the head.

To confirm the presence of trypanosomes in brain tissue following whole animal imaging at D35, the mice were perfused to clear the tissue of blood, and brains were excised and imaged *ex vivo* (Fig. 3.12). Bioluminescence was detectable in all VSL-2-infected mouse brains and was comparable to the signal seen in the head region of the respective intact mice at D35 (Fig. 3.11). In the brain of mouse 2, the signal was most prominent in the olfactory bulb of the brain whereas in mice 1 and 3 the signal non-specifically disseminated through the entire brain, with a high signal (red 'hot spot') in the cerebellum of mouse 3. The remainder of the infected group showed similarly non-specific distribution of bioluminescence in the brain (not shown).

Following *ex vivo* imaging, DNA was extracted from the perfused brains and qPCR was used to determine the parasite load in each brain (Fig. 3.12). Comparing qPCR to bioluminescence signal, the total flux was representative of the number of trypanosomes present. The brain of mouse 3 had areas of higher flux and therefore had an overall higher quantity of trypanosomes. Despite showing differences in the distribution of parasites, a trend can be identified between parasite burden as determined by qPCR and bioluminescence. The control wild type-infected brain had no bioluminescence but high parasitaemia.

Correlation of parasitaemia vs. bioluminescence

To determine if bioluminescence can be used as a quantitative method of evaluating parasitaemia, a correlation analysis of peripheral parasitaemia and whole animal bioluminescence was carried out (Fig. 3.13). From the analysis of BLI and peripheral parasitaemia an *r*-value of 0.28 was calculated, and suggested that the data had a weak positive relationship, as an increase in bioluminescence did not necessarily indicate an increase in parasitaemia. This is especially evident as the highest amount of bioluminescence can be seen when there is little to no parasitaemia.

Limit of Detection

To ascertain the detectable limit of the model within the Lumina IVIS a 0.2 ml serial dilution of parasites (50 – 5 x 10^4 trypanosomes) was prepared and 20 µl of

luciferin added. This was then injected intraperitoneally into CD1 mice and after 10 minutes mice were imaged (Fig 3.14). At the lowest dilution of 50 trypanosomes it can be seen that there is no visible bioluminescence present in the abdomen of the mice. A small signal is detected in mice infected with 1 x 10^2 trypanosomes, and the bioluminescence appeared focused around the site of infection. Mice infected with 5 x 10^2 trypanosomes had a dispersed signal within the abdomen, but still produced bioluminescence at the low end of the heat-map scale. An increase in trypanosomes had little effect on the dispersal of infection at both 1 x 10^3 and 5 x 10^3 trypanosomes, as the bioluminescence remained in the same area as seen in the lower infections, but with an increase in the intensity of the bioluminescence signal. At 1 x 10^4 trypanosomes, the entirety of the abdomen had visible bioluminescence with an area of high intensity around the injection site which can be seen with a red 'hot spot. ' The top dilution of 5 x 10^4 trypanosomes produced wide-spread bioluminescence in the intraperitoneal cavity with a large area of high intensity and bioluminescence.

3.5 Discussion

We demonstrate that the integration of the pTb-AMluc-v construct into *T. b. brucei,* is able to produce a bioluminescence strain that is detectable through whole animal BLI.

The transfected line VSG5 was able to exhibit similar virulence properties compared to the wild type.

The incorporation of bioluminescence into 427 has produced varying results dependent on the type of luciferase that has been used. The strain *T. b. brucei* 427-Rluc-pHD309 contains Renilla luciferase, which emits light in the blue spectrum at 480 nm after the administration of coelentrazine. This emits approximately 10^6 RLU for 1 x 10^6 trypanosomes/ml but is poorly visible within whole animal imaging (Claes *et al*., 2009). Firefly transfected strain (emitting at 562nm), 427-LUC2 transfected with the TbR-LUC2 construct, produced a bioluminescence 1000 times lower than the RLUC line *in vitro* for the same concentration of trypanosomes (~ 10^3-10^4 RLU) but had an improved detectability *in vivo* (Myburgh *et al*., 2013). We have shown that the transfection of a red-shifted luciferase into the 427 parasite may not increase the level of bioluminescence *in*

vitro from what has been seen previously (at approximately 2.5 x10^4 RLUs for 1 x 10^6 trypanosomes/ml), but the VSG5 strain had a far better sensitivity *in vivo* compared to both the firefly transfected TbR-LUC2 and the renilla 427-Rluc-pHD309. Although no parasites can be detected in blood films at D1 p.i a signal is indeed present, indicating that low-level infection can be detected through live imaging.

The data produced demonstrates that from the initial transfection of *T. b. brucei* GVR35 with pTb-AMluc-v to produce 10 bioluminescent lines. The top four lines (VSL-8, VSL-21, VSL-1 and VSL-2) produced a minimum of 3 x 10^4 RLUs greater than the successful 427-VSG5 *in vitro*. Despite the impressive results *in vitro,* only VSL-2 was able to produce a bioluminescence signal in the mouse CNS.

An increase *in vitro* culture time pre and post transfection, affected the infection kinetics of the parasite so that it no longer penetrated the CNS (as seen in VSL-8 and VSL-21 lines). It was decided that parasites would not remain in axenic culture for longer than 7 days (to include pre and post transfection), and the second generation of transfected lines were produced in this manner (VSL-1 and VSL-2).
Further validation of VSL-2 indicated that the transfection with the pTb-AMluc-v construct did little to alter the infectivity of the parasite. The same growth rate *in vitro* was observed, and it was able to produce both early and late stage infection in mice.
During the 35-day validation, VSL-2 was shown to provide higher imaging sensitivity than previous transfected trypanosome strains, with a bioluminescence 1000-fold higher than the GVR35-LUC2 *in vivo* (McLatchie *et al*., 2013, Myburgh *et al*., 2013), with a detectable limit within the IVIS of 100 trypanosomes in a bolus infection.

Despite the improved sensitivity and signal that VSL-2 produced, the bioluminescence was not directly correlated to the peripheral parasitaemia observed in blood films. Literature has documented that the early stage infection of trypanosomiasis infects the haemolymphatic system (Brun *et al*., 2010), and is not solely restricted to the blood system. The data produced in this chapter supports this, as despite peripheral parasitaemia being undetectable in the blood

films, bioluminescence was visible (and in most cases very high). Even when cyclical parasitaemia is observed, bioluminescence remained constant. Further experiments to investigate the bioluminescence and parasite burden (determined by qPCR) within infected lymph nodes would further support studies by Tanner *et al*, that despite parasite fluctuations in the blood, parasites in the lymph nodes remain constant (Kamerkar and Davis, 2012). This however, does mean that bioluminescence imaging can only be used as a qualitative measurement of infection, and further analysis is required to determine parasite burden. Despite this, VSL-2 is an imaging model that could potentially be used in drug development studies. The initial detection of infection through imaging and also the loss of signal after treatment (and reappearance at relapse) can provide a more sensitive, non-invasive drug assessment, with the potential to reduce the time required for drug evaluation.

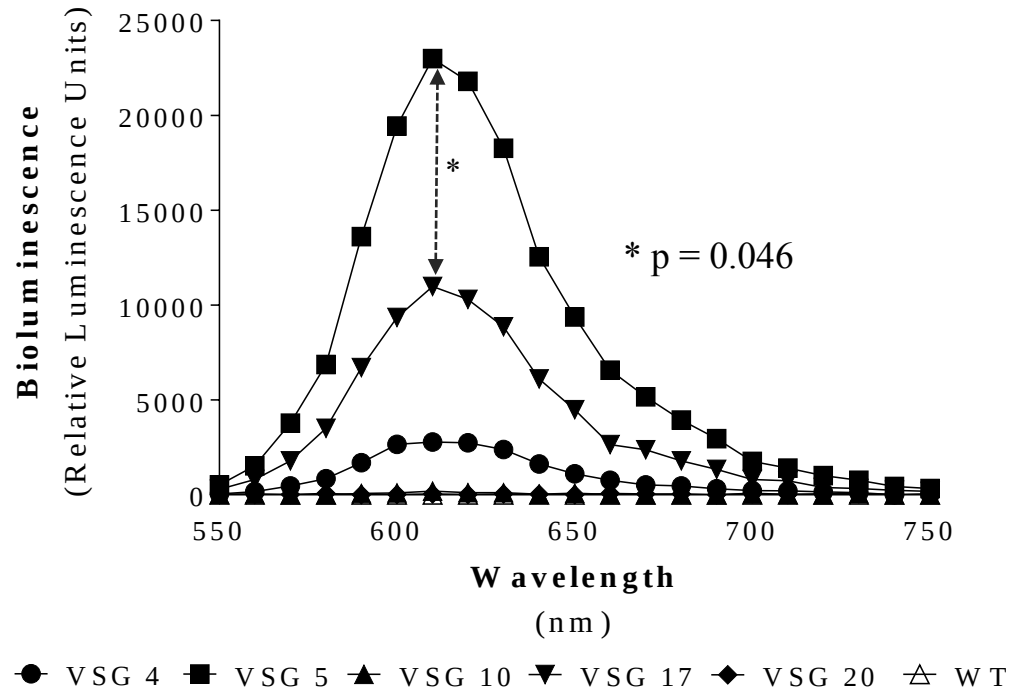

Figure 3.2 Spectral analysis of transfected *T. b. brucei 427*. For each of the transfected strains, 1 x 10^6/ml was analysed over the full spectrum and the RLU was determined.

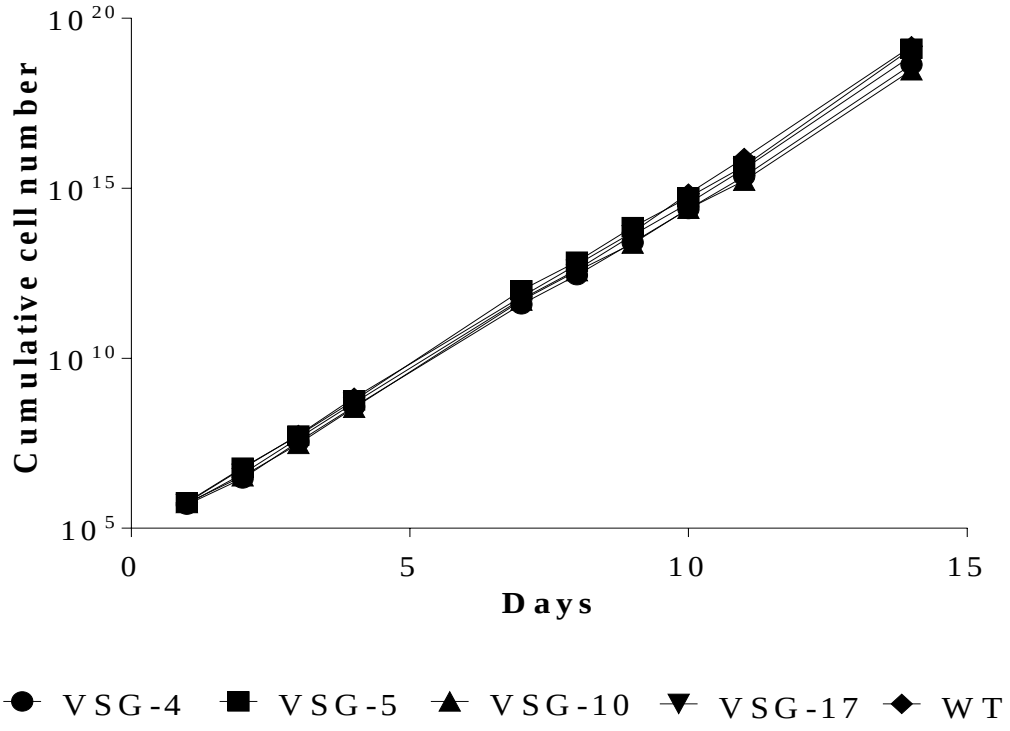

Figure 3.3 Growth curve of transfected *T. b. brucei 427*. The growth rate of transfected 427 was assessed *in vitro* compared to the WT. At each day the parasitaemia was diluted to 1 x 10^5/ml and the cumulative number of parasites was calculated over a 12-day period.

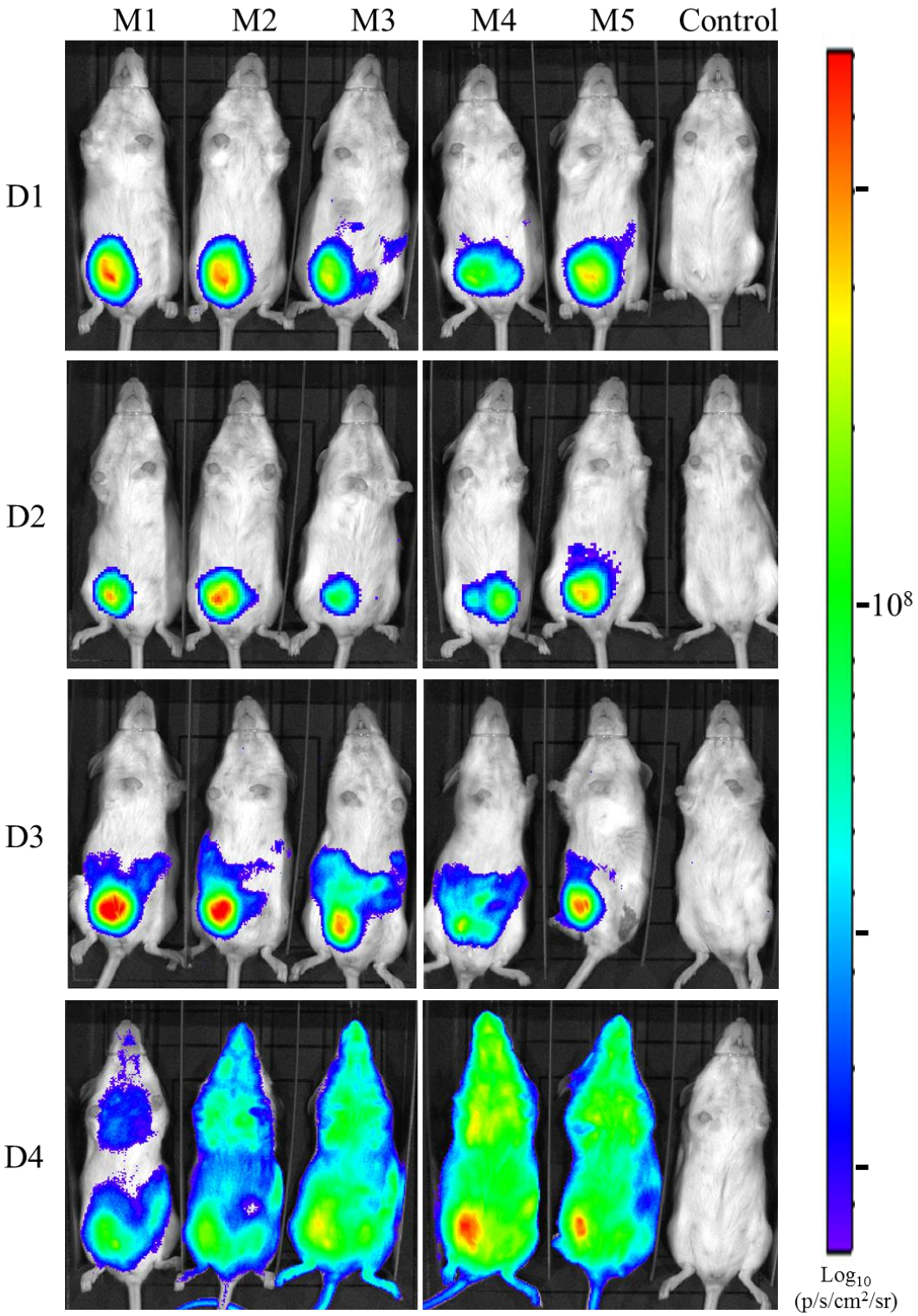

Figure 3.4. *In vivo* imaging of mice infected with VSG5. Five CD1 mice were infected with VSG5 via the i.p route. They were monitored by imaging and blood film acquisition for five days post-infection. Mice imaged at the indicated time points compared to a mouse infected with wild-type 427, showing bioluminescence on a heat-map scale (total flux) where red is an area of high flux i.e., high bioluminescence activity.

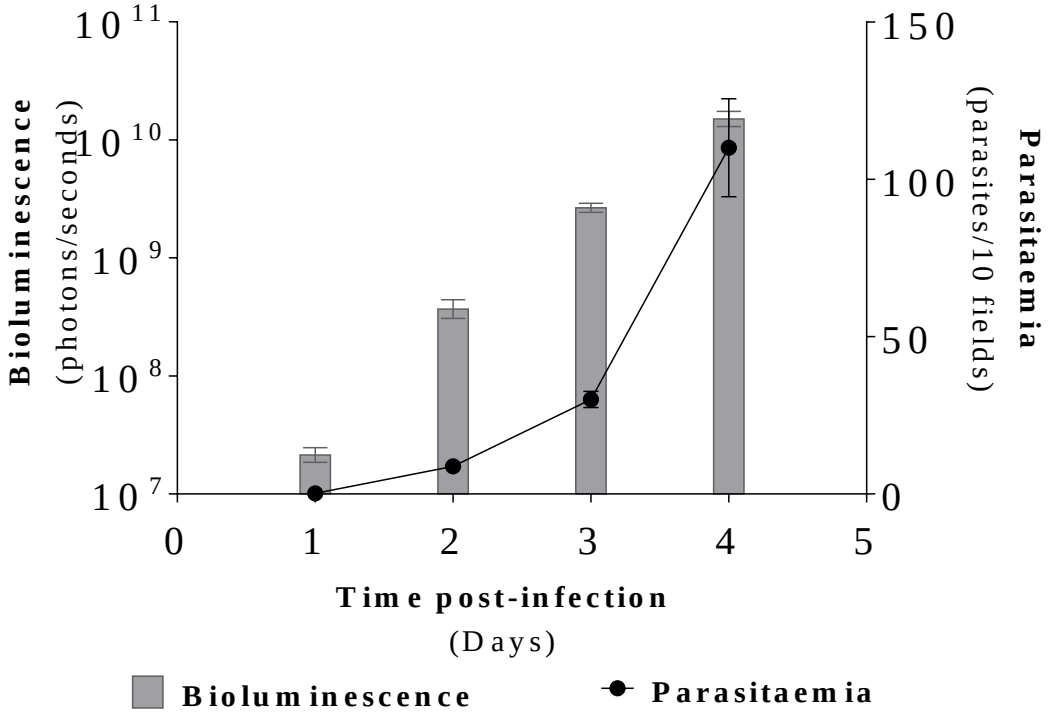

Figure 3.5 Bioluminescence vs. parasitaemia of VSG5. Quantification of average total flux and parasite number from the mice in figure 3.4. Each data point is a mean ± SD of the bioluminescence analysis and microscopic counts.

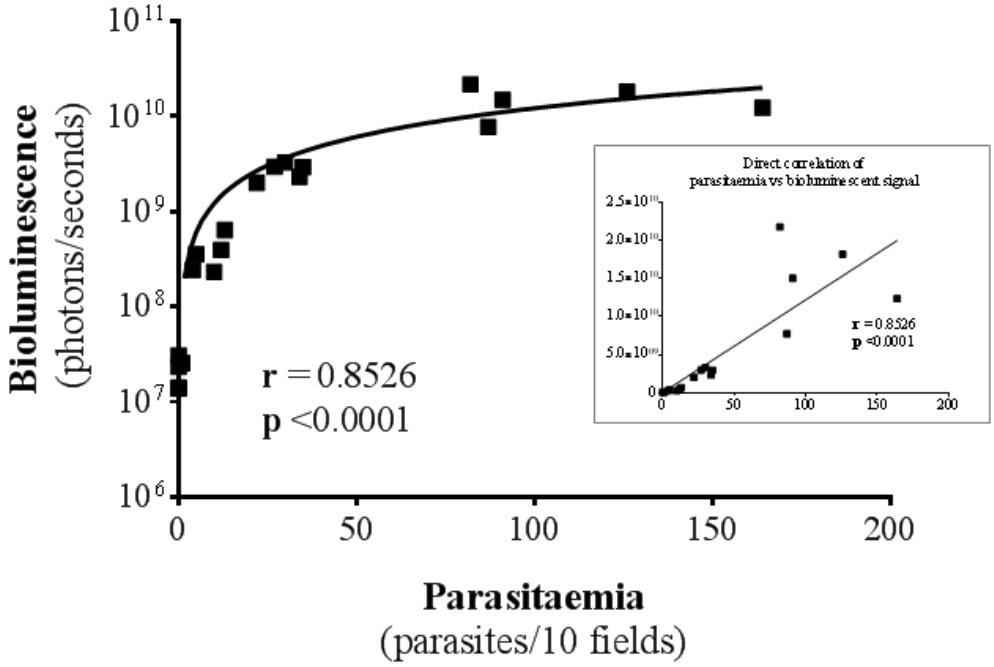

Figure 3.6 Direct correlation of bioluminescence vs parasitaemia of VSG5. A direct correlation analysis determines that it is positively correlated with an r-value of 0.8526. The correlation is also significant which is evident with a p-value of <0.0001. Inset shows correlation data expressed with a linear scale.

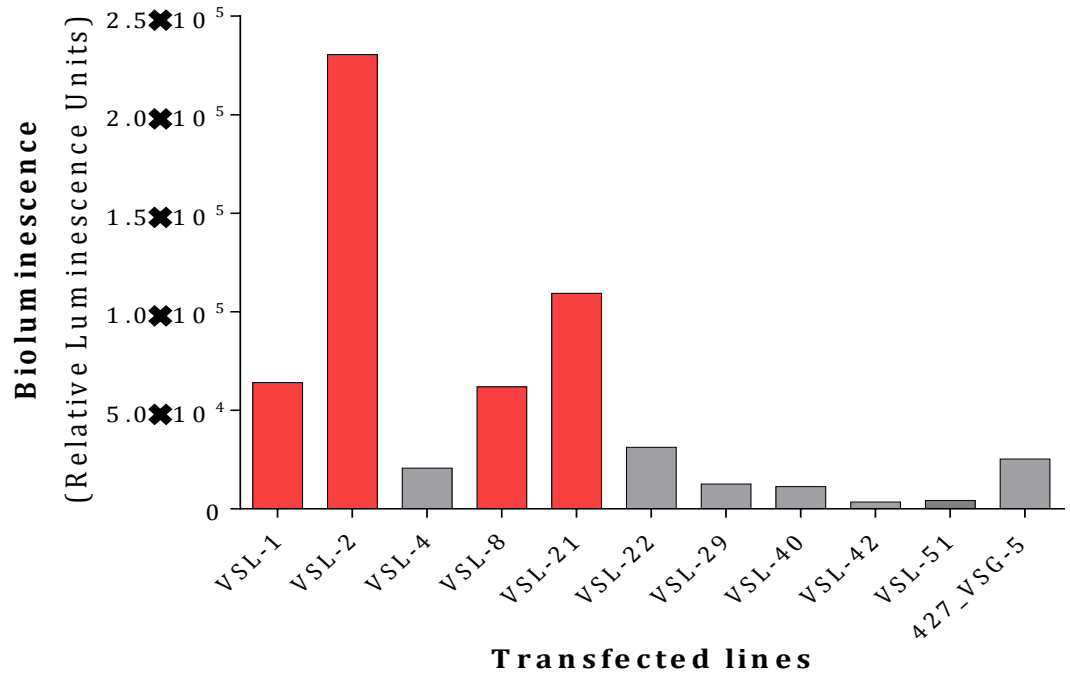

Figure 3.7 Spectral analysis of transfected *T. b. brucei* GVR35. A 1 x 10^6 trypanosomes were lysed using the Promega Luciferase Activity kit and bioluminescence measured. The red bars indicate the strains with the highest *in vitro* bioluminescence.

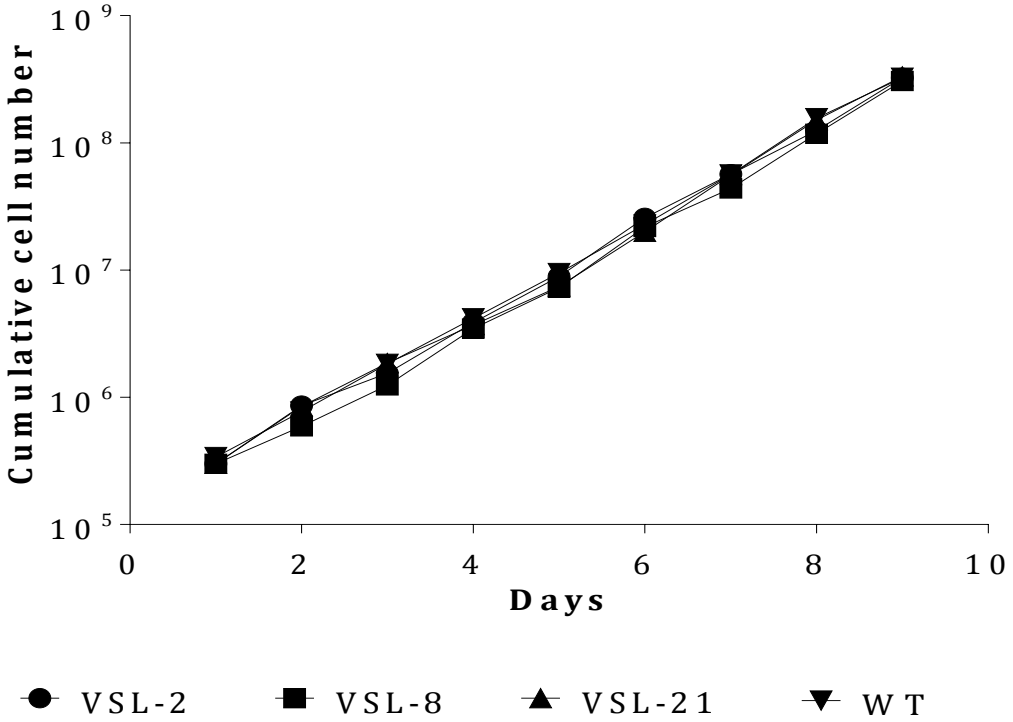

Figure 3.8 The *in vitro* growth rate of three transfected VSL lines. The cumulative growth rate of three transfected lines were compared to the WT strain.

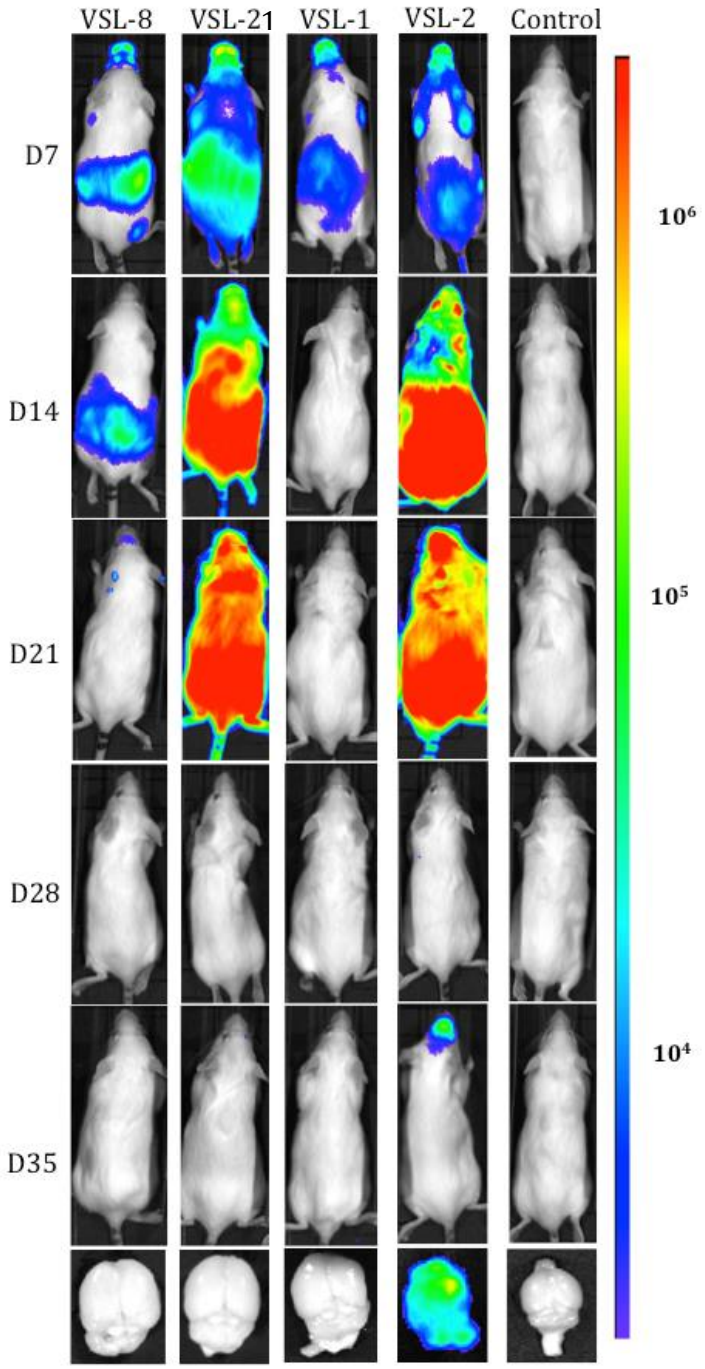

Strain	Trypanosomes/ 50ng of DNA
VSL-8	0
VSL-21	0
VSL-1	6354
VSL-2	9320
Control	10123

Figure 3.9 *In vivo* validation of GVR35 transfected strains. A single representation of three VSL infected mice i.v (VSL-1, VSL-2, VSL-8 and VSL-21) imaged at the indicated time points, showing bioluminescence on a heat-map scale (total flux) where red is an area of high flux i.e., high bioluminescence activity. At D21 mice were treated with DA (b) Excised brains were homogenised and extracted DNA subjected to qPCR

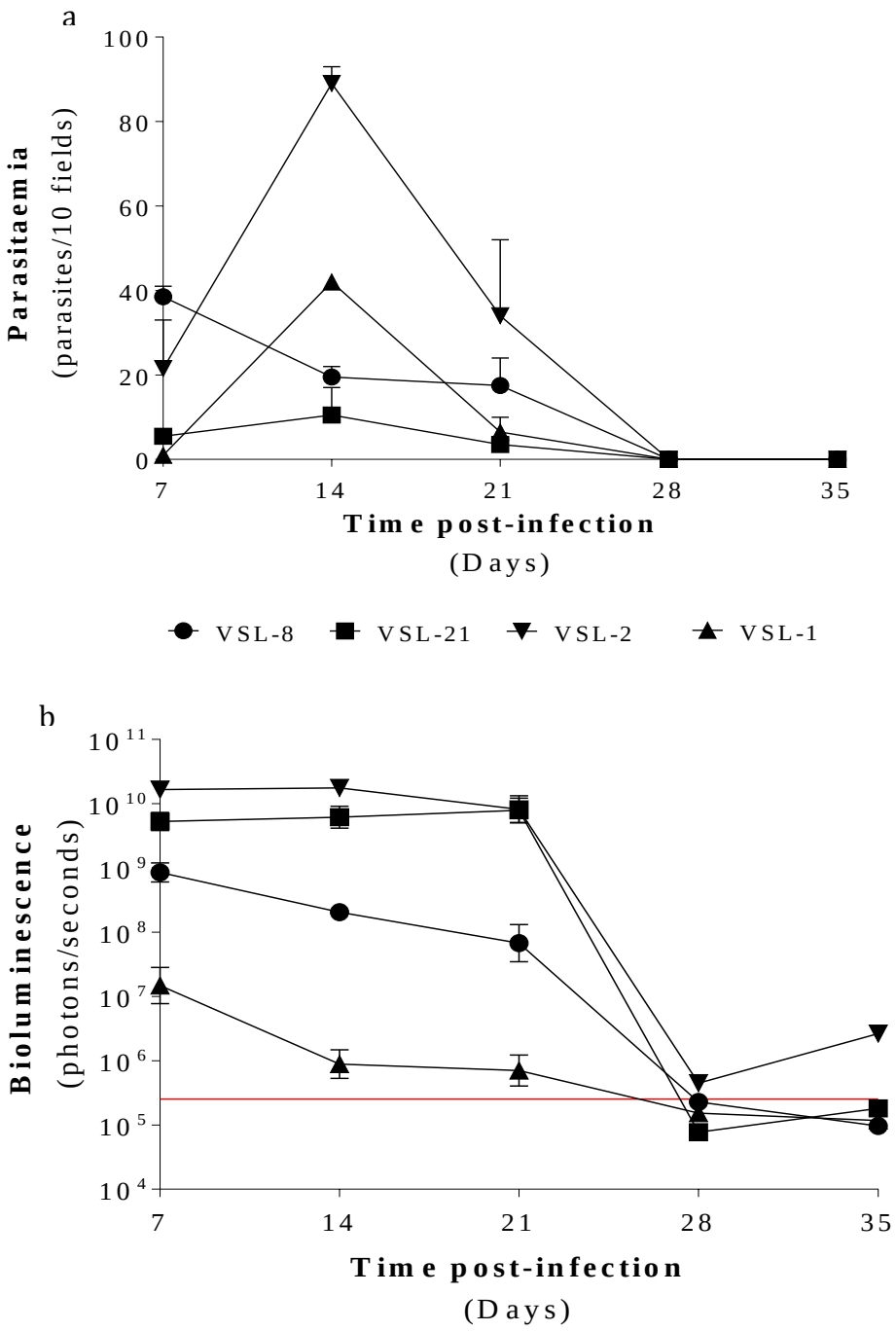

Figure 3.10 Bioluminescence and parasite burden of GVR35 transfected lines (a) peripheral parasitaemia of six mice. (b) Quantification of average total flux as determined by ROI Each data point is a mean ± SD of the bioluminescence analysis and microscopic counts. The red line indicates background bioluminescence which was established by imaging a WT-infected mouse.

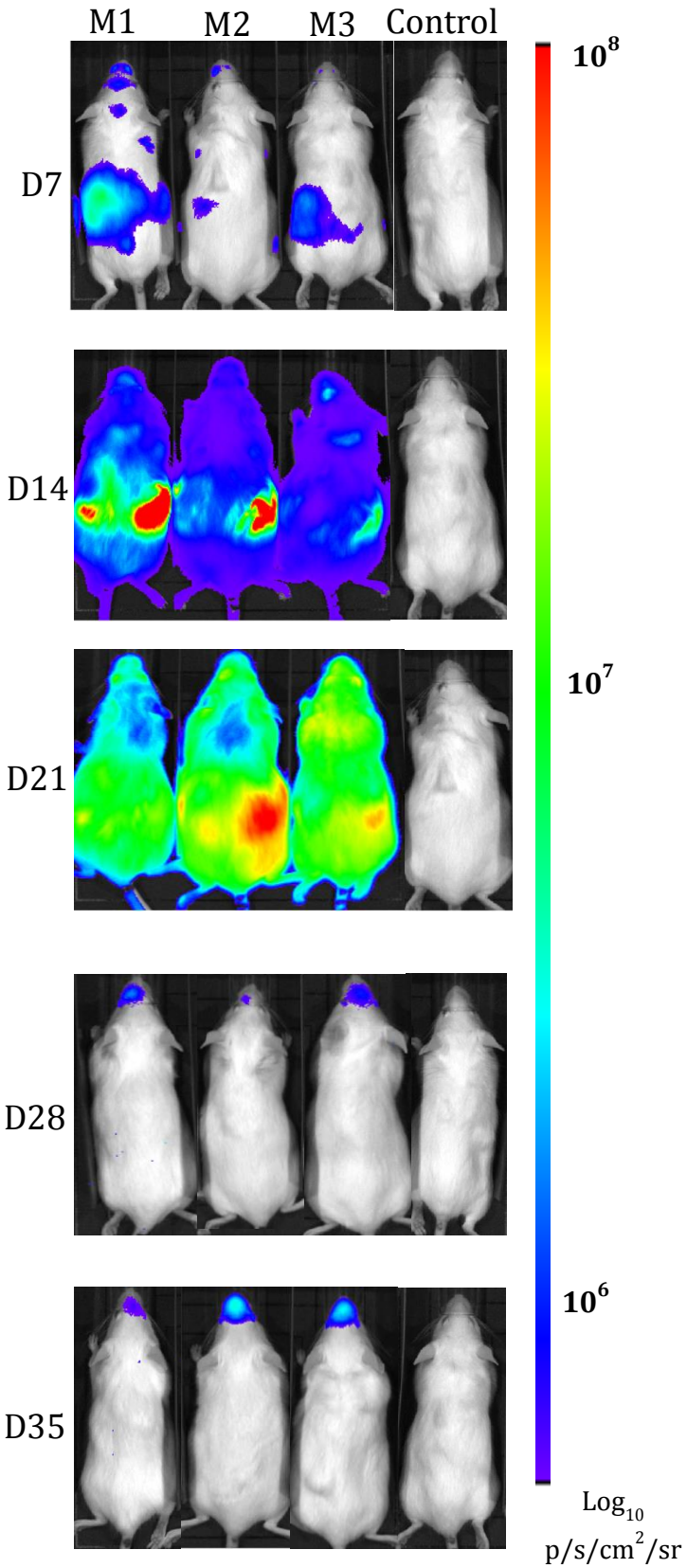

Figure 3.11 Validation of *T. b. brucei* GVR35 VSL-2 Three representative animals of six VSL-2 infected mice i.v (M1, M2 and M3) imaged at the indicated time points compared to a mouse infected with wild-type GVR35, showing bioluminescence on a heat-map scale (total flux) where red is an area of high flux i.e., high bioluminescence activity. At D21 mice were treated with DA.

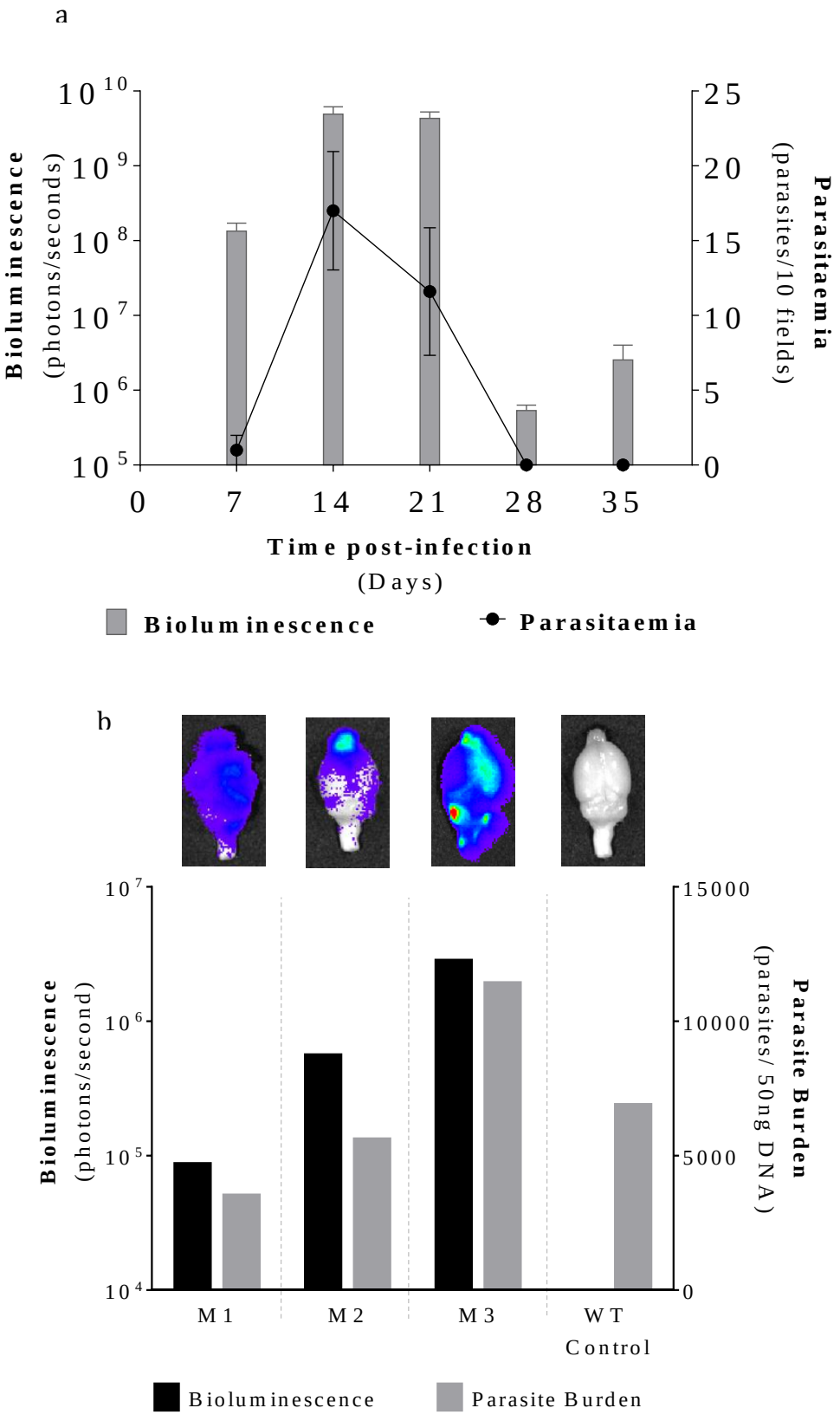

Figure 3.12 Quantification of biolumienscence and parasite burden of VSL-2 (a) Quantification of average total flux as determined by ROI, and peripheral parasitaemia of six mice. Each data point is a mean ± SD of the bioluminescence analysis and microscopic counts. (b) Excised brains were homogenised and extracted DNA subjected to qPCR, and compared to the bioluminescence. The detection limit of the qPCR was 50 trypanosomes/50 ng of DNA.

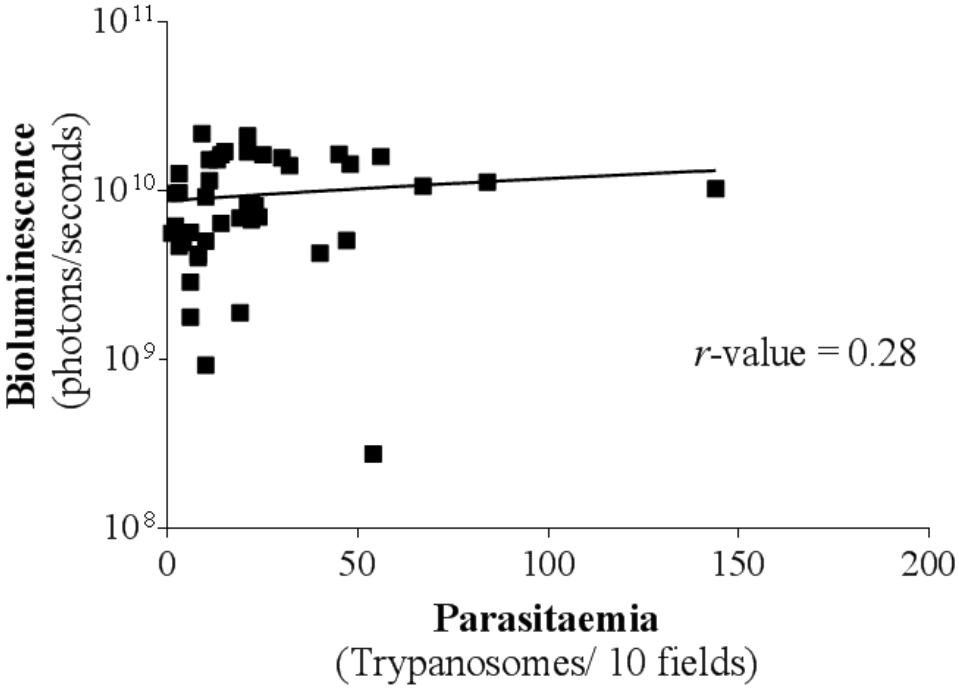

Figure 3.13 Direct correlation of bioluminescene vs Parasitaemia. A direct correlation analysis determined that the data is not correlated with an r-value of 0.28. This indicates that there is no correlation bioluminescence and parasitaemia in VSL-2 strain

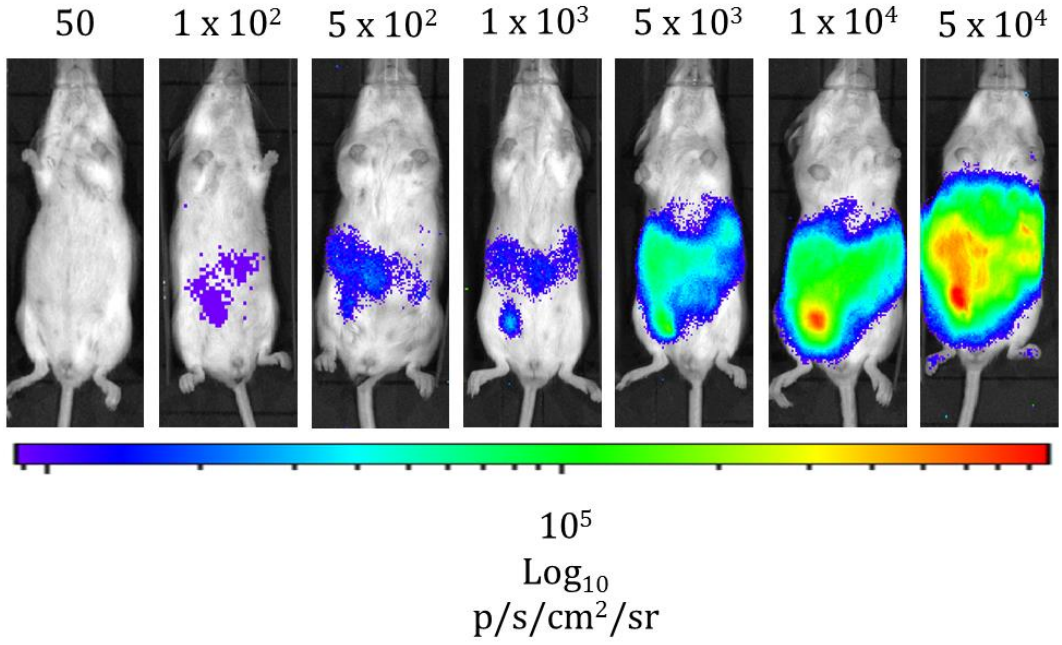

Figure 3.14 Limit of detection of VSL-2 To determine the detectable limit of the VSL-2 model in the IVIS, a bolus of serial diluted trypanosomes and luciferin were infected i.p into an individual mouse per dilution and imaged after 7 minutes.

CHAPTER 4: Validation of VSL-2 using melarsoprol

4.1 Introduction

As detailed in chapter 1, melarsoprol was the most widely used late-stage treatment due to its affordability and cross-sensitivity to both rhodesiense (the only current treatment therapy) and gambiense strains of HAT (Barrett *et al*., 2007).

Melarsoprol is an organoarsenic compound that was developed by adding the heavy metal chelator dimercaptopropanol (BAL) to the trivalent arsenical melarsen oxide (fig. 5.1). The addition of BAL results in a compound that is 100 times less toxic than melarsen oxide alone (trypanocidal active component) (Barrett, 2004).

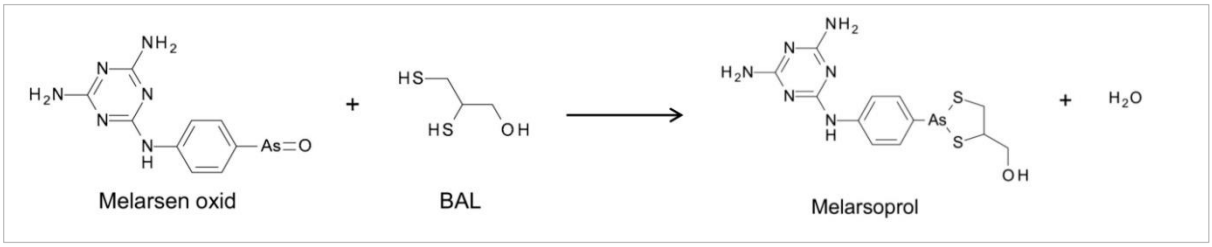

Fig. 4.1 Structure and production of melarsoprol (Adapted from www.parasitesandvectors.com)

Melarsoprol was first introduced in 1949 by Ernst A.H. Friedheim and is now produced and marketed by Sanofi as Arsobal® (Burri, 2004). Due to poor oral bioavailability, melarsoprol treatment regimen consists of intravenous (i.v) injections of 2.2 mg/kg /day for 10 days (Burri, 1993).

Despite widespread use, melarsoprol can produce a severe toxic side effect known as post-treatment reactive encephalopathic (PTRE) syndrome. Symptoms of which can be difficult to distinguish from those of the late-stage infection. They include convulsions, fever, headaches, progressive coma and eventually death (Brun *et al*., 2010). The frequency of the side effects can vary; approximately 4.7% of *gambiense* patients and approximately 8% of *rhodesiense* patients experience PTRE, with a fatality rate of 44% and 57% respectively (Brun *et al*., 2010).

Toxicity is not the only problem with melarsoprol, administration of the drug is painful and it is not uncommon for veins to become thrombotic during treatment. In recent years, the number of treatment failures has risen to 30%, indicating that reduced drug-sensitivity maybe emerging. However, verifying the reduction in

drug sensitivity from samples of relapsed cases in the field, is proving problematic due to difficulties in culturing the human-infective parasite (Barrett *et al*., 2007).

As with most anti-trypanosomal drugs, the mechanism of action is not completely understood. It is known that when the parasites are exposed to melarsoprol they lyse rapidly but 'how' is still under debate. It is thought that melarsoprol forms stable interactions with the dithiol trypanothione, but whether this interaction causes trypanocidal activity is still being explored (Barrett *et al*., 2007). The primary route of uptake of the un-metabolised drug is thought to be through passive diffusion (Scott AG, 1997), whereas melarsen oxide is known to enter the parasite primarily through the nucleoside transporter P2 (Carter, 1993, Beckers, 1981), as the removal of this transporter has shown to provide the trypanosome with a level of resistance to melarsoprol. However, complete resistance does not occur indicating that other secondary routes are also involved (Carter, 1993). It is known that metabolite melarsen oxide is principally responsible for the trypanocidal activity of the drug *in vivo* (Burri, 2004).

Determining the staging of the disease is imperative before starting a treatment regime, as all late-stage treatments require hospitalisation. In most cases, alternative treatment with the nifurtimox-eflornithine combination therapy (NECT) is carried out in *gambiense* patients, thus avoiding the toxic nature of melarsoprol. Alternative dosing routes have been explored but have proven unsuccessful due to poor oral bioavailability and the irritant nature of the adjuvant (propylene glycol). This results in oral and intramuscular administration being impossible (Barrett, 2004).

Presently there are only two registered treatments for late stage HAT, and due to the complexities of treatment regimens of NECT (prolonged treatment times and the requirement of both oral dosing and i.v infusions), melarsoprol is the only drug used as positive control in animal models (Scory *et al*., 1999).

To further validate the model and determine its usability as a drug assessment tool, studies were carried out with melarsoprol to identify if effective dose data

could be obtained and determine if relapse is detected earlier using bioluminescence imaging.

4.2 Aims and Objectives

The work described in this chapter, was to use melarsoprol to further validate VSL-2. This was to show its suitability in the study of drug evaluation and whether current protocols can be carried out in shorter time frames.

The following objectives were investigated:

- Bioluminescence can be used as a qualitative measure of drug efficacy in whole animal imaging.
- The use of qPCR can further confirm dose response seen *in vivo* and *ex vivo* imaging of late stage infection.
- The highly sensitive nature of bioluminescence can detect relapse earlier than with traditional blood films.
- Pharmacokinetics studies can determine the concentration of drug able to pass through the BBB and determine concentrations of 'free' and bound drug.

4.3 Contributors

Within this chapter all *in vivo* experiments were carried out by author, including samples generated for the pharmacokinetic study. Drug extractions of brain and blood were also carried out by author, with LC-MS/MS and analysis carried out by Dr. Hatem Sallam at Pharmidex.

4.4 Results

4.4.1 Drug efficacy

Using bioluminescence to determine dose response, as well as relapse could provide enhanced information on a novel compound's drug efficacy. Mice infected with VSL-2 were treated with melarsoprol at doses of 1, 3, 6 and 10mg/kg i.v for 4 days, as detailed in table 2.2 to provide a dose response. Bioluminescence and parasitaemia were measured at D21 (pre-treatment), 24, 28, 30 and 35 (Fig. 4.2).

The imaging data shows qualitatively that after treatment all mice have undetectable bioluminescence, indicating a clearance of infection that remained undetectable until D30. Despite the initial clearance after treatment, mice treated with 1 mg/kg had detectable bioluminescence at D30 p.i focused in the head and spinal region of the mouse. From its location it can be presumed that the relapsed infection is within the CNS of the spine and brain. By D35 the 1 mg/kg treated mice had full-body bioluminescence and the 3 mg/kg group exhibited bioluminescence within the head region. The region of interest (ROI) quantified the bioluminescence throughout the experiment. Immediately after treatment at D24 p.i both bioluminescence and parasitaemia fell at all doses (Fig. 4.3). As seen in the imaging data, the bioluminescence for the 1 mg/kg treated mice continued to increase and at D35 was 100-fold greater than background at 10^8 photons/second. Two of the five mice treated with 3 mg/kg dose also had visible signs of relapse at D35 located in the head region.

Peripheral parasitaemia could only be detected in mice treated with 1 mg/kg melarsoprol after infection had re-disseminated throughout the entire animal at D35, providing further evidence of the improved sensitivity bioluminescence can provide (Fig. 4.3). At the higher doses of melarsoprol treatment (6 and 10 mg/kg), re-infection was not detectable through both bioluminescence and blood film monitoring during the 35 days.

To quantify parasitic burden after treatment at D35, mouse brains were removed and qPCR analysis was carried out (Fig. 4.4). With the increasing doses of melarsoprol the parasitic burden determined by qPCR decreased, indicating a clear dose-dependent effect. The CNS positive control of DA had a high number of trypanosomes in the brain (1.5×10^4 trypanosomes/50 ng of DNA), confirming that DA was unable to clear parasites in the CNS. The *ex vivo* imaging of the melarsoprol-treated brains correlated with the qPCR data providing evidence that bioluminescence can be used to determine a dose dependent effect.

4.4.2 Drug relapse

To study drug relapse of melarsoprol using the VSL-2 model, a curative dose of 10 mg/kg and non-curative of 6 mg/kg were administered intravenously. Over a 180-

day period bioluminescence and parasitaemia for each individual mouse was monitored (Fig. 4.5).

Mice dosed with 6 mg/kg had undetectable parasitaemia prior to D63 in any animal (Fig 4.5A), after which low numbers of parasites were detectable in the blood of 4 of the 5 animals and an increase of parasitaemia continued until D119. However, according to the blood films, mouse 5 remained aparasitaemic during the 119 days showing few symptoms other than splenomegaly before being culled. Bioluminescence was detected as early as D49 for 3 of the 5 mice, and signal was observed in the remaining mice by D63 (Fig. 4.5A). A fluctuation in bioluminescence was seen over 56-days prior to the termination of the group (at D119) in all mice, however peripheral parasitaemia was not detected.

Parasitaemia was cleared in all mice immediately after treatment of 10 mg/kg melarsoprol and four of the five mice remained blood-film negative throughout the 180 days. At D91 mouse 2 had a peripheral parasitaemia of 14 trypanosomes/10 fields of view (f.o.v), which decreased at D98 before reappearing again 14 days later. The mouse was then culled at D119 after exhibiting lethargy (Fig 4.5A). In the 10 mg/kg treated group, drug relapse for mouse 2 was detected 21 days earlier using BLI than with the traditional blood film method (detected at D70 rather than D91) (Fig. 4.5B). A total flux of 4.64×10^6 photons/seconds (10 fold increase on the background) was observed before the bioluminescence fell below background detection. It reappeared at D84 and spiked at D119 with 1.27×10^{10} photons/second, where the mouse reached its humane endpoint and was culled. BLI was therefore able to detect drug relapse much earlier than traditional blood film.

4.4.3 Melarsoprol dose ranging

All pharmacokinetic studies were carried out on melarsoprol alone and not the metabolites. This was due to melarsen oxide being difficult to fragment and ionize in order to set up a LC-MS/MS method of detection (personal communication with Dr. Hatem Sallam at Pharmidex).

The dose ranging experiments were designed to provide an understanding of the relationship between dose and exposure within the two-compartments of plasma and brain. It is also used to enable modeling of the clinical exposure in humans.

Three doses of melarsoprol were chosen: 0.9, 2.2 and 18 mg/kg and they were administered intravenously to one uninfected mouse per time point (8 time points).

The concentrations of melarsoprol in plasma were rapidly metabolised and removed within 1-2 hours after administration (Fig 4.6). In the brain, only the higher doses of melarsoprol (2.2 and 18 mg/kg) were seen to pass through the blood-brain barrier at detectable levels. (Fig 4.6) The 18 mg/kg dose was rapidly eliminated; mirroring what was seen in plasma but at 100-fold lower concentration.

4.4.4 Melarsoprol binding assays

Using equilibrium assays and LC-MS, the percentage of free and bound fraction of melarsoprol was determined in both uninfected brain and plasma.

	Plasma	**Brain**
Bound	89.1 ± 0.07	91.4 ± 0.3
Free	10.9 ± 0.07	8.6 ± 0.3

Table 4.1. Percentage of bound and free fractions of melarsoprol in plasma and brain ± the standard error of the mean (SEM).

Melarsoprol was predominantly bound to protein in both brain and plasma, with approximately the same affinity. The free fraction of melarsoprol in plasma ($f_{u, plasma}$) was ≈10.9% and for brain ($f_{u, brain}$) was ≈ 8.6%.

4.4.5 Pharmacokinetic study of melarsoprol in mouse model

To study the relationship between dose and exposure of melarsoprol within infected and uninfected animals, 3 mice per time point (8 time points) were treated with a dose of 10 mg/kg and drug extractions from plasma and brain was analysed using LC-MS/MS (Fig. 4.7).

The drug concentration in plasma rapidly decreased in the first 5 minutes from 377 ng/ml to 29 ng/ml in uninfected animals, and 110 ng/ml to 12 ng/ml in VSL-2

infected mice. Over the next two hours the plasma concentrations for both the infected and uninfected mice fluctuated, but at the two hour time point the infected plasma concentrations fell and were below the limit of quantification (LLOQ). However, uninfected plasma continued to fluctuate until it dropped to a low of 8 ng/ml at 4 hours post-dose and further increased to 53 ng/ml (Fig. 4.7A), indicating a longer exposure time of melarsoprol in the uninfected mice. The brain concentrations of the infected and uninfected mice followed the same pattern by decreasing in the first 30 minutes (36 ng/g uninfected and 61 ng/g), but the levels of melarsoprol increased at 1 hour post exposure, with both infected and uninfected mice having brain concentrations of 243 ng/g and 235 ng/g respectively (Fig. 4.7B).

4.5 Discussion

Chapter 3 showed that VSL-2 was a highly sensitive imaging model that was able to detect infection earlier through BLI than with traditional blood films. The model was tested with melarsoprol to establish if bioluminescence can be used as a tool in determining drug efficacy.

Currently, pre-clinical drug evaluation requires mice to be monitored for up to 180 days post-infection, with relapse being detected when parasites re-establish an infection in the periphery and are detectable via blood films (Kennedy *et al*., 1997). Presently, there is no established *in vivo* test to determine the dose-dependent effect of trypanocidal drugs in the CNS. Here we have shown that by using a combination of bioluminescence and qPCR, we are able to detect parasite persistence within tissues after drug treatment and provide a visual marker of parasite clearance. Parasite quantification by qPCR added to the sensitivity of the model, but parameters need to be established to define when successful treatment has occurred, i.e. 100% clearance of all parasites.

As the model is able to produce detailed data of drug efficacy in real-time through *in vivo* imaging and definitive parasite load through qPCR, the likelihood of treatment failures at later experimental studies is limited, but this may also result in fewer drugs making it through to the next phase of clinical trials.

The current experimental model requires a time period of six months, which is not appropriate for drug development, and a new approach is required to speed up the process and provide data on time-to-kill and parasite distribution. At present there is no current model for assessing a dose dependent effect in CNS *in vivo*, as it is not possible to determine parasite persistence within tissues using contemporary techniques.

Bioluminescent model systems using luciferase have been described for the assessment of drugs for other diseases and infections (Barman *et al*., 2011, Andreu *et al*., 2010, Claes *et al*., 2009). The development of the green luciferase LUC2 and red-shifted VSL-2 strain has paved the way for a new mouse model of HAT that is both highly sensitive and non-invasive.

VSL-2 provides an improved imaging sensitivity than previous transfected trypanosome strains, which enables a dose-dependent effect to be detected in whole mouse imaging after treatment with melarsoprol.

The shortened experimental time of 35 days is sufficient to confirm anti-trypanosomal activity on late-stage HAT by loss of bioluminescence in the brain, which has been difficult to determine *in vivo* before now.

The increased sensitivity of BLI is demonstrated further in the analysis of drug relapse. By D60, a clear indication of sub-curative clearance (in this case 6mg/kg) is evident and by 90 days p.i relapse is detected, resulting in the reduction of experimental time by 50%. The non-invasive nature of the model also provides an option to extend the time required to follow the animals with minimal invasion.

Although 10 mg/kg appeared as a curative dose in 4 of the 5 mice through the assessment of peripheral parasitaemia on blood films and bioluminescence, mouse 2 showed that parasites could persist long after treatment with increasing flux around D60, and then again at D81 to D112 suggesting relapse. Early studies carried out by Poltera on melarsoprol showed that the regimen of 10 mg/kg x 3 days i.v, gave no relapse in peripheral parasitaemia detected by blood films, but two-thirds of the mice in the study died (Poltera *et al*., 1981). Poltera concluded that melarsoprol was curative as no parasites were found in the peripheral blood or brain tissue in all of the mice as determined by histopathological study and immunofluorescence (Poltera *et al*., 1981). Data shown here supports that peripheral parasitaemia was not detected, but bioluminescence re-emerged after

treatment in one of the five mice through the 180-day experiment, lending further evidence to the hypothesis that the lymphatic system is involved in parasite latency, and also raises the question on how 'cure' can be defined in the mouse model.

The dose ranging studies showed that the rapid decrease of melarsoprol in plasma in the first 20 minutes was representative of the distribution of the drug from the plasma/blood (central compartment) into the brain (peripheral compartment). Over the next 100 minutes the decrease in concentration is gradual as drug metabolism and excretion occurred.

By moving into the infected host, the pharmacokinetic studies carried out on melarsoprol did not show a difference in drug concentrations in either the plasma or brain compartments, of the infected and uninfected mice. This suggests, that the infection had not altered the permeability of the BBB, to either let more drug into the brain or to prevent it.

The biggest limitation from the studies was the inability to detect and measure the active component of melarsoprol, melarsen oxide. The restriction was due to the inability to produce ionisable fragments for LC-MS/MS analysis.

The pharmacokinetics of melarsoprol as a whole compound does not provide accurate information of the drug activity within the animal host.

In summary, we have presented evidence here that the red-shifted bioluminescent GVR35 VSL-2 model, has the capability of providing a sensitive drug assessment system by non-invasive imaging, with the ability to reduce the current screening time by 90 days. In addition to this, the high sensitivity of the imaging combined with quantitative methods of qPCR, have allowed a new methodology to be developed that can assess drug efficacy of novel drugs for treatment of late stage of human African trypanosomiasis.

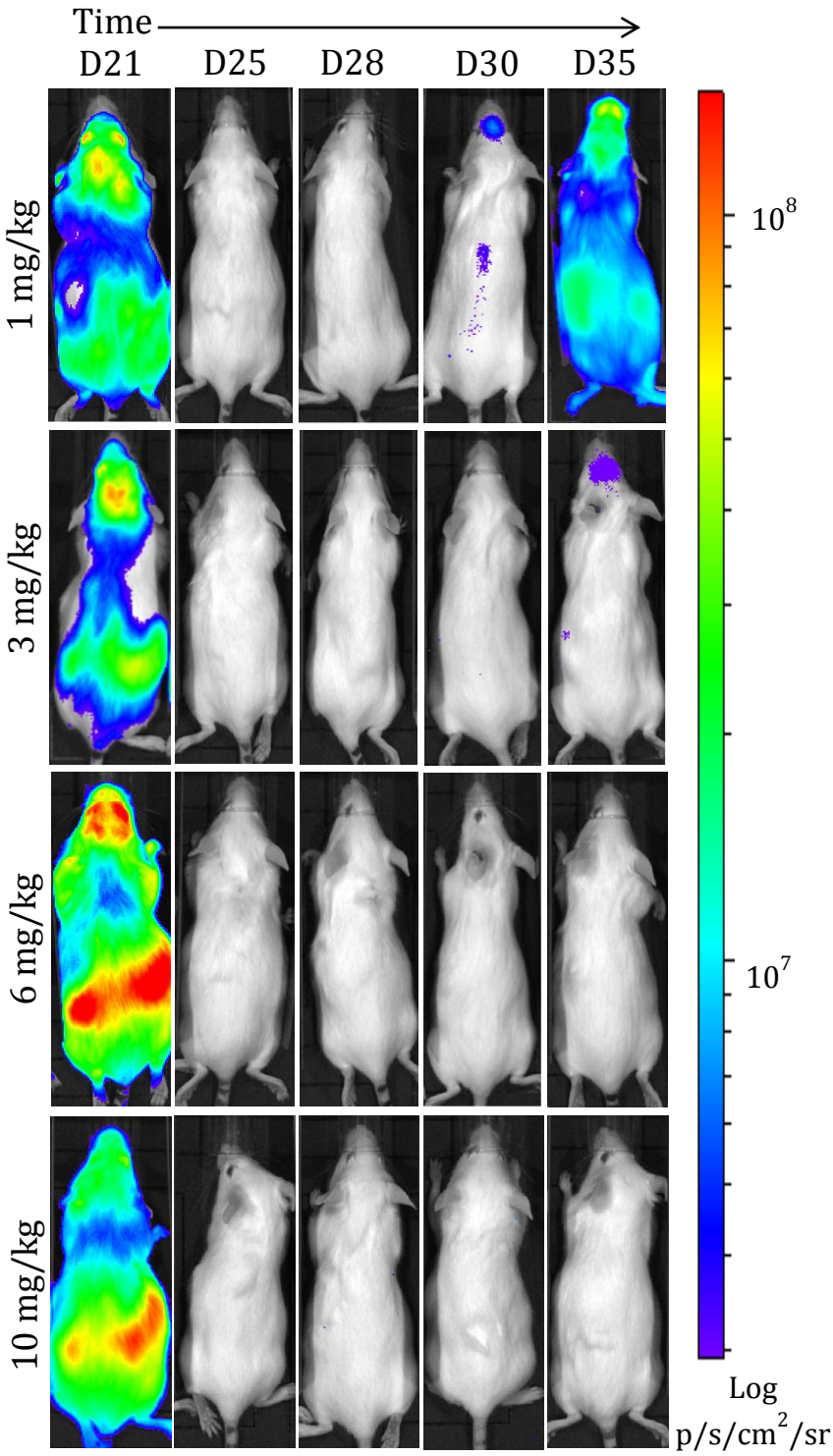

Figure 4.2 Drug efficacy of melarsoprol using bioluminescence imaging. Infected CD1 mice were split into groups of six and treated with varying doses of melarsoprol from D21 and monitored until D35. A single representative mouse (1 mouse from group of six) from all doses 10 mg/kg – 1 mg/kg, showing bioluminescence on a heat map scale (red representing maximum flux) before and after treatment.

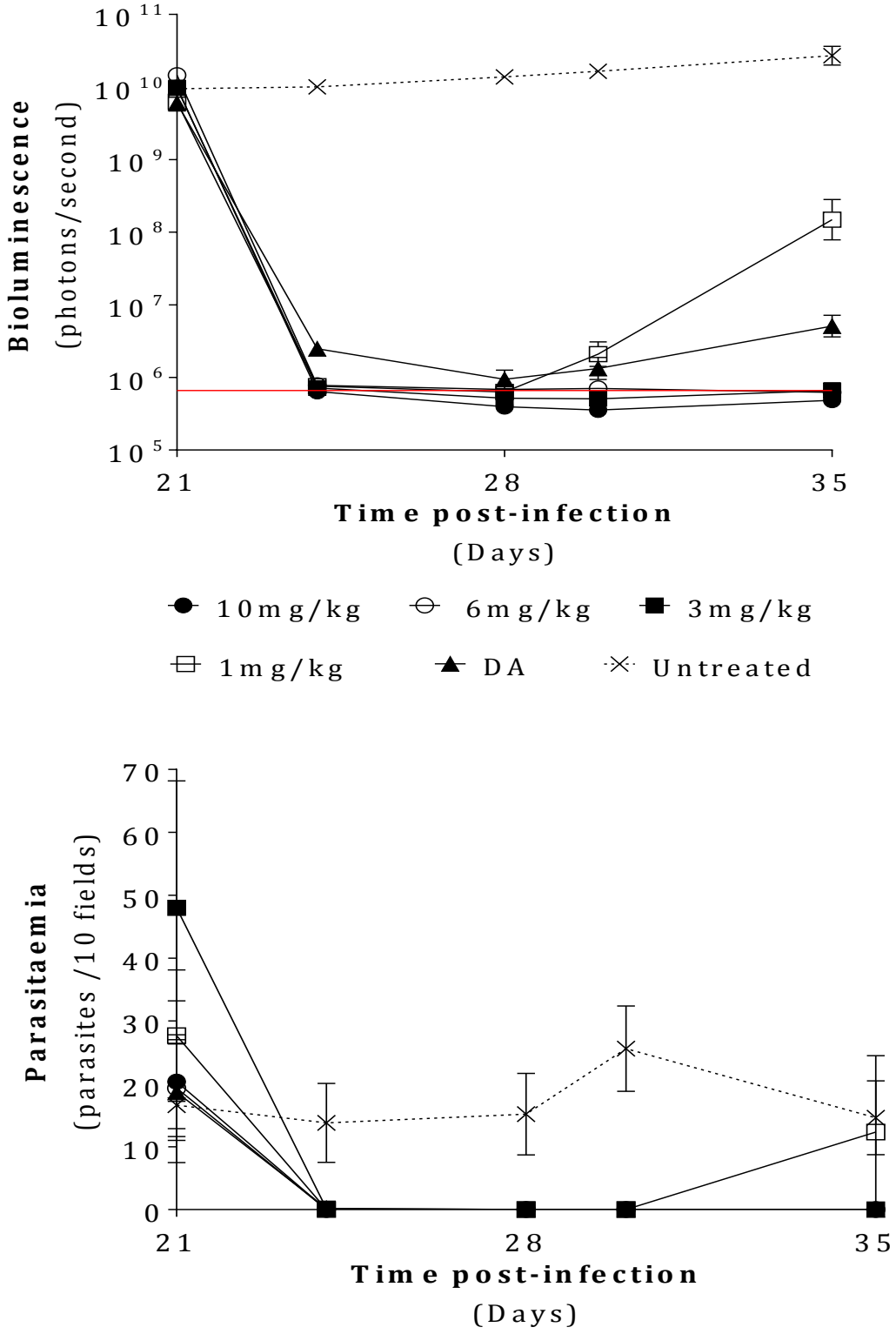

Figure 4.3 Bioluminescence and parasitaemia after melarsoprol treatment. The average (of six mice) quantification of total flux and parasite number. Each data point is a mean ± SD of the bioluminescence analysis and microscopic counts. Red line indicates background bioluminescence measured by the BLI of a WT infected mouse

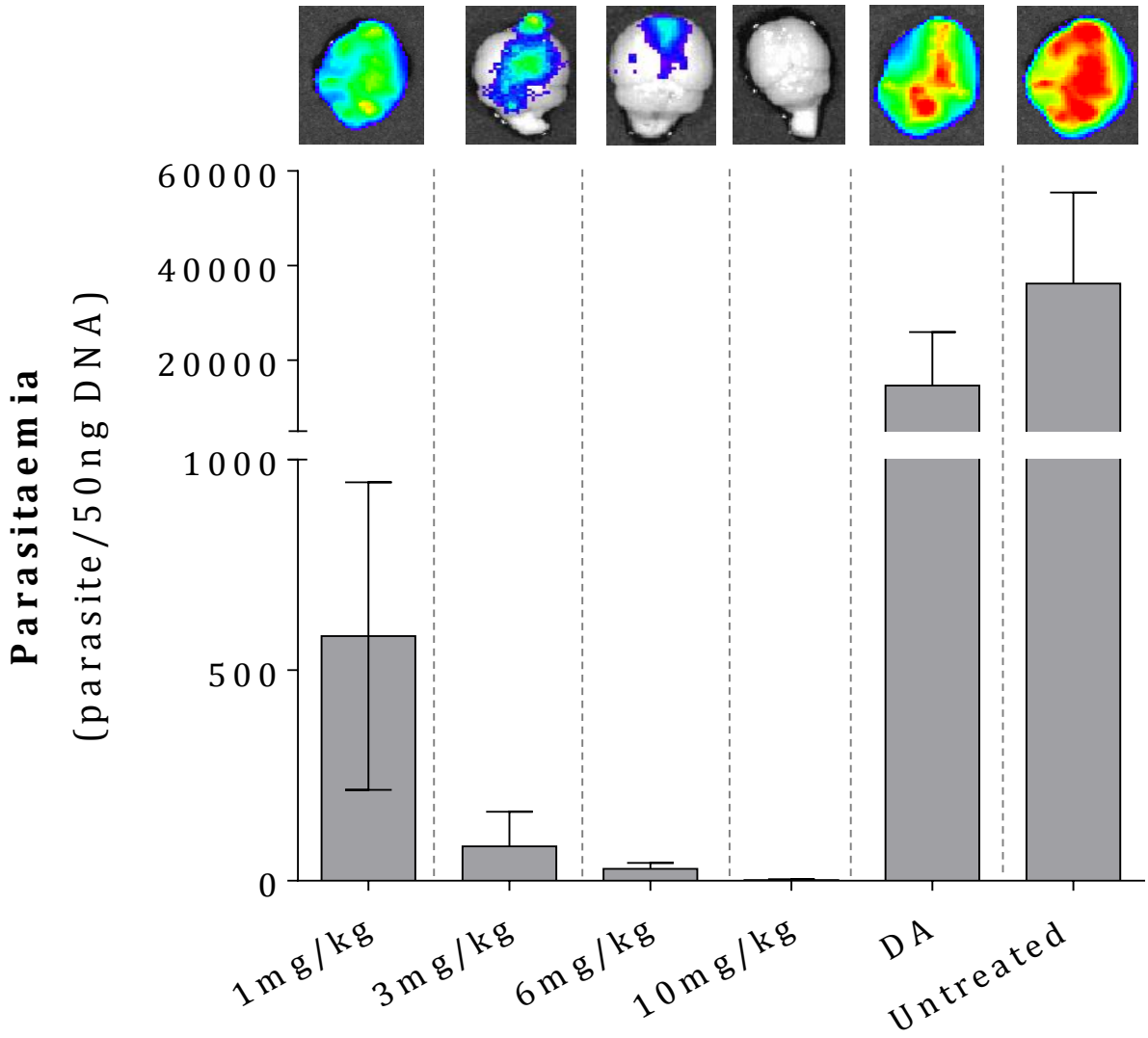

4.4 *Ex vivo* imaging and parasite burden of excised brain. Brains were removed after perfusion and brain homogenates from each of the mice from 4.3 were extracted for DNA and analysed using qPCR. Graph shows mean of six mice ± SD of the number of parasites in 50 ng of DNA. The detection limit of the qPCR was 50 trypanosomes/50 ng of DNA.

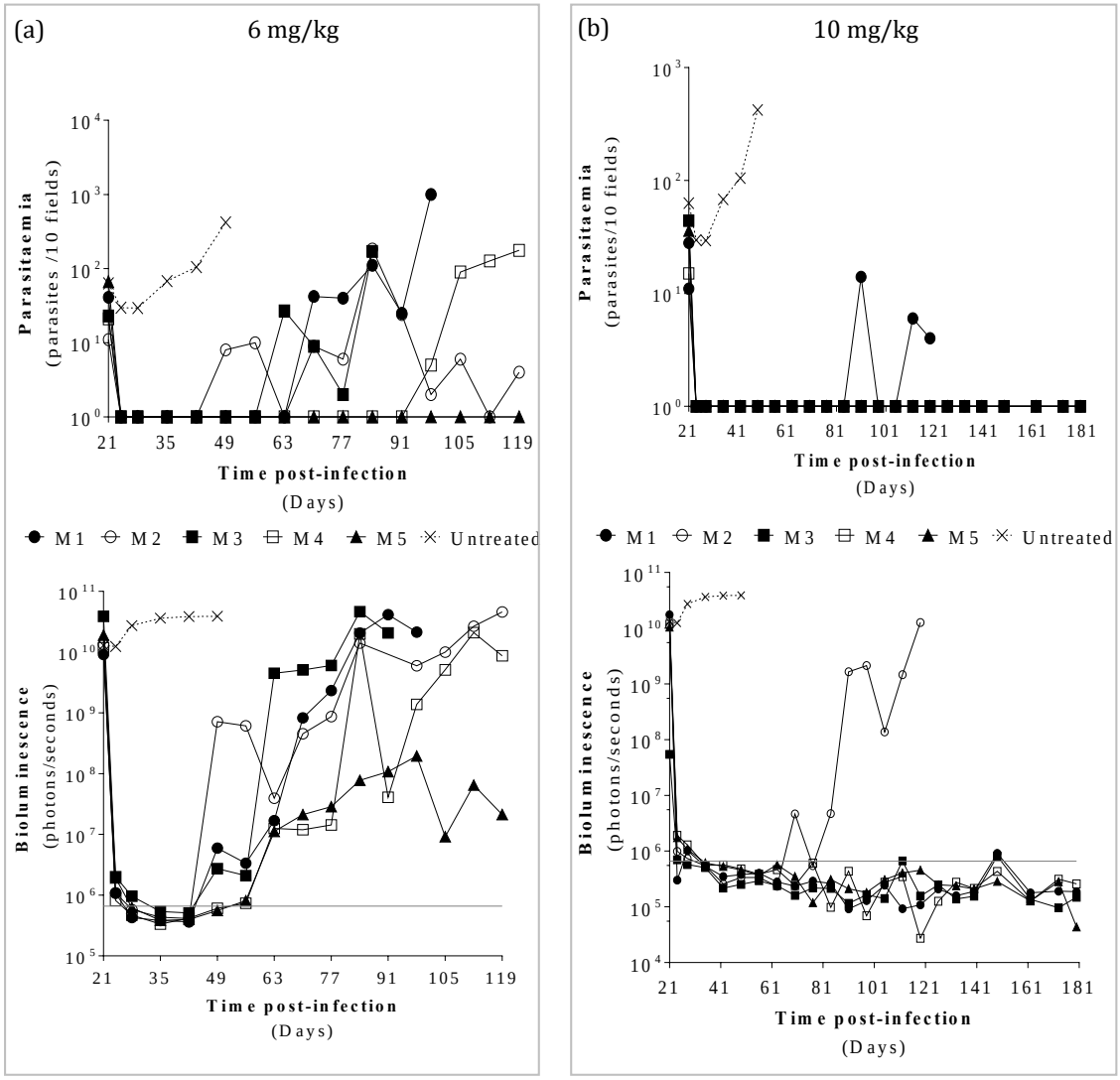

4.5 Drug relapse analysis. Early detection of drug relapse of melarsoprol using VSL-2. Mice infected with VSL-2 via the intravenous route were imaged and blood filmed at weekly intervals post-dose of melarsoprol. Graphs show the bioluminescence and peripheral parasitaemia from a group of five mice (M1, M2, M3, M4, and M5) dosed with (a) 6 mg/kg melarsoprol and (b) 10 mg/kg melarsoprol.

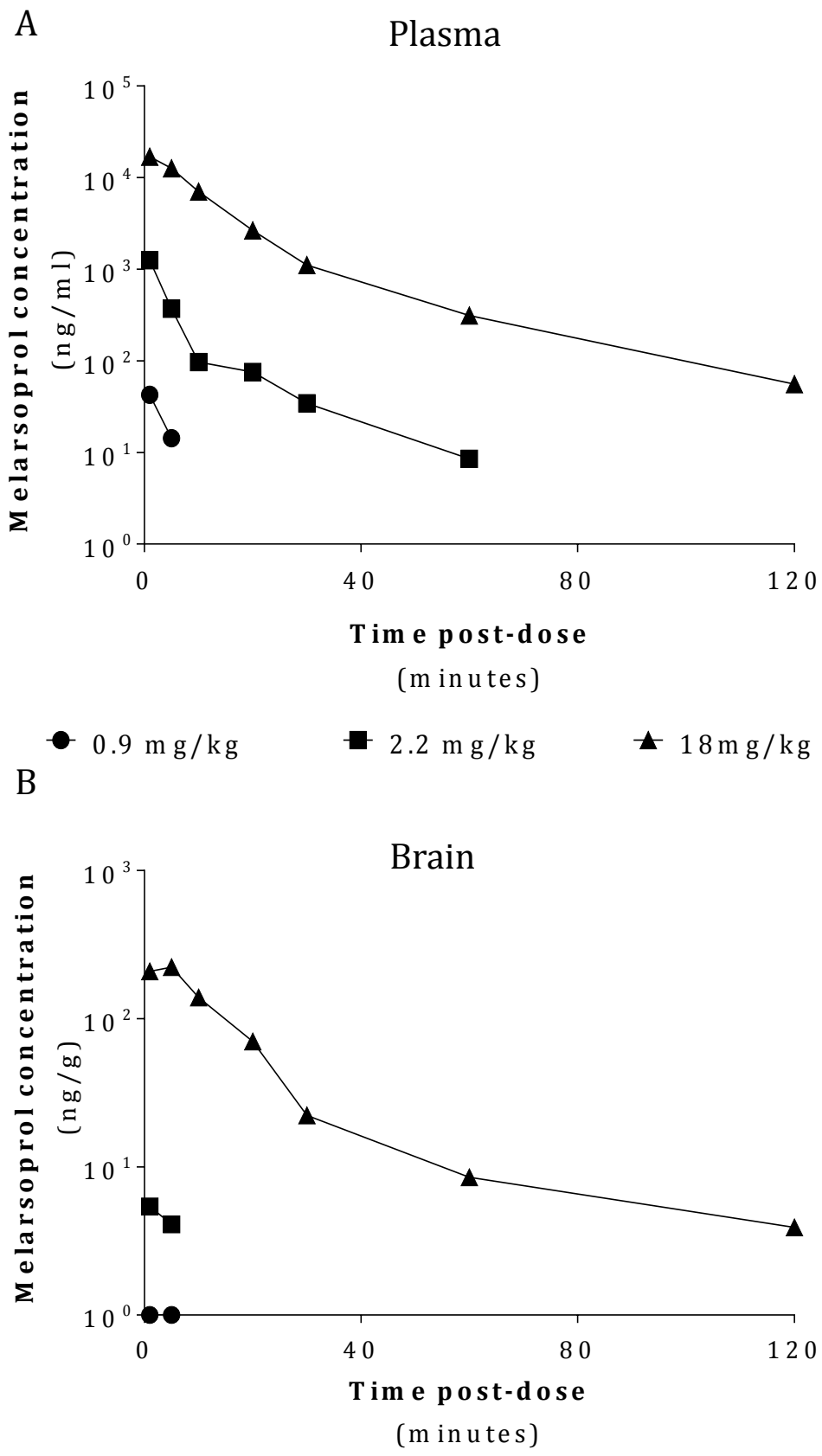

Figure 4.6 Dose ranging studies of melarsoprol. A dose range of melarsoprol was administered intravenously and melarsoprol concentrations determined via LC-MS/MS. (A) Shows the decreasing concentration of melarsoprol in plasma of the three doses over 120 minute period. (B) Shows the decreasing concentration of melarsoprol in brain for 18 mg/kg and 2.2 mg/kg doses over 120 minute period.

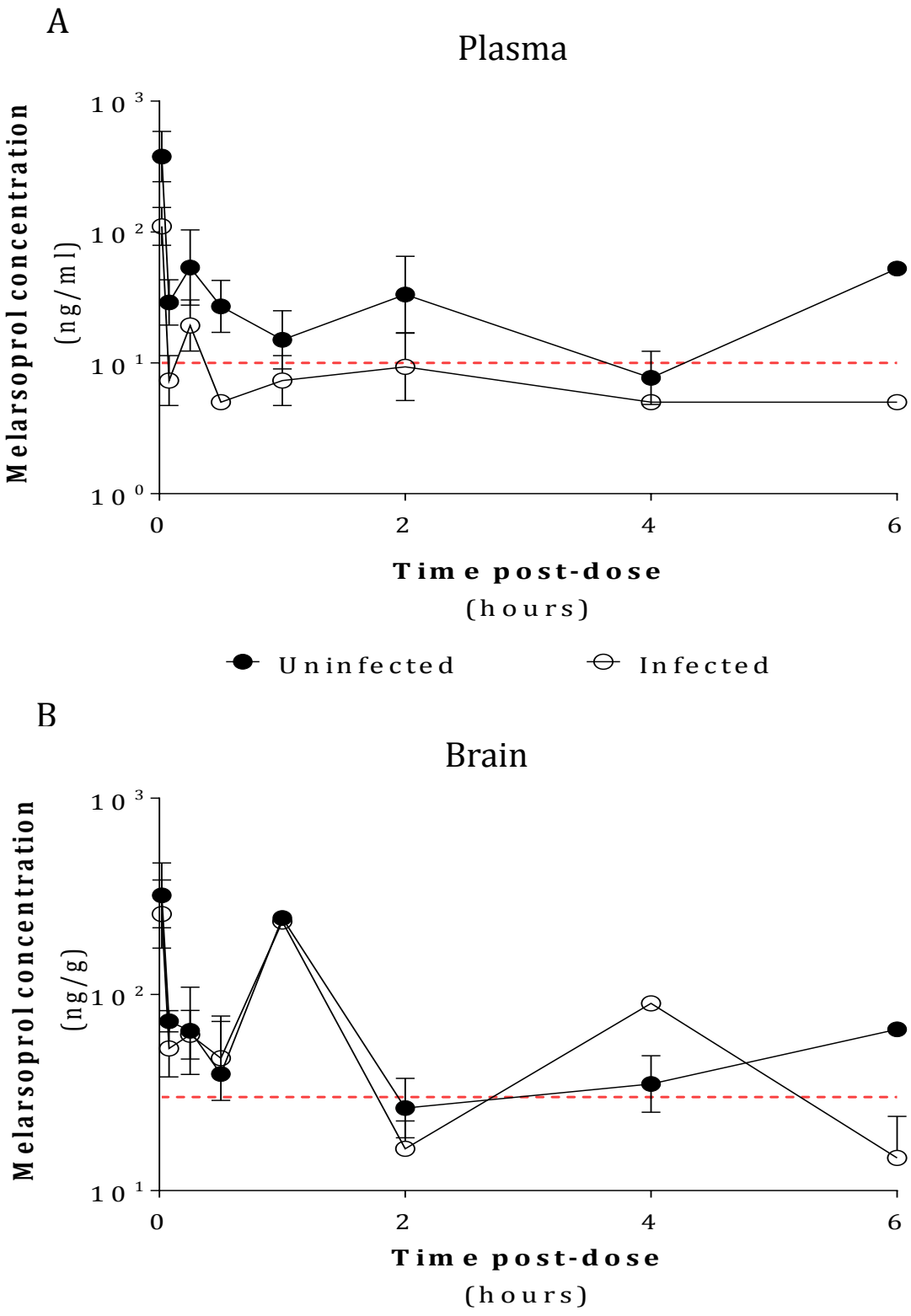

Figure 4.7 Pharmacokinetic study of melarsoprol in VSL-2 infected and uninfected mice. Mice dosed with 10 mg/kg were culled at time points 1, 5, 15, 30 minutes, 1, 2, 4 and 6 hours post dose. Drug was extracted from plasma and brains and analysed through LC-MS/MS. (A) Concentrations of melarsoprol in plasma (central compartment) over 6 hours in infected and uninfected mice. The lower limit of quantification (LLOQ) was 10 ng/ml (indicated by dotted red line). (B) Brain concentration of melarsoprol in infected and uninfected mice. The LLOQ was 30 ng/g (indicated by dotted red line).

CHAPTER 5: Bioluminescence as a tool for detection of early drug treatment failure with nifurtimox and DFMO

5.1 Introduction

Since its introduction in 2009, the first line drug for the treatment of gambiense late-stage HAT has been the co-administration therapy NECT (nifurtimox and eflornithine combination therapy) (Simarro, 2011). Prior to the inclusion of NECT onto the WHO Essentials Medicine List there had been no new or improved treatment options for HAT for 25 years (Stein *et al*., 2014).

Nifurtimox is a 5-nitrofuran pro-drug (Fig 5.1), produced by Bayer under the brand name Lampit®. As a monotherapy, nifurtimox produced disappointing results with 63 % of patients relapsing after treatment with a high frequency of adverse reactions (Pepin *et al*., 1989, Bisser *et al*., 2007). Because of this, nifurtimox currently remains un-registered as a monotherapy treatment of HAT (Burri, 2004).

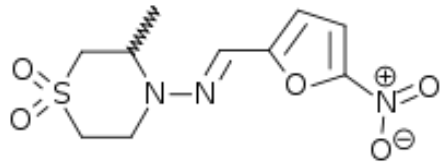

Fig. 5.1 Structure of Nifurtimox. (Source: http://en.wikipedia.org/wiki/File:Nifurtimox.svg)

The mechanism of action of nifurtimox is still largely unknown. Recently, studies have shown that as a prodrug it requires activation by a nitroreductase (NTR) in the *T. brucei* parasite (Hall *et al*., 2011). Type 1 NTRs are predominantly found within bacteria (although in rare cases they have been found in eukaryotes) and facilitates the nitroreduction of the nitro groups found in nitroheterocyclic drugs (Hall *et al*., 2011). The presence of type 1 NTR in trypanosomes results in the trypanocidal selectivity of nifurtimox, as although mammalian cells have the oxygen-sensitive type II NTR, studies by Hall *et al* have shown that it is the type I NTRs that are responsible for the metabolism of nifurtimox (Hall *et al*., 2011).
The type I NTR present in the mitochondria of the trypanosome reduces nifurtimox to a reactive nitrile derivative, which induces a trypanocidal effect, the mechanism of which is still under investigation. (Hall *et al*., 2011, Croft, 1999).

In early studies of nifurtimox monotherapy against melarsoprol-relapsed HAT (when melarsoprol treatment had failed), a range of doses and treatment durations were attempted, but adverse reactions (including vomiting, insomnia and headaches) occurred which appeared to be both dose and duration dependent (Bisser *et al.*, 2007).

Prior to the introduction of NECT, DFMO (eflornithine) was the only alternative to melarsoprol treatment-failures in gambiense infections. The use of DFMO in the treatment of rhodesiense infections is strongly discouraged due to the drugs poor efficacy to the strain (Burri, 2004).

DFMO is an analogue of the amino acid ornithine (Fig. 5.2) and is an irreversible inhibitor of ornithine decarboxylase (ODC), which is responsible for polyamine biosynthesis (Burri, 2004).

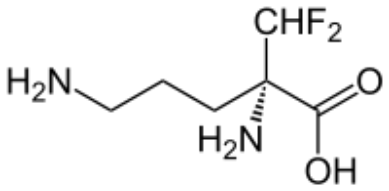

Fig. 5.2 Structure of α-difluoromethylornithine (DFMO) (Source: http://en.wikipedia.org/wiki/Eflornithine)

The mechanism of action of DFMO against trypanosomes is well documented. It is understood that the disruption in polyamine synthesis by irreversibly inhibiting ODC results in a depletion of polyamines which are essential in the process of growth and multiplication within the trypanosomes. The inability of the trypanosome to proliferate, in combination with damage caused by the depleting polyamines eventually causes the trypanosomes to differentiate to the non-replicating stumpy form, leaving the parasite open to attack from the host immune system. In addition to the disruption in polyamine biosynthesis, changes occur in cellular levels within trypanosomes. After DFMO treatment an increase in levels of S-adenosyl methionine (hindering the proper methylation of proteins, nucleic acids and lipids) and a depletion of trypanothione has been observed, both of

which may result in the parasite becoming more susceptible to oxidative stress (Yarlett and Bacchi, 1988, Fairlamb *et al*., 1987).

The ODC enzyme is found in all eukaryotic cells, but within mammalian cells ODC has a rapid turnover of between 10-30 minutes. The slow turnover rate of between 18-19 hours in *T. b. gambiense* is thought to be why the drug is so effective and non-toxic. In comparison, *T. b. rhodesiense* has a much higher turnover rate (half-life of 4.3 hours), which is believed to be why DFMO is ineffective against this strain (Barrett *et al*., 2007, Babokhov *et al*., 2013).

DFMO was introduced as a first-line monotherapy treatment for gambiense HAT in 1990 after nearly a decade of clinical trials (Milord *et al*., 1992). Field studies carried out by Medécins Sans Frontières (MSF) in 2000 found that despite the drug being free-of-charge, few patients were treated with it. This was due to a lack of necessary equipment needed for intravenous infusion administration (catheters, bags of sterile water, needles etc.) being available. To overcome this issue, WHO provided free kits to include all essential items as well as the drug. DFMO monotherapy was considerably more expensive, with estimated costs of $350 per person for the drug alone (Burri, 2004).

The combination NECT has greatly reduced the length of DFMO treatment required. A daily dose of 400mg/kg is still required but can be carried out over two i.v infusions and for only 7-days (as opposed to the original 14), combined with oral tablets of nifurtimox at 15mg/kg for 10days. This combination has been shown to have a cure rate of approximately 98% and the use of a combinational therapy greatly reduces the risk of drug resistance occurring (Priotto, 2006).

The cost and ability to transport NECT to remote rural areas makes the treatment far from ideal, as the current NECT kit provided by WHO to treat four patients (includes all necessary items for DFMO infusion as detailed above, and the drugs) weighs approximately 39kg, making it logistically impractical to transport (Eperon *et al*., 2014).

Both nifurtimox and DFMO present challenges when used for *in vivo* studies. The use of intravenous infusions within mice is not possible and, as previously discussed, nifurtimox has shown poor efficacy against the parasite. In this chapter we use bioluminescence to determine whether the activity of either of these two poorly efficacious drugs can be detected in the VSL-2 model of late-stage HAT.

5.2 Aims and objectives

- Bioluminescence imaging (BLI) can demonstrate the dose dependent effect of the monotherapy regimes of DFMO and nifurtimox
- Investigate the limitations of the model by assessing poorly efficacious drugs

5.3 Contributors

All work within this chapter was carried out solely by the author, with consultation from Dr. Hatem Sallam regarding dose ranges for eflornithine.

5.4 Results

We have demonstrated in the previous chapter that BLI can be used to show the effect of drugs on parasite burden. Here we assess the trypanocidal activity of DFMO and nifurtimox monotherapies within the bioluminescence model.

5.4.1 DFMO monotherapy against late-stage trypanosomiasis

VSL-2 infected mice were dosed intravenously with DFMO at 200, 400, 800 and 1000 mg/kg for four days as detailed in Table 2.1. Doses were chosen as the maximum tolerable dose for intravenous administration, determined by carrying out a dose setting experiment (data not shown). Mice were imaged at D21 (pre-treatment), D24, D28 and D35 (Fig 5.3). The imaging data indicated that the treatment regime used for DFMO was not effective in reducing parasite burden.

For all doses of DFMO the bioluminescence did not decrease after treatment, with a rise in bioluminescence intensity visible from D28 to D35 in all doses, producing saturated images. In contrast the DA treated mice had an immediate drop in

bioluminescence at D24 which further decreased to produce a focal bioluminescence signal in the head region.

The quantification of the bioluminescence (Fig 5.4) parallels the imaging data. All groups of mice had approximately the same bioluminescence throughout the experiment at 10^9 to 10^{10} photons/second. Despite the increase in doses, the bioluminescence is equivalent to that of the untreated mice until D35 when the treated mice had a bioluminescence of $\sim 2 \times 10^{10}$ photons/second. In contrast the untreated mice had a bioluminescence at 6.4×10^9 photons/second. As with the qualitative imaging data, the bioluminescence in the DA treated mice dropped after treatment from 2.9×10^9 photons/second to just above background at 9.9×10^5 at D28. It then proceeded to increase to 4.4×10^6 photons/second as the signal appeared in the head region of the mice.

5.4.2 Nifurtimox monotherapy against late stage trypanosomiasis

Mice infected with VSL-2 were treated with a dose of nifurtimox at 200 mg/kg for four days via the oral route. The dose was chosen on the advice of Dr. Hatem Sallam to provide a high but tolerable dose that could provide anti-trypanosomal activity. (Table 2.1). Mice were imaged at D21 pre-treatment, at D24 (the end of treatment) and then at D28 and D35 (Fig 5.5). After treatment the bioluminescence did decrease with partial clearance within the whole animal. A reduction in bioluminescence in the lower back region was visible, with the highest level of bioluminescence being present in the snout of the mouse. By D28, the bioluminescence had disseminated throughout the mice with larger areas of signal being present around the head and lower back regions. At D35 all mice had relapsed with a total dissemination of bioluminescence throughout the animal. The control groups of DA (CNS control group) and the melarsoprol (MelB) treated group (drug control) had a reduction in bioluminescence after treatment, with MelB treated mice remaining clear until the end of the experiment. The DA mice had a clear focal bioluminescence signal present in the head from D25 until D35, at which point low levels of signal were also present on the back of the mouse.

The ROI data acquired from the images (Fig 5.6) shows that after nifurtimox treatment the bioluminescence drops from 6.6×10^9 photons/second to 2.4×10^8

photons/second. The bioluminescence then gradually increased over the 11-days, returning to the starting bioluminescence prior to treatment of 6.2 x 10^9 photons/second.

5.5 Discussion

In the previous chapter we showed that the dose dependent effect and relapse of a drug can be detected through BLI. By assessing the monotherapies of nifurtimox and DFMO with BLI we are able to show how the bioluminescence model of VSL-2 can be used in the study of less efficacious trypanosomal drugs.

The use of DFMO in the treatment of HAT involves a long, complex regimen consisting of a continuous 14-day treatment of intravenous infusions of 100 mg/kg every six hours (Matovu and Mäser, 2010). This method of treatment is impossible to mimic in the animal model due to ethical restrictions. The original studies carried out by Bacchi *et al* administered DFMO to mice in drinking water (after being deprived of water for 12 hours). By using this method, mice were continuously exposed to the drug therefore enabling constant drug levels to be established (Bacchi *et al*., 1983). However this method of administration makes it difficult to determine the exact dose each mouse receives, and in cases of treatment failures it is impossible to determine if individual mice received the same dose as other animals in the group. Based on this we chose to administer DFMO via a single intravenous injection daily to enable controlled administration with improved bioavailability (oral bioavailability of DFMO is ~ 50%) (Burri, 2004).

The limited trypanocidal efficacy of nifurtimox in humans as well as the adverse reactions, prevented this drug from being used as a monotherapy treatment (Barrett *et al*., 2007). Pharmacokinetic studies showed that the serum levels of nifurtimox after oral administration are low, with a half-life elimination of only three hours. The accumulation of nifurtimox across the BBB is also poor at only 50% of that of serum levels (Burri, 2004). This explains why nifurtimox had a poor efficacy within this study. Despite the poor efficacy, BLI was still able to detect the low trypanocidal activity.

The additive effect of NECT was discovered by Priotto *et al*, when a number of different drug combinations were tested in field clinical trials (Priotto, 2006). Many of the dual treatments produced a toxic effect (melarsoprol with DFMO and melarsoprol with nifurtimox), but the combination of NECT produced an additive effect by reducing adverse reactions, but also produced cure rates equivalent to monotherapies (Priotto, 2006).

It was shown that nifurtimox induced oxidative stress in the trypanosome (although the exact mechanism is unknown), and DFMO reduced levels of trypanothione which has been shown to protect the pathogen against oxidative stress. It is this combined effect which leads to the greater therapeutic nature of this dual drug treatment (Barrett *et al*., 2007).

The differences in bioluminescence and therefore parasite burden between NECT and the monotherapies, would ideally have been demonstrated in this study providing a conclusive data set for NECT treatment. However due to the problems of mimicking the DFMO dosing used in NECT treatment, as well as the poor effect of the single i.v administration in the monotherapy experiment, it was decided not to carry out a combination study.

The three *T. brucei* strains; *T. b. brucei, T. b. gambiense* and *T. b. rhodesiense* all share similar genetic and morphological profiles, which is one of the main reasons why *T. b. brucei* GVR35 is used as a predictive model of the human infection. As mentioned in chapter 1 it is important to establish that the use of predictive models still have limitations. Although the three strains show similarities, it is understood that *T. b. brucei* is closely related to the zoonotic *T. b. rhodesiense*. This close relationship could explain why DFMO in the GVR35 model is ineffective, as this strain may have a more rapid turnover of ODC than the gambiense strain, resulting in DFMO being unable to clear parasitaemia. In addition the single i.v daily dose, may not have been able to provide sufficient drug concentration levels in the plasma and brain to result in a trypanostatic effect. Despite this, GVR35 is currently the only model available for late stage HAT within an immunocompetent system, but care must be taken when extrapolating data to the human infection.

We have shown that despite GVR35 being a successful model of HAT (both in terms of gambiense and rhodesiense), there are limitations to its use when considering specific drug targets. Whilst it can be argued that GVR35 is not a true predictor of gambiense HAT in DFMO studies, the data described in this chapter shows that GVR35 mimics the action of DFMO in rhodesiense HAT infection.

With the use of bioluminescence, poor efficacy of both DFMO and nifurtimox was identified at early treatment stages. Although a reduction in bioluminescence, and therefore parasite burden, could not be detected using DFMO the study was still able to show how the bioluminescence model can be used to indicate treatment failures; with the ability to show varying degrees of efficacy as seen in the nifurtimox treatment group.

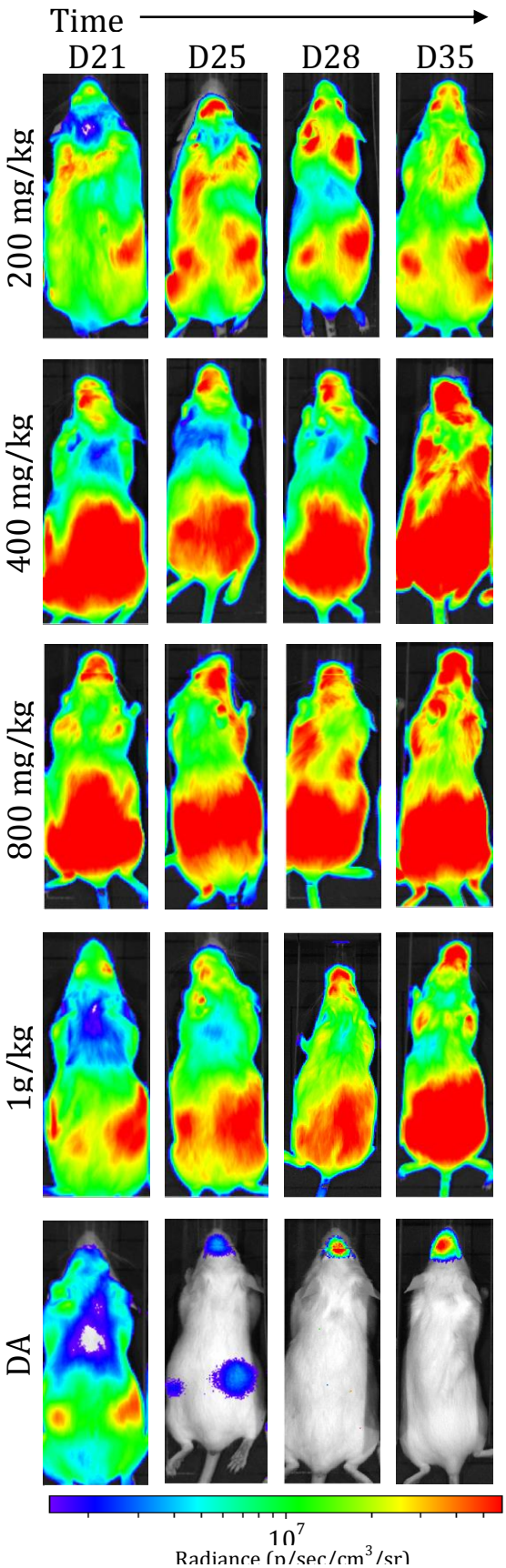

Figure 5.3. BLI evaluation of DFMO treated mice. Groups of six mice were infected with VSL-2 as described in 2.5.2, and at D21 were treated with DFMO at 1 g/kg, 800 mg/kg, 400mg/kg and 200mg/kg for 5 days i.v. A CNS control group treated with a single dose of DA at 40 mg/kg was included Mice were imaged at D21, D25, D28 and D35 post-infection. A single representative of groups is represented here against a heat-map scale.

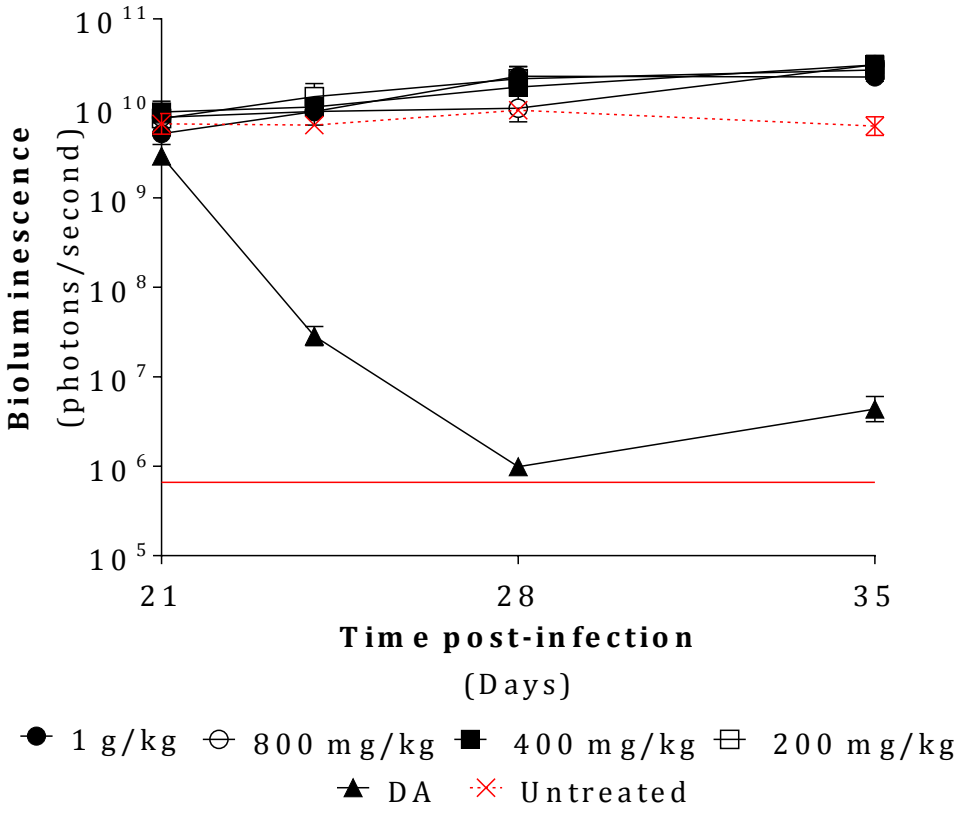

Figure 5.4 Bioluminescence after DFMO treatment. The average bioluminescence of the six mice per group from figure 5.3 was quantified using Living Image software. All data points are presented as mean ± SD**.** Red line indicates background bioluminescence determined by the BLI of a WT-infected mouse.

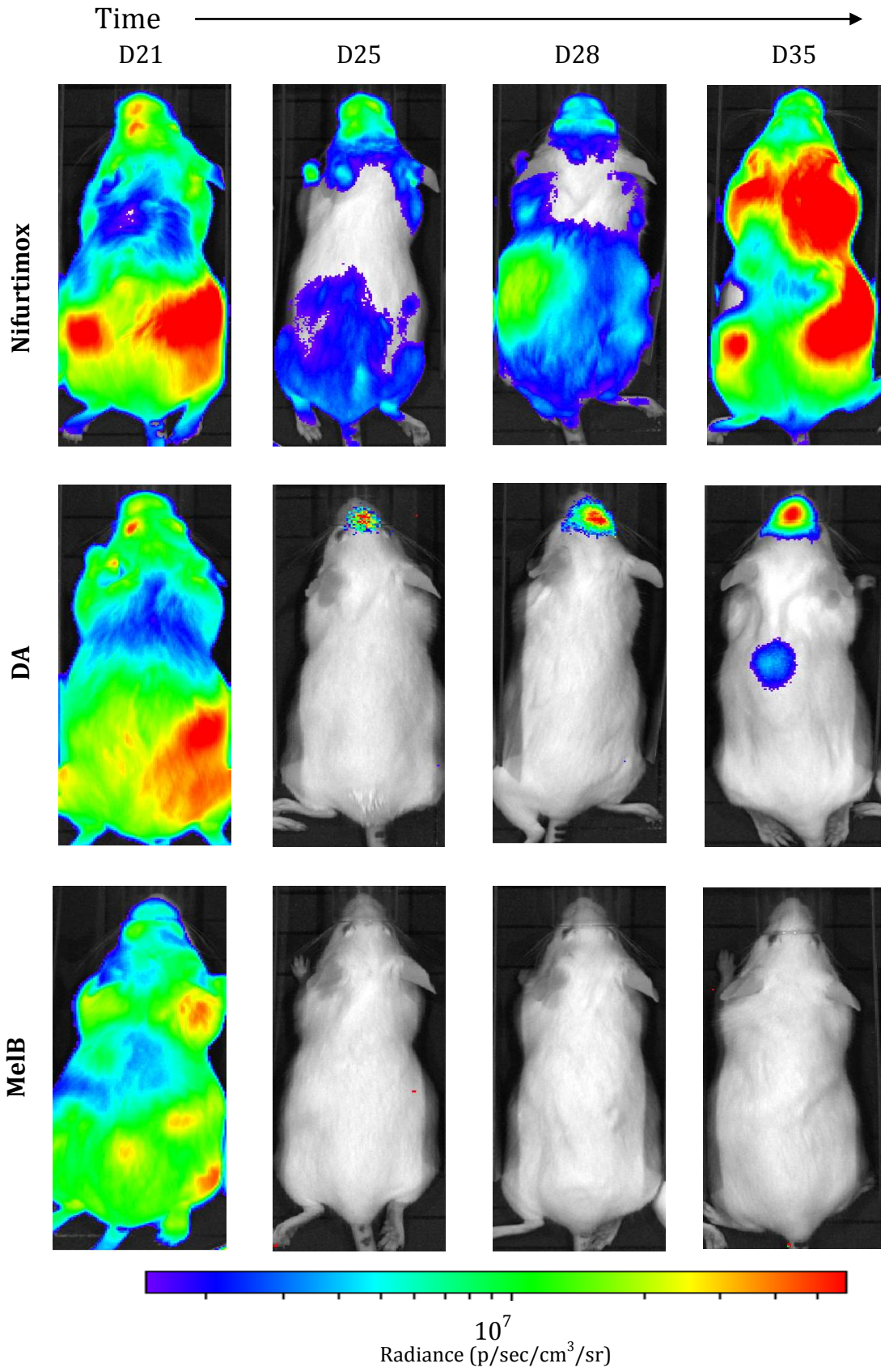

Figure 5.5 BLI evaluation of nifurtimox monotherapy Groups of six mice were infected with VSL-2 as described in 2.5.2, and at D21 were treated with Nifurtimox at 200 mg/kg for 4 days p.o. A CNS control group treated with a single dose of DA at 40 mg/kg and a drug control group of MelB treated mice (15 mg/kg for 3 days i.v) was included. Mice were imaged at D21, D25, D28 and D35 post-infection. A single representative of groups is represented here against a heat-map scale.

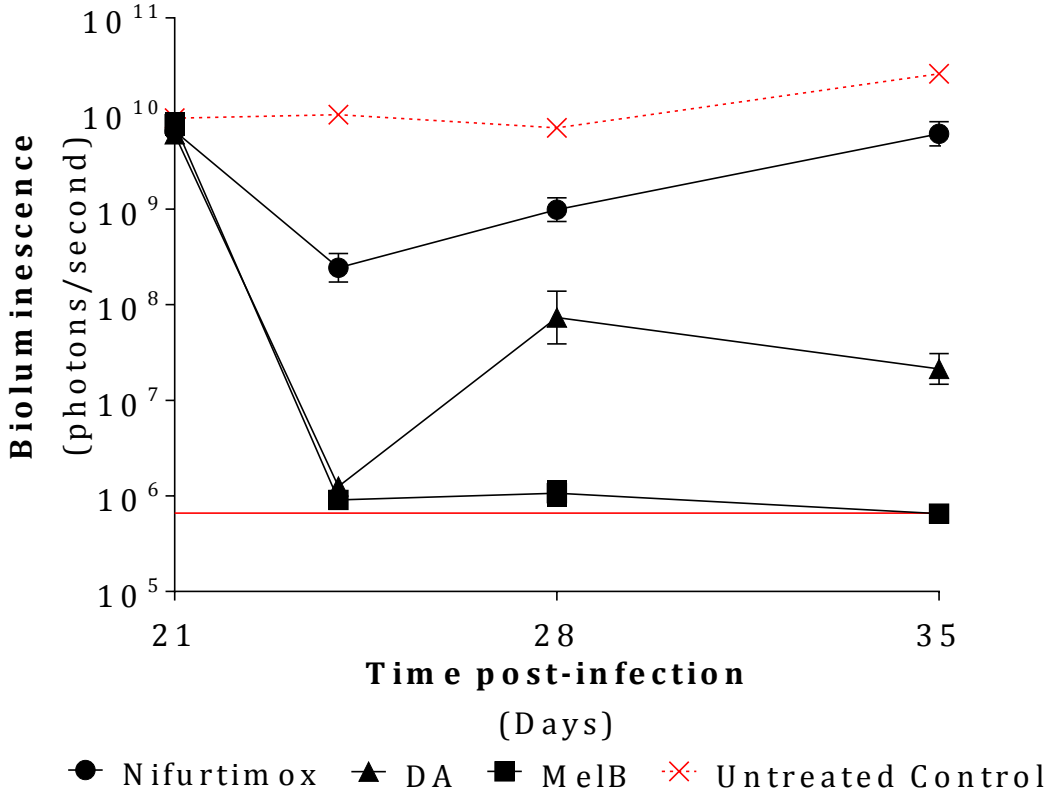

Figure 5.6 Bioluminescence after nifurtimox treatment. The average bioluminescence of the six mice per group from figure 5.5 was quantified using Living Image software. All data points are presented as mean ± SD. Red line indicates background bioluminescence determined by the BLI of a WT-infected mouse.

CHAPTER 6: Assessment of the dose dependent effect of fexinidazole using BLI model

6.1 Introduction

Fexinidazole looks set on becoming the newest addition to the family of HAT treatment therapies, but despite being in phase II/III clinical trials, fexinidazole is far from being a "new" drug (Tarral *et al*., 2014).

The nitroimidazole was re-discovered by the Drugs for Neglected Diseases initiative (DNDi) in 2005 through the use of compound mining, i.e. searching public and pharmaceutical drug databases for potential candidates (Mogk *et al*., 2014).

Fexinidazole was first in preclinical development as a broad-spectrum antiprotozoal agent in the 1970s and 1980s by Hoeschst AG (now Sanofi-Aventis). Its ease of chemical synthesis and the confirmation of *in vitro* activity against *T. brucei* in 1983 made it an ideal candidate in the treatment of HAT (Torreele *et al*., 2010). However, further development of the drug ceased as fexinidazole returned positive results in the Ames test (the mutagenic potential of new compounds based on a biological assay using bacteria), indicating potential toxicity (Torreele *et al*., 2010).

Despite this result DNDi felt that the compound needed further investigation due to current therapies (namely melarsoprol) exhibiting serious toxic effects in patients and therefore needing to be replaced. Studies carried out with Sanofi and the Swiss Tropical and Public Health Institute (Swiss TPH) in collaboration with DNDi re-evaluated the efficacy and preclinical profile of fexinidazole and found that, despite producing a positive result in the Ames test, it was shown not to be mutagenic to mammalian cells (both *in vitro* and *in vivo*) (Torreele *et al*., 2010).

Fexinidazole is a pro-drug and is rapidly metabolized into two active metabolites: fexinidazole sulfoxide and fexinidazole sulfone (Fig. 6.1) (Tarral *et al*., 2014)

Figure 6.1 Metabolism of fexinidazole. Fexinidazole (1-methyl-2-((p-(methylthio) phenoxy) methyl)-5-nitroimidazole is rapidly metabolized by oxidation by either cytochrome P450 (CYP) or flavin-containing monooxygenase (FMO) to produce the active metabolites sulfoxide and sulfone.

The mechanism of action of fexinidazole is currently unknown but research indicates that it has a similar action to other 5-nitroimidazoles by causing a negative redox potential within the trypanosome during the reduction to the sulfone and sulfoxide metabolites (Eperon *et al*., 2014).

The oral administration of fexinidazole has shown to cure acute (early stage) *T. b. rhodesiense* and *T. b. gambiense* in *in vivo* models with a four-day treatment regimen of 100 mg/kg/day. More importantly however, a five-day oral treatment regimen of 200 mg/kg/day provided cure in 7/8 mice for up to ~162-days before relapse occurred, using the late-stage GVR35 mouse model (Torreele *et al*., 2010).

Current phase II/III clinical trials are being carried out in Africa and are looking at fexinidazole treatment in comparison with the combinational therapy NECT in terms of safety and efficacy. The 10-day oral treatment regimen currently being studied is split in to two parts: the first consists of 1800 mg/day dose (3 x 600 mg tablet taken with food) for four days, followed by six days at 1200 mg/day (2 x 600mg to be taken with food). The trial will also look at dose ranging to determine if lower doses and shorter treatment regimens can be used (DNDi, 2014).

Compared to the current treatment therapy of melarsoprol, the doses involved in fexinidazole treatment are large. Melarsoprol treatment is currently 2.2 mg/kg x 10 days i.v, whilst NECT therapy is complex with a combination of nifurtimox tablets being administered three times a day (total 15 mg/kg/day) x 10 days in addition to twice daily two hour i.v infusions of 200 mg/kg of eflornithine. If fexinidazole is successful in clinical trials it will become the first oral drug for early and late stage HAT. This would enable effective treatment in rural endemic areas

where complex treatments requiring hospitalization are currently limiting the curing of the disease (DNDi, 2014).

To further validate the model and determine its usability as a drug assessment tool, studies were carried out with fexinidazole to identify if effective dose data could be obtained using bioluminescence imaging.

6.2 Aims and objectives

The main aim of this chapter was to compare the drug sensitivity of VSL-2 to the wild type (WT) GVR35 strain and to investigate the relationship between parasite and drug distribution using BLI and PK analysis. The following objectives were investigated:

- Bioluminescence can be used as a qualitative measure of drug efficacy in whole animal imaging and provide a qualitative example of a time-kill effect of the drug.
- Quantitative PCR can further confirm dose effect seen *in vivo* and *ex vivo* imaging of late stage infection.
- Determine that there is no significant difference in the drug sensitivity of fexinidazole in WT and VSL-2 infected mice.
- PK analysis on fexinidazole and active metabolites can provide information on the relationship of drug and parasite distribution.

6.3 Contributors

Within this chapter all *in vivo* experiments were carried out by the author including the preparation of samples for PK analysis. PK analysis was carried out by Dr. Andy Harris at Pharmidex, UK.

6.4 Results

6.4.1 Drug efficacy

VSL-2 infected mice were treated with a fexinidazole dose range of 7.4, 22.2, 66.7 and 200 mg/kg with six mice per dose (Table 2.1). The dose of 200mg/kg has been shown to be effective in mouse studies carried out by Torreele *et al* and was

therefore chosen to be the curative dose of this study (Torreele *et al*., 2010). Bioluminescence and parasitaemia were assessed prior to treatment at D21 p.i and then at D25, 28, 30 and 35 (Fig. 6.2).

The BLI data shows that after treatment (D25) 66.7 mg/kg and 200 mg/kg treated mice were the only doses able to clear the infection. At the lower doses of 7.4 mg/kg and 22.2 mg/kg, bioluminescence was detected immediately after treatment at D25. The bioluminescence in 7.4 mg/kg treated mice decreased after treatment (indicated as blue areas) but was still above background detection, whereas the 22.2 mg/kg treated mice exhibited an almost complete clearance in bioluminescence with just the highly vascular areas of the nose and feet having detectable signal. Three days later at D28, mice treated with the top doses of 66.7 and 200 mg/kg were still negative for detectable bioluminescence, indicating a clearance in trypanosome infection. Bioluminescence in mice treated with 22.2 mg/kg did not increase in intensity but dissemination through the mouse was present. Relapse of trypanosome infection occurred in the 7.4 mg/kg treated mice at D28 with disseminated bioluminescence similar to D21.

At the end of the experiment three of the four doses had relapsed, as shown by varying bioluminescence, indicating a dose dependent effect. The 66.7 mg/kg treatment group, despite presenting with no detectable bioluminescence seven days prior, had early stages of drug relapse with bioluminescence being present throughout the entire animal. Mice treated with 200 mg/kg presented with no bioluminescence at D35 indicating that the mice were clear of infection.

In order to quantify the dose dependent effect the average bioluminescence of each group was determined (Fig 6.3A). The quantification of the bioluminescence provided further evidence that BLI can provide dose effect data. All four doses showed an initial drop in bioluminescence from $\sim 10^{10}$ photons/second (p/s) to 2.8 x 10^9 p/s (7.4 mg/kg group), 8.5 x 10^7 p/s (22.2 mg/kg group) and to just above background at 1 x 10^6 for 66.7 mg/kg and 200mg/kg treated mice. Bioluminescence in the three relapsed doses (7.4, 22 and 66.7 mg/kg) increased as the infection reappeared from D28.

A rapid drop in bioluminescence from 10^{10} photons/second to below background detection of 6 x 10^5 photons/second was seen in the 200 mg/kg treated group, where it remained until the end of the experiment. The blood films (Fig 6.3B) also detected the initial drop in parasitaemia after treatment, with all treated groups except the low dose of 7.4 mg/kg (parasitaemia of 9 trypanosomes/ 10 f.o.v), exhibiting undetectable parasitaemia.
At D28, the 7.4 mg/kg treated group had a slight increase in parasitaemia to 28 trypanosomes/ 10-f.ov. Mice treated with 200 mg/kg of fexinidazole and DA remained blood-film negative until the end of the experiment.

At the end of the 35-day experiment both the VSL-2 and WT mice were culled and the perfused brains removed for qPCR analysis to determine parasite burden (2.10 for details). The excised brains of the VSL-2 mice were also imaged prior to freezing (Fig. 6.4). The BLI and qPCR data of the excised brains reflected what was seen in whole animal imaging: that the increasing doses of fexinidazole produced lower bioluminescence and a decrease in parasitic burden. As seen in chapter 4 in the study of melarsoprol, the BLI and qPCR data shows a strong correlation, indicating that bioluminescence can be used as a viable tool in CNS drug efficacy studies.

6.4.2 Comparison of VSL-2 and GVR35 WT

To determine if the VSL-2 model reacted with the same drug sensitivity as the established GVR35 WT strain a comparative study was carried out. Mice were split into two groups and infected with either the VSL-2 or the WT strain as detailed in 2.4.2. The mice were further sub-grouped and treated with four varying doses of fexinidazole (7.4, 22.2, 66.7 ad 200 mg/kg), six mice per dose per strain. At D35 p.i mice were culled and the parasite burden within the brain was determined by qPCR (Fig. 6.5).

At each dose there was no significant difference between VSL-2 and WT response to fexinidazole. At 66.7 mg/kg the difference between the two strains was greater with the VSL-2 strain having a burden of 439 trypanosomes/50ng of DNA whilst the WT had just over four times less parasites with a burden of 105

trypanosomes/ 50ng of DNA. The DA and untreated data for the VSL-2 and WT strains was impressive, with VSL-2 having a similar parasite burden to the WT.

6.4.3 Pharmacokinetic analysis of fexinidazole and metabolites.

A preliminary qualitative pharmacokinetic study to look at the relationship between dose and exposure of fexinidazole and metabolites was carried out within infected and uninfected animals. 3 mice per time point (8 time points) were treated with a dose of 200 mg/kg, and drug extractions from plasma and brain was analysed using LC-MS/MS. The data is presented as the mean peak area of the LC-MS/MS trace (Fig. 6.6).

The time-dependent plasma PK profile of infected mice, show that after fexinidazole administration there was an initial decrease as the drug was absorbed and distributed throughout the body. At one hour post-administration, approximately a 20-fold increase in fexinidazole occurred, before drug levels stabilized and decreased over the 21-hour period as the drug was metabolised. The fexinidazole plasma levels in the uninfected mice had a shorter peak (at 2 hours post dose) and a more rapid decrease and elimination of the drug occurred over the 21-hours. As the parent compound was metabolised, levels of both sulfoxide and sulfone gradually increased, with sulfone remaining at a constant concentration for 8 hours (providing a longer drug exposure) before being gradually metabolised.

The time-dependent profile within the brain showed that unlike the levels of fexinidazole in plasma, the drug level is 2-fold higher in the uninfected brain than the infected brain. At the beginning of sampling (T0) both the uninfected and infected brains have low levels of drug (< 10000) before a 6-fold and 2-fold increase for the uninfected and infected brains respectively. The drug is then rapidly eliminated with the infected brain retaining a longer exposure at 2-4 hours than the uninfected brain. The profiles of both of the metabolites within the brain mimicked the plasma profile but approximately 10-fold lower.

6.5 Discussion

Earlier chapters within this study have shown the sensitivity of the VSL-2 model and its ability to detect early drug relapse and cure. Presently there is no reliable method to determine dose dependent effect in real-time late stage HAT. In support of the data found in chapter 4 we show that a clear dose effect can be determined through both BLI and qPCR.

When determining the pharmacodynamics-pharmacokinetic (PK/PD) parameters of a new anti-protozoal, studies predominantly look at the static approach of an MIC (minimum inhibitory concentration, the lowest concentration required to inhibit growth) which is often determined with an endpoint *in vitro* assay (Mueller *et al*., 2004).

Pro-drugs tend to perform poorly in *in* vitro assays as the process of metabolism into the active metabolites is hindered *in vitro*. Studies on the *in vitro* efficacy of fexinidazole, for example, indicated a moderate activity of 0.1 – 0.8 μg/ml against *T. b. gambiense* and *T. b. rhodesiense*. However *in vivo* studies against the acute and chronic stages found that doses of 100 and 200 mg/kg/day produced cure (Torreele *et al*., 2010), which mirrors what this study found in the dose dependent studies with the VSL-2 line.

By determining parasite clearance *in vivo* the active metabolites are taken into consideration providing a better understanding of the drug effect in infected patients.

The use of static PK/PD models to evaluate preclinical drug profiles has not accounted for drug-parasite interactions or how well the drug distributes through both the plasma and tissue (Nielsen *et al*., 2007). By using a dynamic model that looks at the relationship between drug distributions within the plasma and tissue and the rate-of-kill of a drug (concentration and/or time dependent), an understanding of drug-exposure can be established (Mueller *et al*., 2004). By using the bioluminescence model to detect the dose dependent effect of fexinidazole the time-kill properties of the drug during a real-time infection can be assessed, as the

non-invasive nature of BLI allows infected mice to be imaged a number of times post dose.

The preliminary PK profiles of fexinidazole and the metabolites in both the plasma and brain showed that fexinidazole and metabolites were able to pass through the blood brain barrier at levels similar to that of the plasma. It also showed that as the fexinidazole was metabolised, the levels of both sulfoxide and sulfone increased, with sulfone having a longer exposure time than sulfoxide, supporting previous studies by Tarral and Torreele that sulfone is the more active of the metabolites (Tarral *et al*., 2014, Torreele *et al*., 2010). The profiles also showed that the slow elimination of the 200 mg/kg dose of fexinidazole would result in the parasite being exposed to the drug for up to 24 hours, meaning that daily dosing regimens are possible. Whilst exact concentrations of the drugs cannot be determined from this study, further experiments are currently underway. Studies are also in progress to determine the concentrations of fexinidazole and metabolites in regions of the brain using microdialysis. This data as well as the quantitative PK analysis can provide information on how much drug is present in the brain and how well it is distributed. The microdialysis data of drug distribution in the brain can then be compared to parasite distribution in the brain by using BLI of brain slices. Providing a better understanding of the relationship between drug exposure, parasite distribution and rate of kill.

Fexinidazole has also shown promising results in other kinetoplastid diseases, with its efficacy being assessed against Chagas and leishmaniasis. Studies carried out on Chagas disease found that the active metabolites of sulfoxide and sulfone were more effective in treating an acute *in vivo* mouse model of *T. cruzi* than the parent drug (Bahia *et al*., 2014). In visceral leishmaniasis both fexinidazole and its metabolites were shown to be orally effective with a good distribution and absorption of the drug in the target organs of the liver and spleen (Wyllie *et al*., 2012). Both preliminary studies indicate that fexinidazole could be a potentially useful new oral treatment for the kinetoplastid diseases.

This chapter also addresses the issue of whether the transfection of luciferase in the parasite affected its drug sensitivity. This is especially important in drug

models where the death of the transfected pathogen may cause an up-regulation of cellular markers. If the luciferase is located within an up-regulated marker, an overexpression of luciferase may occur and thereby produce a false positive (high bioluminescence despite the pathogen dying).

We have shown here that under drug pressure the VSL-2 strain reacts to the same drug sensitivity as the WT, with no significant difference at any of the doses. This provides evidence that VSL-2 can be used to replace the current drug evaluation model T. *b. brucei* GVR35.

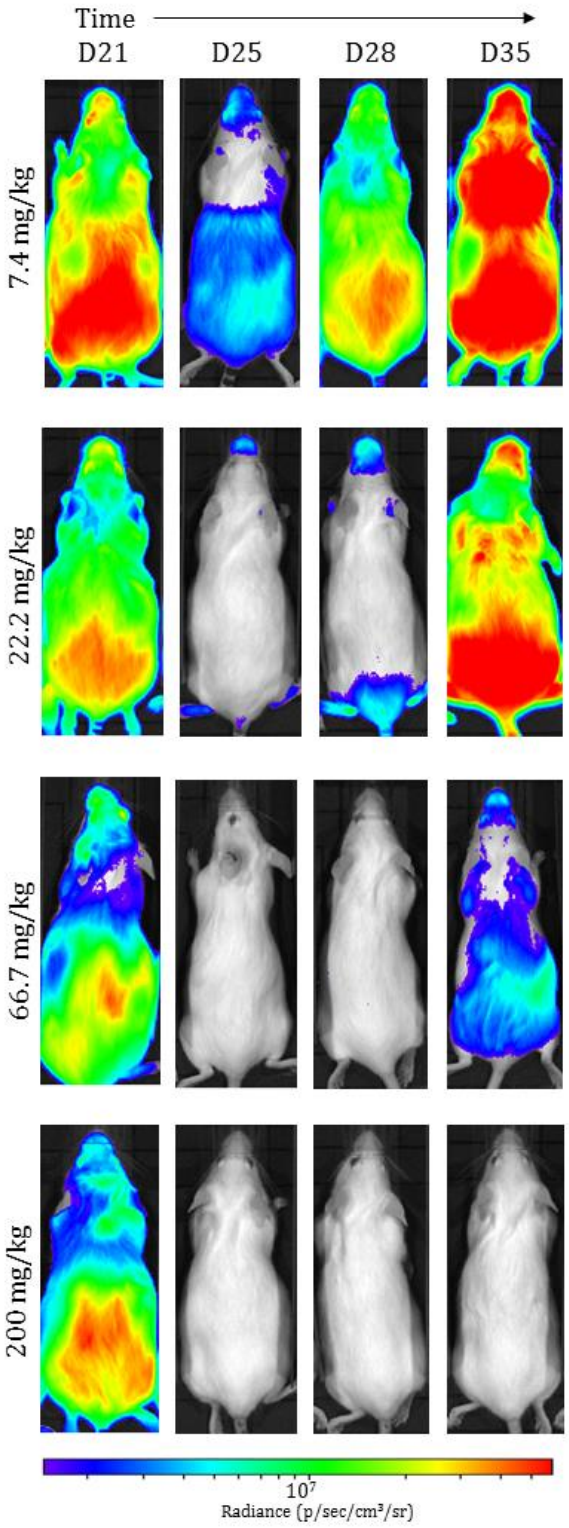

Figure 6.2 Dose effect determined by bioluminescence. Determining fexinidazole drug efficacy using bioluminescence and qPCR. Infected CD1 mice were split into groups of six and treated with varying doses of fexinidazole from D21 and monitored until D35. (a) A single representative mouse (1 mouse from group of six) from each dose, showing bioluminescence on a heat map scale (red representing maximum flux) before and after treatment.

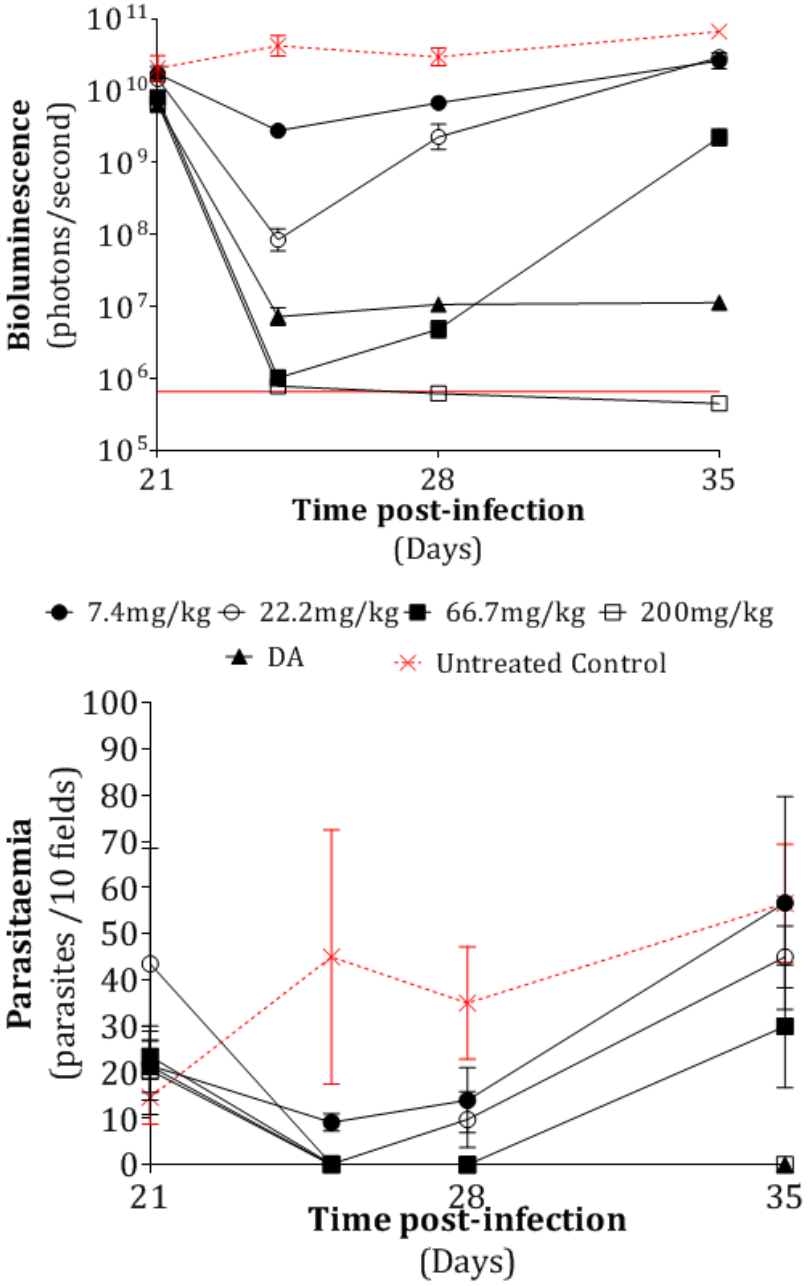

Figure 6.3 Quantification of bioluminescence and parasitaemia The average (of six mice) quantification of total flux and parasite number. (A) Each data point is a mean ± SD of the bioluminescence analysis as determined by the ROI of the whole animal as detailed in 2.5.4. Red line indicates background bioluminescence determined by the BLI of a WT-infected mouse. (B) The average microscopic counts from Giemsa-stained blood films, each data point is a mean ± SD.

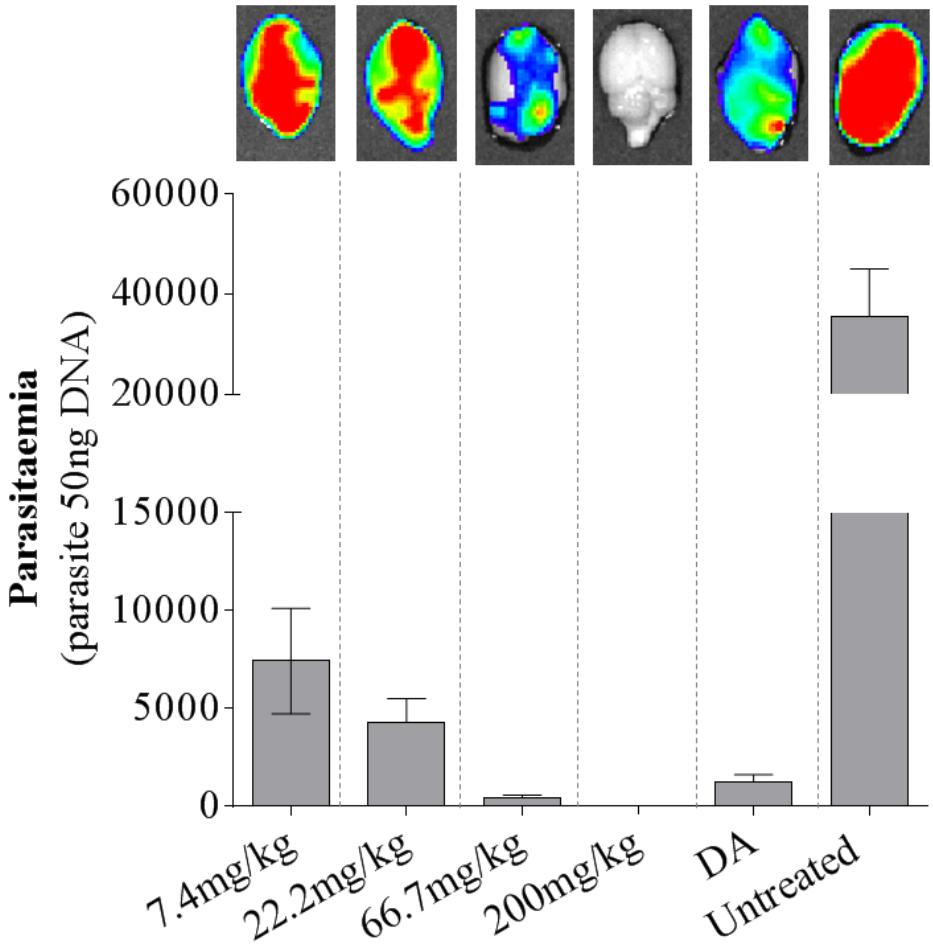

Figure 6.4 *Ex vivo* imaging of perfused brain and related qPCR Parasite burden determined by brain homogenates from each of the mice from 6.2 were extracted for DNA and analysed using qPCR. Graph shows mean of six mice ± SD of the number of parasites in 50 ng of DNA. *Ex vivo* images were obtained by adding 50 µl of luciferin to perfused brains and imaging using the IVIS Lumina. The detection limit of the qPCR was 50 trypanosomes/50 ng of DNA.

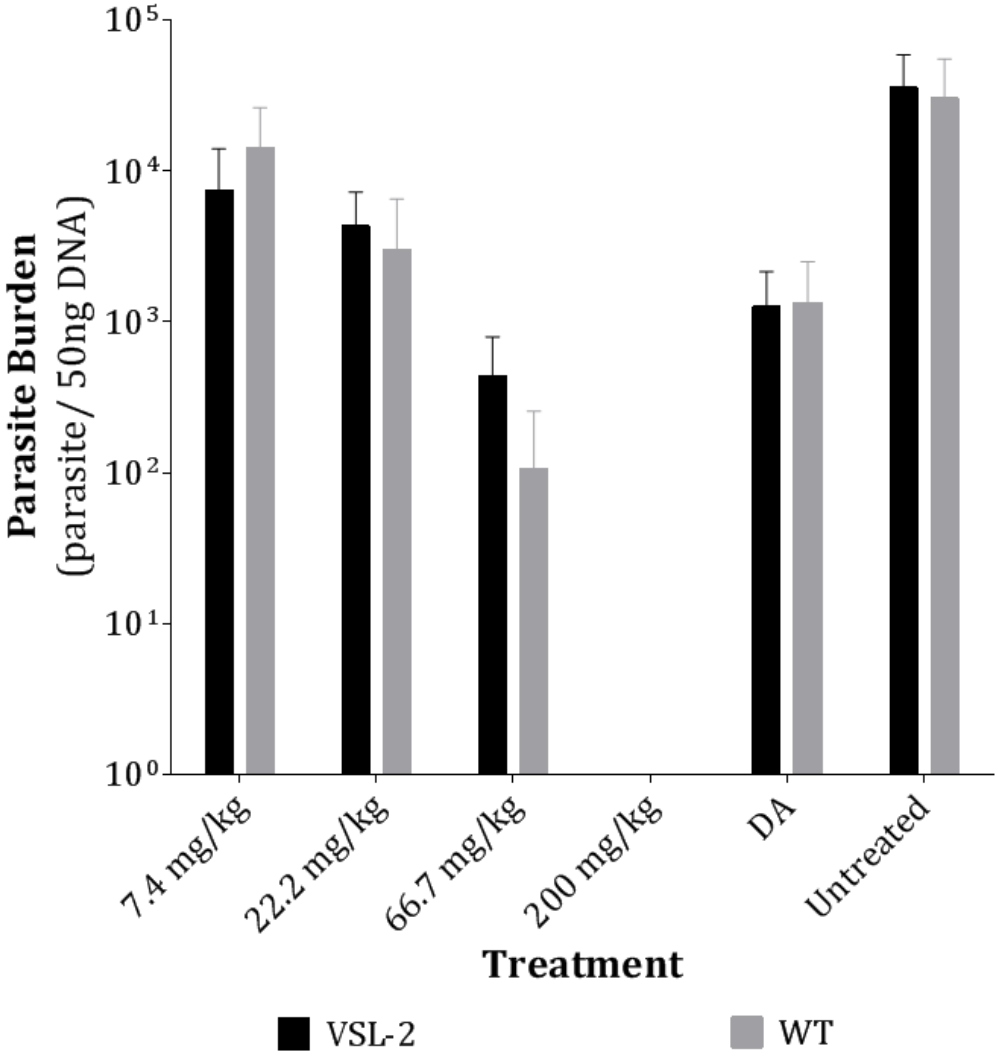

Figure 6.5 Drug sensitivity of VSL-2 vs WT after fexinidazole treatment The parasite burden was determined using qPCR and calculated as the number for trypanosomes/ 50 ng of DNA (as quantified by Nanodrop of extraction). A two-way ANOVA analysis to determine if the difference between the two strains and at each dose was significant. Between each data set it was found to not be significant with a p-value > 0.05.

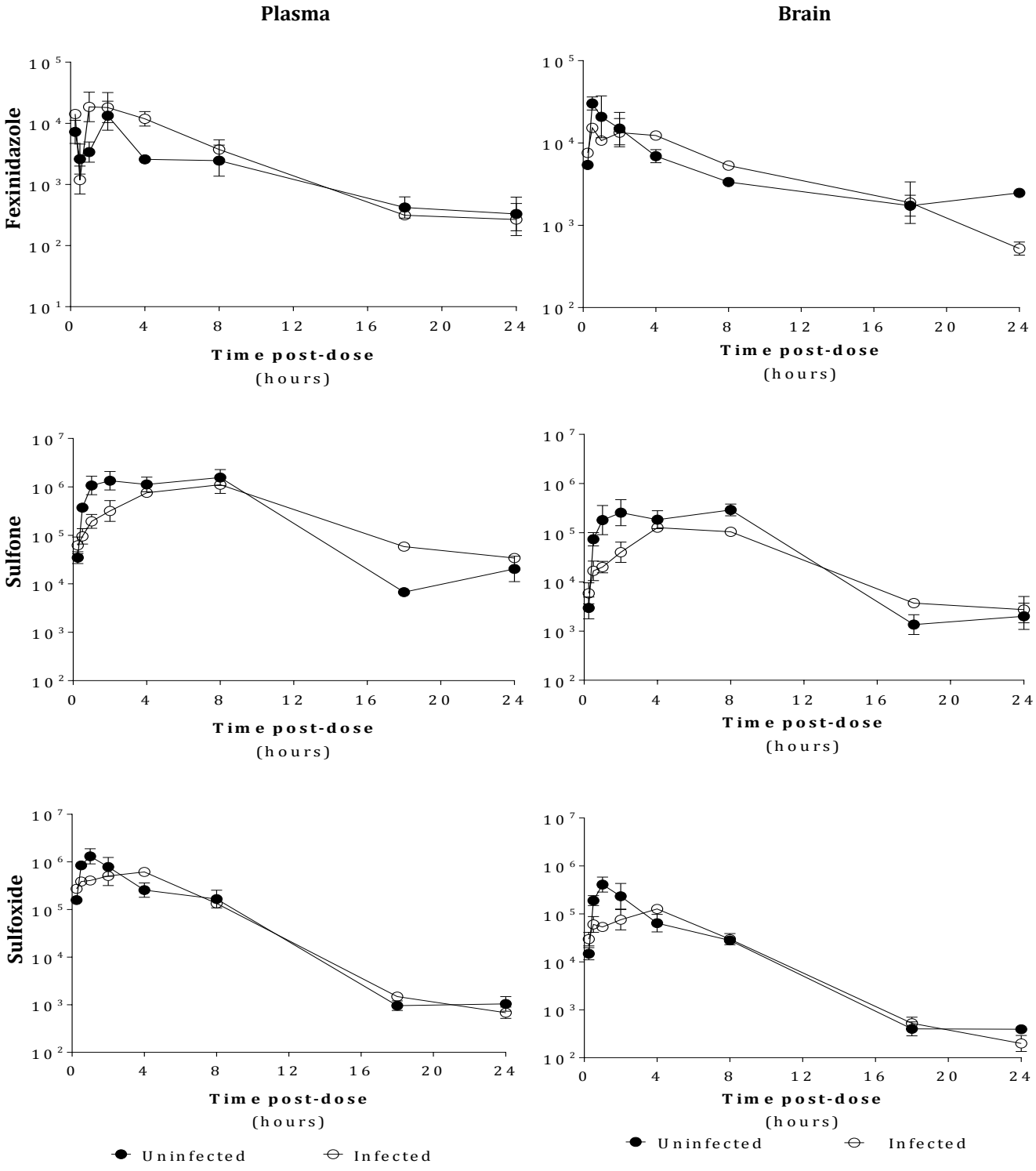

Figure 6.6 The pharmacokinetic profile of fexinidazole and metabolites. A qualitative study on the time-dependent PK profile of fexinidazole, sulfoxide and sulfone. Sampling was carried out at the following time points post-dose; 15, 30 minutes, 1, 2, 4, 8, 18 and 24 hours. Data is presented as the mean peak area (of LC-MS/MS trace) ± SD over time. (A) Fexinidazole in plasma and brain, (B) Sulfone in plasma and brain, (C) Sulfoxide.

CHAPTER 7: Discussion

At present, the *in vivo* drug evaluation tools for HAT require lengthy 180-day relapse experiments, with no definitive data on the parasite burden within the CNS until animals are culled (Kennedy *et al*., 1997). The *in vitro* drug assay using resazurin is also restrictive, as it requires long incubation times, thus preventing time-kill data from being easily determined (Raz *et al*., 1997). The development of an imaging model utilizing bioluminescent *T. b. brucei* enables the real-time assessment of both infection kinetics and drug activity in *in vitro* and *in vivo* studies. In this study we have developed and validated a red-shifted bioluminescent strain of both the monomorphic *T. b. brucei* Lister 427 and pleiomorphic *T. b. brucei* GVR35 to aid drug discovery and development.

When evaluating new compounds for potential anti-trypanosomal activity, the initial *in vitro* assessment is carried out using the 72 hour Alamar blue®/ resazurin assay. The REDOX indicator of resazurin detects parasite proliferation and is ultimately used as an end-point assay. Although resazurin is non-toxic, the long incubation time of 4-6 hours of the fluorometric dye means that the ability to assess the rate of kill of a drug is impossible, as early time points after drug exposure are not detectable.

T. b. brucei 427-VSG5 was originally generated to determine the optimal bioluminescent reporter for future studies in the pleiomorphic line. But its creation has provided advancement in time-kill and efficacy assays. VSG5 has shown the same growth patterns as the WT line both *in vitro* and *in vivo*, suggesting that the incorporation of the construct has not had a negative effect on the trypanosome (McLatchie *et al*., 2013).

The two published bioluminescent 427 strains 427-Rluc-pHD309 (renilla luciferase) and 427-LUC2 (green firefly luciferase) show strong bioluminescence activity *in vitro* but fail to produce high bioluminescence when being transferred into animal models. Despite the VSG5 line demonstrating similar *in vitro* results, the activity demonstrated *in vivo* was far greater. This would enable the strain to be used in time-kill studies *in vivo* to determine time-concentration dependent data in the acute infection.

A number of lines were produced by transfection of the pleiomorphic strain GVR35 with varying degrees of success. Initially the four strains VSL-1, 2, 8 and 21 had a high level of bioluminescence intensity *in vitro*, but the move into animals produced different results. With the exception of VSL-2, all lines failed to produce a detectable signal in the CNS, with VSL-8 and 21 demonstrating altered infection kinetics which resulted in a failure to produce a late-stage infection. High bioluminescence intensity of VSL-2 both *in vitro* and *in vivo* was due to the luciferase being under the control of a strong promoter within the parasite, which enabled a high level of expression of the luciferase (McLatchie *et al*., 2013). In addition to the strong promoter, the red-shifted firefly luciferase (PpyRE9) had been further modified to match a human codon bias, which is similar to that of *T. b. brucei.* This resulted in an improved integration and stability of the luciferase reporter within the parasite (McLatchie *et al*., 2013).

The VSL-2 line provided a higher imaging sensitivity (as few as 100 trypanosomes can be detected) than the previous pleiomorphic trypanosome strains AnTaR1-RLuc (renilla luciferase), GVR35-LUC2 (firefly luciferase), AnTaR1-CBR (click beetle luciferase) and AnTaR1-P9 (red-shifted FLuc) (Myburgh *et al*., 2013, McLatchie *et al*., 2013, Van Reet *et al*., 2014).

The panel of AnTaR1 bioluminescent lines produced by Van Reet *et al* showed the difference between various luciferase reporters, with the RLuc transfected lines having the weakest signal *in vivo* of approximately 10^7 average radiance (photons/s/sr/cm^2), and whilst the red-shifted line was transfected with the same PpyRE9 luciferase as VSL-2, it produced a 10-fold lower bioluminescent signal (Van Reet *et al*., 2014).

At present there is no model for assessing dose dependent drug efficacy, as contemporary techniques (blood films) are unable to determine the level of parasite persistence within tissues. The experimental time of the pre-clinical drug evaluation model of six months is a hindrance in developing new drug treatments, and a new innovative approach is needed.

The combination of BLI and the VSL-2 model can be used in a shortened experimental time of 35 days to confirm drug activity on late-stage HAT by loss of bioluminescence in the brain, and qPCR analysis on the excised brains subsequently confirms parasite burden.

The high-sensitivity and non-invasive nature of the VSL-2 model was able to assess for the first time the dose-dependent effect of the current anti-trypanocidal drug treatment; melarsoprol, DFMO, nifurtimox and fexinidazole.

Using melarsoprol and fexinidazole, the VSL-2 model was able to demonstrate positive clearance of infection, relapse and drug failure. Importantly, the VSL-2 model was able to detect drug relapse 21 days earlier than the conventional method of blood films used in the current pre-clinical model (Kennedy *et al*., 1997).

A quicker assessment of drugs is not the only requirement for a new model, the ability to assess drug activity in real-time to understand time-kill activity will help pharmacokinetic studies. We have carried out preliminary pharmacokinetic studies on a limited number of uninfected mice with nifurtimox, and found that the drug was rapidly metabolised within brain homogenate. Further investigations will be carried out to determine the metabolites and carry out the study on a larger group of infected and uninfected mice.

Here we have demonstrated that a dose-dependent effect can be established in 35 days p.i. By 60 days p.i, a sub curative effect can be detected with relapse observable by 90 days p.i. These findings reduce the experimental time of the current models by 50%. Due to the non-invasive nature of BLI, the monitoring of infection can be extended further if required.

In order to replace the current *T. b. brucei* GVR35 wild type model, the new VSL-2 line needed to mimic the WT infection kinetics, growth and drug sensitivities. Whilst there is evidence to indicate that the transfection of microorganisms can alter their ability to maintain growth rates and infections relative to that of the WT (Andreu *et al*., 2011), the transfection of pTbAMLuc-v into *T. b. brucei* resulted in growth rates, infection kinetics and drug sensitivity mirroring that of the wild type, as indicated in the drug sensitivity study carried out with fexinidazole and *in vitro* growth curves.

There are limitations in the use of animal models for human infections, and it is important to address these issues before data is extrapolated to human level. Many of the mouse models commonly used for HAT studies (including the one presented here) use the animal parasite *T. b. brucei,* which is non-infectious to humans

(making it a safer alternative within the laboratory), and may not provide a true representation of the human infection (Kennedy, 2007).

Although models have been established using the human-infective forms *T. b. rhodesiense* and *T. b. gambiense* within mice, they are harder to use due to the higher level of containment and health risks associated with them. Rhodesiense lines produce an acute infection in immunocompetent mice with a survival of approximately 6 days p.i similar to the *T. b. brucei* 427 strain (but with a higher risk of human infection) (Baltz *et al*., 1985). Gambiense infection in mice is complex, with low virulence in immunocompetent mice and parasitaemia taking months to appear in the periphery (Beckers, 1981). Whilst the use of immunosuppression (through the use of either SCID or immunosuppressant drugs such as cyclophosphamide) produces a quicker infection with higher parasitaemia, studies using minocycline (drug that reduces the number of immune cells invading the CNS) carried out by Masocha *et al* have shown that a strong immune response is involved with the invasion of trypanosomes into the brain, providing complications in the use of SCID mice in the study of late stage infection (Brun, 1999, Masocha *et al*., 2004).

Despite these issues, the use of mouse models (and predominantly *T. b. brucei* models) has been essential in identifying potential therapeutic targets as well as assessing new drug compounds in pre-clinical trials, and until viable alternatives have been established, advancements and improvements on the usability of these models are imperative in the understanding of infectious diseases.

VSL-2 has provided evidence to support that trypanosomes are present in the brain during a late-stage infection. Previous data of direct detection of

trypanosomes in the brain has been sparse, as histopathological studies have shown the characteristic immune response to the disease rather than actual parasites in brain parenchyma (Rodgers, 2010). The high sensitivity of the model is also able to provide early detection of drug relapse and efficacy compared to the wild type, but its uses can extend beyond drug development,

It is known that trypanosomiasis is a haemolymphatic disease with parasites residing in both the blood and lymphatic systems, and the aspiration of the cervical lymph node can be used as a diagnostic method, providing parasitological confirmation of infection (Brun *et al*., 2010). The VSL-2 model showed that the peripheral parasitaemia could not be correlated with bioluminescence during infection. One explanation for this is that the bioluminescence was able to detect parasites present within tissues and the lymphatic system. To confirm this, a study on the infection kinetics of trypanosomiasis through the early to late stage of infection over 35 days could provide further information on where the trypanosomes reside. A similar study by Lewis *et al* on the infection kinetics of a bioluminescent *T. cruzi* strain showed surprising results of the parasite location. By tracking the parasite distribution using BLI during a chronic infection, and subsequently carrying out *ex vivo,* histopathology and qPCR analysis, the authors found that the *T. cruzi* parasite resided in the gastrointestinal tract to allow long-term parasite persistence (Lewis *et al*., 2014a). By using the method of BLI combined with *ex vivo* imaging, histopathology and qPCR described by Lewis *et al* with the VSL-2 model, we could gain an understanding of where the parasites reside during an infection and their movements within the CNS infection.

At present we are still unsure of where trypanosomes migrate to from the brain, but by using BLI we can track even low levels of infection *ex vivo.* This study could

be taken further by assessing parasite load in regions of the brain. This can be done by imaging thick slices of VSL-2 infected brain tissue, and areas of bioluminescence can be subsequently dissected for qPCR analysis or histopathological evaluation, thus reducing the current 'needle in a haystack' approach of finding trypanosomes in tissue sections.

The ability to detect trypanosomes within tissue sections has been difficult, but could be improved by using dual-reporter lines. Although bioluminescence is advantageous in *in vitro* assays and *in vivo* imaging of whole animals and organs, its use in histology is limited. The requirement of a catalytic reaction of the bioluminescent substrate means that the parasites need to be metabolically active (therefore alive) to produce a light signal, this is not possible when preparing sections for microscopic visualisation. By adding a fluorescent protein into the construct the parasite can be imaged both macroscopically and microscopically. The bioluminescent reporter can be detected in whole animal imaging, and the fluorescence detected in microscopy or flow cytometry.

The combination of a dual reporter line with fluorescent immunostaining of host cells could provide evidence of the interactions of the trypanosomes with immune cells at the BBB and therefore determine mechanisms of parasite invasion.

In conclusion, in this study we have developed and validated a red-shifted bioluminescence model of *T. b. brucei*, which provides a sensitive drug assessment system through non-invasive BLI, which reduces the current screening time by 120 days. By combining the high sensitivity of the VSL-2 model with quantitative methods of qPCR, we have developed a new methodology that can assess the dose dependent effect of novel drugs for the treatment of late stage human African

trypanosomiasis, as well as assessing the rate of kill of a drug in a real-time infection. The reduction in drug evaluation time that can now be applied to pre-clinical drug testing will speed up drug development and aid the ongoing progress to HAT elimination.

CHAPTER 8: REFERENCES

ADAMS, S., BROWN, H. & TURNER, G. 2002. Breaking down the blood-brain barrier: signaling a path to cerebral malaria? *Trends Parasitol,* 18**,** 360-6.

ANDREU, N., ZELMER, A., FLETCHER, T., ELKINGTON, P. T., WARD, T. H., RIPOLL, J., PARISH, T., BANCROFT, G. J., SCHAIBLE, U., ROBERTSON, B. D. & WILES, S. 2010. Optimisation of bioluminescent reporters for use with mycobacteria. *PLoS One,* 5**,** e10777.

ANDREU, N., ZELMER, A. & WILES, S. 2011. Noninvasive biophotonic imaging for studies of infectious disease. *FEMS Microbiol Rev,* 35**,** 360-94.

BABOKHOV, P., SANYAOLU, A. O., OYIBO, W. A., FAGBENRO-BEYIOKU, A. F. & IRIEMENAM, N. C. 2013. A current analysis of chemotherapy strategies for the treatment of human African trypanosomiasis. *Pathog Glob Health,* 107**,** 242-52.

BACCHI, C. J., GAROFALO, J., MOCKENHAUPT, D., MCCANN, P. P., DIEKEMA, K. A., PEGG, A. E., NATHAN, H. C., MULLANEY, E. A., CHUNOSOFF, L., SJOERDSMA, A. & HUTNER, S. H. 1983. In vivo effects of alpha-DL-difluoromethylornithine on the metabolism and morphology of Trypanosoma brucei brucei. *Mol Biochem Parasitol,* 7**,** 209-25.

BACCHI, C. J., NATHAN, H.C.,HUNTER, S.H., MC CANN, P.P., SJOERDSMA, A. 1980. Polyamine metabolism: a potential therapeutic target in trypanosomes. *Science,* 210**,** 332-334.

BADR, C. E. & TANNOUS, B. A. 2011. Bioluminescence imaging: progress and applications. *Trends Biotechnol,* 29**,** 624-33.

BAHIA, M. T., NASCIMENTO, A. F., MAZZETI, A. L., MARQUES, L. F., GONCALVES, K. R., MOTA, L. W., DINIZ LDE, F., CALDAS, I. S., TALVANI, A., SHACKLEFORD, D. M., KOLTUN, M., SAUNDERS, J., WHITE, K. L., SCANDALE, I., CHARMAN, S. A. & CHATELAIN, E. 2014. Antitrypanosomal activity of fexinidazole metabolites, potential new drug candidates for Chagas disease. *Antimicrob Agents Chemother,* 58**,** 4362-70.

BALTZ, T., BALTZ, D., GIROUD, C. & CROCKETT, J. 1985. Cultivation in a semi-defined medium of animal infective forms of Trypanosoma brucei, T. equiperdum, T. evansi, T. rhodesiense and T. gambiense. *EMBO J,* 4**,** 1273-7.

BARMAN, T. K., RAO, M., BHATI, A., KISHORE, K., SHUKLA, G., KUMAR, M., MATHUR, T., PANDYA, M. & UPADHYAY, D. J. 2011. Non invasive real-time monitoring of bacterial infection & therapeutic effect of anti-microbials in five mouse models. *Indian J Med Res,* 134**,** 688-95.

BARRETT, M. P., BOYKIN, D. W., BRUN, R. & TIDWELL, R. R. 2007. Human African trypanosomiasis: pharmacological re-engagement with a neglected disease. *Br J Pharmacol,* 152**,** 1155-71.

BARRETT, M. P., COOMBS, G. H. & MOTTRAM, J. C 2004. Future Prospects in Chemotherapy for Trypanosomiasis. *In:* MAUDLIN, I. H., P.H. & MILES, M. A. (ed.) *The Trypanosomiases.* Oxfordshire: CABI Publishing.

BARRY, D. C., M. 2004. Antigenic Variation *In:* MAUDLIN, I. H., P.H. & MILES, M. A. (ed.) *The Trypanosomiases.* Oxfordshire: CABI Publishing.

BARRY, J. D., MCCULLOCH, R. 2001. Antigenic variation in trypanosomes: enhanced phenotypic variation in a eukaryotic parasite. *Advances in Parasitology,* 49**,** 1-70.

BECKERS, A. W., M., VAN MARCK, E., GIGASE, P. 1981. Experimental infections of laboratory rodents with recently isolated stocks of *Trypanosoma brucei gambiense*. 1. Parasitological investigations. *Z Parasitenkd,* 60**,** 285-296.

BISSER, S., N'SIESI, F. X., LEJON, V., PREUX, P. M., VAN NIEUWENHOVE, S., MIAKA MIA BILENGE, C. & BUSCHER, P. 2007. Equivalence trial of melarsoprol and nifurtimox monotherapy and combination therapy for the treatment of second-stage Trypanosoma brucei gambiense sleeping sickness. *J Infect Dis,* 195**,** 322-9.

BRANCHINI, B. R., ABLAMSKY, D. M., DAVIS, A. L., SOUTHWORTH, T. L., BUTLER, B., FAN, F., JATHOUL, A. P. & PULE, M. A. 2010. Red-emitting luciferases for bioluminescence reporter and imaging applications. *Anal Biochem,* 396**,** 290-7.

BRUN, R., BLUM, J., CHAPPUIS, F. & BURRI, C. 2010. Human African trypanosomiasis. *Lancet,* 375**,** 148-59.

BRUN, R. K., R. 1999. Animal Models of Acute (1st Stage) Sleeping Sickness. *In:* SANDE, O. Z. M. A. (ed.) *Handbook of Animal Models of Infection.* London: Academic Press.

BURGOS, J. S., ROSOL, M., MOATS, R. A., KHANKALDYYAN, V., KOHN, D. B., NELSON, M. D., JR. & LAUG, W. E. 2003. Time course of bioluminescent signal in orthotopic and heterotopic brain tumors in nude mice. *Biotechniques,* 34**,** 1184-8.

BURKARD, G., FRAGOSO, C. M. & RODITI, I. 2007. Highly efficient stable transformation of bloodstream forms of Trypanosoma brucei. *Mol Biochem Parasitol,* 153**,** 220-3.

BURRI, C. B., T. GIROUND, C. DOUA, F. WELKER, H. A. BRUN, R. 1993. Pharmacokinetic properties of trypanocidal drug Melarsoprol. *Chemotherapy,* 39**,** 225-234.

BURRI, C. S., A. & BRUN, R. 2004. Current Chemotherapy of Human African Trypanosomiasis. *In:* MAUDLIN, I. H., P.H. & MILES, M. A. (ed.) *The Trypanosomiases.* Oxfordshire: CABI Publishing.

BYSCHER, P. L., V. 2004. Diagnosis Of Human African Trypanosomiasis. *In:* MAUDLIN, I. H., P.H. & MILES, M. A. (ed.) *The Trypanosomiases.* Oxfrodshire: CABI Publishing.

CARTER, N. S., FAIRLAMB, A. H. 1993. Arsenical-resistant trypanosomes lack an unusual adenosine transporter. *Nature,* 361**,** 173-176.

CDC. 2009. *Trypanosomiasis, African* [Online]. Available: http://www.google.co.uk/url?sa=t&rct=j&q=cdc%20african%20tryps%20life%20cycle&source=web&cd=2&ved=0CC0QFjAB&url=http%3A%2F%2Fdpd.cdc.gov%2Fdpdx%2Fhtml%2FFrames%2FS-Z%2FTrypanosomiasisAfrican%2Fbody_TrypanosomiasisAfrican_Page1.htm&ei=OkSpTpSJC5HD8QPl9K2hDA&usg=AFQjCNG9hsISECk6jix8SQJP_8hVezLzLA [Accessed 27/10/2011 2011].

CLAES, F., VODNALA, S. K., VAN REET, N., BOUCHER, N., LUNDEN-MIGUEL, H., BALTZ, T., GODDEERIS, B. M., BUSCHER, P. & ROTTENBERG, M. E. 2009. Bioluminescent imaging of Trypanosoma brucei shows preferential testis dissemination which may hamper drug efficacy in sleeping sickness. *PLoS Negl Trop Dis,* 3**,** e486.

CROFT, S. L. 1999. Pharmacological approaches to antitrypanosomal chemotherapy. *Mem Inst Oswaldo Cruz,* 94**,** 215-20.

CUI, K., XU, X., ZHAO, H. & WONG, S. T. 2008. A quantitative study of factors affecting in vivo bioluminescence imaging. *Luminescence,* 23**,** 292-5.

DELIOLANIS, N., WURDINGER, T., TANNOUS, BA., SHAH, K., NTZIACHRISTOS, V. 2008. Performance of the red-shifted flourescent proteins in deep-tissue molecular imaging applications. *Journal of Biomed Opt,* 4.

DNDI. 2014. *Clinical Trials Protocols* [Online]. Switzerland. Available: http://www.dndi.org/diseases-projects/clinical-trial-protocols.html [Accessed 13Nov 2014].

DORLO, T. P. & KAGER, P. A. 2008. Pentamidine dosage: a base/salt confusion. *PLoS Negl Trop Dis,* 2**,** e225.

DRUSANO, G. L. 2004. Antimicrobial pharmacodynamics: critical interactions of 'bug and drug'. *Nat Rev Microbiol,* 2**,** 289-300.

EPERON, G., BALASEGARAM, M., POTET, J., MOWBRAY, C., VALVERDE, O. & CHAPPUIS, F. 2014. Treatment options for second-stage gambiense human African trypanosomiasis. *Expert Rev Anti Infect Ther,* 12**,** 1407-17.

FAIRLAMB, A. H., HENDERSON, G. B., BACCHI, C. J. & CERAMI, A. 1987. In vivo effects of difluoromethylornithine on trypanothione and polyamine levels in bloodstream forms of Trypanosoma brucei. *Mol Biochem Parasitol,* 24**,** 185-91.

FINSTERER, J. & AUER, H. 2013. Parasitoses of the human central nervous system. *J Helminthol,* 87**,** 257-70.

FRANKE-FAYARD, B., JANSE, C. J., CUNHA-RODRIGUES, M., RAMESAR, J., BUSCHER, P., QUE, I., LOWIK, C., VOSHOL, P. J., DEN BOER, M. A., VAN DUINEN, S. G., FEBBRAIO, M., MOTA, M. M. & WATERS, A. P. 2005. Murine malaria parasite sequestration: CD36 is the major receptor, but cerebral pathology is unlinked to sequestration. *Proc Natl Acad Sci U S A,* 102**,** 11468-73.

HALL, B. S., BOT, C. & WILKINSON, S. R. 2011. Nifurtimox activation by trypanosomal type I nitroreductases generates cytotoxic nitrile metabolites. *J Biol Chem,* 286**,** 13088-95.

HIRUMI, H., DOYLE, J. J. & HIRUMI, K. 1977. Cultivation of bloodstream Trypanosoma brucei. *Bull World Health Organ,* 55**,** 405-9.

HIRUMI, H. & HIRUMI, K. 1994. Axenic culture of African trypanosome bloodstream forms. *Parasitol Today,* 10**,** 80-4.

HITZIGER, N., DELLACASA, I., ALBIGER, B. & BARRAGAN, A. 2005. Dissemination of Toxoplasma gondii to immunoprivileged organs and role of Toll/interleukin-1 receptor signalling for host resistance assessed by in vivo bioluminescence imaging. *Cell Microbiol,* 7**,** 837-48.

HUTCHENS, M. & LUKER, G. D. 2007. Applications of bioluminescence imaging to the study of infectious diseases. *Cell Microbiol,* 9**,** 2315-22.

HYLAND, K. V., ASFAW, S. H., OLSON, C. L., DANIELS, M. D. & ENGMAN, D. M. 2008. Bioluminescent imaging of Trypanosoma cruzi infection. *Int J Parasitol,* 38**,** 1391-400.

IDRO, R., MARSH, K., JOHN, C. C. & NEWTON, C. R. 2010. Cerebral malaria: mechanisms of brain injury and strategies for improved neurocognitive outcome. *Pediatr Res,* 68**,** 267-74.

JANNIN, J. & GABRIELLI, A. F. 2013. Neurological aspects of neglected tropical diseases: an unrecognized burden. *Handb Clin Neurol,* 114**,** 3-8.

JAYAKUMAR, P. N., CHANDRASHEKAR, H. S. & ELLIKA, S. 2013. Imaging of parasitic infections of the central nervous system. *Handb Clin Neurol,* 114**,** 37-64.

JENNINGS, F. W., RODGERS, J., BRADLEY, B., GETTINBY, G., KENNEDY, P. G. & MURRAY, M. 2002. Human African trypanosomiasis: potential therapeutic benefits of an alternative suramin and melarsoprol regimen. *Parasitol Int,* 51**,** 381-8.

JENNINGS, F. W. W., D. D. URQUHART, G.M 1977. The relationship between duration of infection with *Trypanosoma brucei* in mice and the efficacy of chemotherapy. *Parasitology,* 75**,** 143-153.

JOHANSON, C. E., STOPA, E. G. & MCMILLAN, P. N. 2011. The blood-cerebrospinal fluid barrier: structure and functional significance. *Methods Mol Biol,* 686**,** 101-31.

KAISER, M., BRAY, M. A., CAL, M., TRUNZ, B. B., TORREELE, E. & BRUN, R. 2011. Anti-trypanosomal activity of Fexinidazole - A New Oral Nitroimidazole Drug Candidate for the Treatment of Sleeping Sickness. *Antimicrob Agents Chemother*.

KAMERKAR, S. & DAVIS, P. H. 2012. Toxoplasma on the brain: understanding host-pathogen interactions in chronic CNS infection. *J Parasitol Res,* 2012**,** 589295.

KENNEDY, P. G. 2007. Animal models of human African trypanosomiasis--very useful or too far removed? *Trans R Soc Trop Med Hyg,* 101**,** 1061-2.

KENNEDY, P. G., RODGERS, J., JENNINGS, F. W., MURRAY, M., LEEMAN, S. E. & BURKE, J. M. 1997. A substance P antagonist, RP-67,580, ameliorates a mouse meningoencephalitic response to Trypanosoma brucei brucei. *Proc Natl Acad Sci U S A,* 94**,** 4167-70.

KEYAERTS, M., CAVELIERS, V. & LAHOUTTE, T. 2012. Bioluminescence imaging: looking beyond the light. *Trends Mol Med,* 18**,** 164-72.

KILKENNY, C., BROWNE, W. J., CUTHILL, I. C., EMERSON, M. & ALTMAN, D. G. 2010. Improving bioscience research reporting: the ARRIVE guidelines for reporting animal research. *PLoS Biol,* 8**,** e1000412.

KRISTENSSON, K., MASOCHA, W. & BENTIVOGLIO, M. 2013. Mechanisms of CNS invasion and damage by parasites. *Handb Clin Neurol,* 114**,** 11-22.

LACHENMAIER, S. M., DELI, M. A., MEISSNER, M. & LIESENFELD, O. 2011. Intracellular transport of Toxoplasma gondii through the blood-brain barrier. *J Neuroimmunol,* 232**,** 119-30.

LANG, T., GOYARD, S., LEBASTARD, M. & MILON, G. 2005. Bioluminescent Leishmania expressing luciferase for rapid and high throughput screening of drugs acting on amastigote-harbouring macrophages and for quantitative real-time monitoring of parasitism features in living mice. *Cell Microbiol,* 7**,** 383-92.

LEWIS, M. D., FORTES FRANCISCO, A., TAYLOR, M. C., BURRELL-SAWARD, H., MCLATCHIE, A. P., MILES, M. A. & KELLY, J. M. 2014a. Bioluminescence imaging of chronic Trypanosoma cruzi infections reveals tissue-specific parasite dynamics and heart disease in the absence of locally persistent infection. *Cell Microbiol,* 16**,** 1285-300.

LEWIS, M. D., FRANCISCO, A. F., TAYLOR, M. C. & KELLY, J. M. 2014b. A New Experimental Model for Assessing Drug Efficacy against Trypanosoma cruzi Infection Based on Highly Sensitive In Vivo Imaging. *J Biomol Screen*.

MADIGAN, M. T. M., . MARTINKO, J. M., BROCK, T. D. 2006. *Brock: Biology of Microoganisms,* New Jersey, Pearson Prentice Hall.

MASOCHA, W. & KRISTENSSON, K. 2012. Passage of parasites across the blood-brain barrier. *Virulence,* 3**,** 202-12.

MASOCHA, W., ROBERTSON, B., ROTTENBERG, M. E., MHLANGA, J., SOROKIN, L. & KRISTENSSON, K. 2004. Cerebral vessel laminins and IFN-gamma define Trypanosoma brucei brucei penetration of the blood-brain barrier. *J Clin Invest,* 114**,** 689-94.

MATOVU, E. & MÄSER, P. 2010. Drug Resistance in African Trypanosomiasis. *In:* SOSA, A. D. J., BYARUGABA, D. K., AMÁBILE-CUEVAS, C. F., HSUEH, P.-R., KARIUKI, S. & OKEKE, I. N. (eds.) *Antimicrobial Resistance in Developing Countries.* Springer New York.

MCLATCHIE, A. P., BURRELL-SAWARD, H., MYBURGH, E., LEWIS, M. D., WARD, T. H., MOTTRAM, J. C., CROFT, S. L., KELLY, J. M. & TAYLOR, M. C. 2013. Highly sensitive in vivo imaging of Trypanosoma brucei expressing "red-shifted" luciferase. *PLoS Negl Trop Dis,* 7**,** e2571.

MEDANA, I. M. & TURNER, G. D. 2006. Human cerebral malaria and the blood-brain barrier. *Int J Parasitol,* 36**,** 555-68.

MILORD, F., PEPIN, J., LOKO, L., ETHIER, L. & MPIA, B. 1992. Efficacy and toxicity of eflornithine for treatment of Trypanosoma brucei gambiense sleeping sickness. *Lancet,* 340**,** 652-5.

MOGK, S., MEIWES, A., BOSSELMANN, C. M., WOLBURG, H. & DUSZENKO, M. 2014. The lane to the brain: how African trypanosomes invade the CNS. *Trends Parasitol,* 30**,** 470-7.

MUELLER, M., DE LA PENA, A. & DERENDORF, H. 2004. Issues in pharmacokinetics and pharmacodynamics of anti-infective agents: kill curves versus MIC. *Antimicrob Agents Chemother,* 48**,** 369-77.

MYBURGH, E., COLES, J. A., RITCHIE, R., KENNEDY, P. G., MCLATCHIE, A. P., RODGERS, J., TAYLOR, M. C., BARRETT, M. P., BREWER, J. M. & MOTTRAM, J. C. 2013. In vivo imaging of trypanosome-brain interactions and development of a rapid screening test for drugs against CNS stage trypanosomiasis. *PLoS Negl Trop Dis,* 7**,** e2384.

NA-BANGCHANG, K., DOUA, F., KONSIL, J., HANPITAKPONG, W., KAMANIKON, B., KUZOE, F. 2004. The pharmocokinetics of eflornithine (alpha-fifluoromethylornithine) in patients with late-stage *T. b. gambiense* sleeping sickness. *European Journal of Clinical Pharmacology,* 60**,** 269-278.

NARE, B., WRING, S., BACCHI, C., BEAUDET, B., BOWLING, T., BRUN, R., CHEN, D., DING, C., FREUND, Y., GAUKEL, E., HUSSAIN, A., JARNAGIN, K., JENKS, M., KAISER, M., MERCER, L., MEJIA, E., NOE, A., ORR, M., PARHAM, R., PLATTNER, J., RANDOLPH, R., RATTENDI, D., REWERTS, C., SLIGAR, J.,

YARLETT, N., DON, R. & JACOBS, R. 2010. Discovery of novel orally bioavailable oxaborole 6-carboxamides that demonstrate cure in a murine model of late-stage central nervous system african trypanosomiasis. *Antimicrob Agents Chemother,* 54**,** 4379-88.

NAU, R., SORGEL, F. & EIFFERT, H. 2010. Penetration of drugs through the blood-cerebrospinal fluid/blood-brain barrier for treatment of central nervous system infections. *Clin Microbiol Rev,* 23**,** 858-83.

NEWTON, C. R., HIEN, T. T. & WHITE, N. 2000. Cerebral malaria. *J Neurol Neurosurg Psychiatry,* 69**,** 433-41.

NIELSEN, E. I., VIBERG, A., LOWDIN, E., CARS, O., KARLSSON, M. O. & SANDSTROM, M. 2007. Semimechanistic pharmacokinetic/pharmacodynamic model for assessment of activity of antibacterial agents from time-kill curve experiments. *Antimicrob Agents Chemother,* 51**,** 128-36.

NOLAN, D. P., GARCIA-SALVEDO, J.A. ET AL 2004. Communication in Trypanosomatids. *In:* MAUDLIN, I. H., P.H. & MILES, M. A. (ed.) *The Trypanosomiases.* Oxfordshire: CABI Publishing.

OBERHEIM, N. A., TAKANO, T., HAN, X., HE, W., LIN, J. H., WANG, F., XU, Q., WYATT, J. D., PILCHER, W., OJEMANN, J. G., RANSOM, B. R., GOLDMAN, S. A. & NEDERGAARD, M. 2009. Uniquely hominid features of adult human astrocytes. *J Neurosci,* 29**,** 3276-87.

PENTREATH, V. W. K., P. G. E 2004. Pathogenesis of Human African Trypanosomiasis. *In:* MAUDLIN, I. H., P.H. & MILES, M. A. (ed.) *The Trypanosomiases.* Oxfordshire: CABI Publishing.

PEPIN, J., MILORD, F., MPIA, B., MEURICE, F., ETHIER, L., DEGROOF, D. & BRUNEEL, H. 1989. An open clinical trial of nifurtimox for arseno-resistant Trypanosoma brucei gambiense sleeping sickness in central Zaire. *Trans R Soc Trop Med Hyg,* 83**,** 514-7.

PITTELLA, J. E. 2013. Pathology of CNS parasitic infections. *Handb Clin Neurol,* 114**,** 65-88.

POLTERA, A. A., HOCHMANN, A. & LAMBERT, P. H. 1981. Trypanosoma brucei brucei: the response to Melarsoprol in mice with cerebral trypanosomiasis. An immunopathological study. *Clin Exp Immunol,* 46**,** 363-74.

POSTELS, D. G. & BIRBECK, G. L. 2013. Cerebral malaria. *Handb Clin Neurol,* 114**,** 91-102.

PRIOTTO, G., FOGG, C. BALASEGARAM, M., ERPHAS, O. LOUGA, A., CHECCHI, F. ET AL 2006. Three drug combinations for late-stage *Trypanosoma brucei gambiense* sleeping sickness: a randomised clinical trial in Uganda. *PloS Clinical Trials,* 1**,** 39.

RAZ, B., ITEN, M., GRETHER-BUHLER, Y., KAMINSKY, R. & BRUN, R. 1997. The Alamar Blue assay to determine drug sensitivity of African trypanosomes (T.b. rhodesiense and T.b. gambiense) in vitro. *Acta Trop,* 68**,** 139-47.

RODGERS, J. 2010. Trypanosomiasis and the brain. *Parasitology,* 137**,** 1995-2006.

SAADATNIA, G. & GOLKAR, M. 2012. A review on human toxoplasmosis. *Scand J Infect Dis,* 44**,** 805-14.

SADIKOT, R. T. & BLACKWELL, T. S. 2005. Bioluminescence imaging. *Proc Am Thorac Soc,* 2**,** 537-40, 511-2.

SAEIJ, J. P., BOYLE, J. P., GRIGG, M. E., ARRIZABALAGA, G. & BOOTHROYD, J. C. 2005. Bioluminescence imaging of Toxoplasma gondii infection in living mice reveals dramatic differences between strains. *Infect Immun,* 73**,** 695-702.

SCORY, S., CAFFREY, C. R., STIERHOF, Y. D., RUPPEL, A. & STEVERDING, D. 1999. Trypanosoma brucei: killing of bloodstream forms in vitro and in vivo by the cysteine proteinase inhibitor Z-phe-ala-CHN2. *Exp Parasitol,* 91**,** 327-33.

SCOTT AG, T. A., TURNER CMR 1997. Trypanosoma brucei: lack of cross-resistance to melarsoprol in vitro by cymelarsan-resistant parasites. *Experimental Parasitology***,** 181-190.

SIMARRO, P. P., DIARRA, A. RUIZ POSTIGO, J. A., FRANCO, J. R>, JANNIN, J. G. 2011. The Human African Trypanosomiasis Control Surveillance Programme of the World Health Organisation 2000-2009: The Way Forward. *PLoS Negl Trop Dis,* 5**,** 1-7.

SIMEONOVA, I. & HUILLARD, E. 2014. In vivo models of brain tumors: roles of genetically engineered mouse models in understanding tumor biology and use in preclinical studies. *Cell Mol Life Sci,* 71**,** 4007-26.

STEIN, J., MOGK, S., MUDOGO, C. N., SOMMER, B. P., SCHOLZE, M., MEIWES, A., HUBER, M., GRAY, A. & DUSZENKO, M. 2014. Drug development against sleeping sickness: old wine in new bottles? *Curr Med Chem,* 21**,** 1713-27.

STERNBERG, J. M. & MACLEAN, L. 2010. A spectrum of disease in human African trypanosomiasis: the host and parasite genetics of virulence. *Parasitology,* 137**,** 2007-15.

STEVENS, J. R. A. B., S. 2004. Systemics of Trypanosomes of Medical and Veterinary Importance. *In:* MAUDLIN, I. H., P.H. & MILES, M. A. (ed.) *The Trypanosomiases.* Oxfordshire: CABI Publishing.

STEVERDING, D. 2008. The history of African trypanosomiasis. *Parasites & Vectors,* 12.

TARRAL, A., BLESSON, S., MORDT, O. V., TORREELE, E., SASSELLA, D., BRAY, M. A., HOVSEPIAN, L., EVENE, E., GUALANO, V., FELICES, M. & STRUB-WOURGAFT, N. 2014. Determination of an optimal dosing regimen for fexinidazole, a

novel oral drug for the treatment of human African trypanosomiasis: first-in-human studies. *Clin Pharmacokinet,* 53**,** 565-80.

TAYLOR, M. C. & KELLY, J. M. 2014. Optimizing bioluminescence imaging to study protozoan parasite infections. *Trends Parasitol,* 30**,** 161-2.

TORREELE, E., BOURDIN TRUNZ, B., TWEATS, D., KAISER, M., BRUN, R., MAZUE, G., BRAY, M. A. & PECOUL, B. 2010. Fexinidazole--a new oral nitroimidazole drug candidate entering clinical development for the treatment of sleeping sickness. *PLoS Negl Trop Dis,* 4**,** e923.

VAN NIEUWENHOVE, S., DECLERCQ, J. Difluoromethylornithine: a new promising drug against *gambiense* sleeping sickness. . Proceedings 17th meeting ISCTRC, Arusha, 1981b Nairobi. 213.

VAN REET, N., VAN DE VYVER, H., PYANA, P. P., VAN DER LINDEN, A. M. & BUSCHER, P. 2014. A panel of Trypanosoma brucei strains tagged with blue and red-shifted luciferases for bioluminescent imaging in murine infection models. *PLoS Negl Trop Dis,* 8**,** e3054.

WEISS, N., MILLER, F., CAZAUBON, S. & COURAUD, P. O. 2009. The blood-brain barrier in brain homeostasis and neurological diseases. *Biochim Biophys Acta,* 1788**,** 842-57.

WHO. 2009. *WHO includes combination of eflornithine and nifurtimox in its Essential List of Medicines for th treatment of human African Trypanosomiasis* [Online]. Available: /www.who.int/neglected_diseases/disease_management/drug_combination/en/index.html [Accessed 20March2012 2012].

WHO 2013. Control and surveillance of human African trypanosomiasis. *In:* ORGANISATION, W. H. (ed.) *WHO Technical Report Series.* Geneva, Switzaland: World Health Organisiation.

WRING, S., GAUKEL, E., NARE, B., JACOBS, R., BEAUDET, B., BOWLING, T., MERCER, L., BACCHI, C., YARLETT, N., RANDOLPH, R., PARHAM, R., REWERTS, C., PLATNER, J. & DON, R. 2014. Pharmacokinetics and pharmacodynamics utilizing unbound target tissue exposure as part of a disposition-based rationale for lead optimization of benzoxaboroles in the treatment of Stage 2 Human African Trypanosomiasis. *Parasitology,* 141**,** 104-18.

WYLLIE, S., PATTERSON, S., STOJANOVSKI, L., SIMEONS, F. R., NORVAL, S., KIME, R., READ, K. D. & FAIRLAMB, A. H. 2012. The anti-trypanosome drug fexinidazole shows potential for treating visceral leishmaniasis. *Sci Transl Med,* 4**,** 119re1.

YARLETT, N. & BACCHI, C. J. 1988. Effect of DL-alpha-difluoromethylornithine on polyamine synthesis and interconversion in Trichomonas vaginalis grown in a semi-defined medium. *Mol Biochem Parasitol,* 31**,** 1-9.

APPENDIX

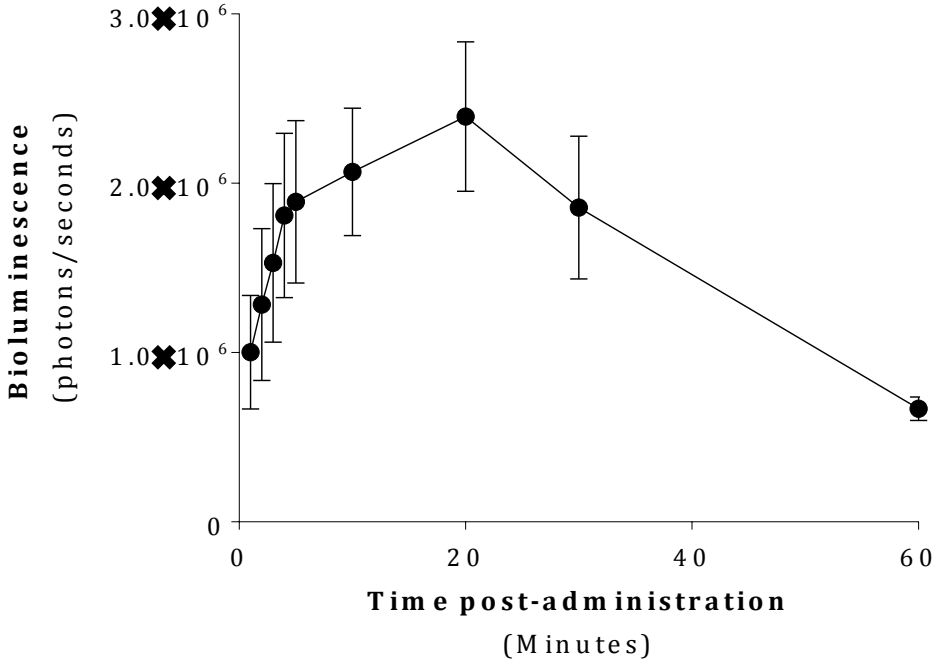

Luciferin. Three VSL-2 infected CD1 mice were injected with 150 mg/kg i.p of luciferin and placed immediately within the IVIS Lumina. The mice were imaged over 60 minutes and their bioluminescence was calculated to determine the optimum imaging window after luciferin administration